

MDPI

Review

# Advancing Hydrogen Gas Utilization in Industrial Boilers: Impacts on Critical Boiler Components, Mitigation Measures, and Future Perspectives

Edem Honu 1,\*, Shengmin Guo 20, Shafiqur Rahman 30, Congyuan Zeng 10 and Patrick Mensah 1

- Department of Mechanical Engineering, Southern University and A & M College, Baton Rouge, LA 70807, USA; congyuan.zeng@sus.edu (C.Z.); patrick\_mensah@subr.edu (P.M.)
- Department of Mechanical & Industrial Engineering, Louisiana State University, Baton Rouge, LA 70803, USA; sguo2@lsu.edu
- Department of Mechanical Engineering, Louisiana Tech University, Ruston, LA 71272, USA; srahman@latech.edu
- \* Correspondence: edem.honu@sus.edu; Tel.: +1-225-407-6554

Abstract: This review sets out to investigate the detrimental impacts of hydrogen gas (H<sub>2</sub>) on critical boiler components and provide appropriate state-of-the-art mitigation measures and future research directions to advance its use in industrial boiler operations. Specifically, the study focused on hydrogen embrittlement (HE) and high-temperature hydrogen attack (HTHA) and their effects on boiler components. The study provided a fundamental understanding of the evolution of these damage mechanisms in materials and their potential impact on critical boiler components in different operational contexts. Subsequently, the review highlighted general and specific mitigation measures, hydrogen-compatible materials (such as single-crystal PWA 1480E, Inconel 625, and Hastelloy X), and hydrogen barrier coatings (such as TiAlN) for mitigating potential hydrogen-induced damages in critical boiler components. This study also identified strategic material selection approaches and advanced approaches based on computational modeling (such as phase-field modeling) and data-driven machine learning models that could be leveraged to mitigate potential equipment failures due to HE and HTHA under elevated H<sub>2</sub> conditions. Finally, future research directions were outlined to facilitate future implementation of mitigation measures, material selection studies, and advanced approaches to promote the extensive and sustainable use of H<sub>2</sub> in industrial boiler operations.

Keywords: boilers; hydrogen; embrittlement; hydrogen attack; sustainability



Citation: Honu, E.; Guo, S.; Rahman, S.; Zeng, C.; Mensah, P. Advancing Hydrogen Gas Utilization in Industrial Boilers: Impacts on Critical Boiler Components, Mitigation Measures, and Future Perspectives. *Hydrogen* 2024, 5, 574–623. https://doi.org/10.3390/hydrogen5030032

Academic Editor: Zhang-Hui Lu

Received: 27 June 2024 Revised: 21 August 2024 Accepted: 28 August 2024 Published: 1 September 2024



Copyright: © 2024 by the authors. Licensee MDPI, Basel, Switzerland. This article is an open access article distributed under the terms and conditions of the Creative Commons Attribution (CC BY) license (https://creativecommons.org/licenses/by/4.0/).

# 1. Introduction

Boilers, critical pressure vessels for heating water and generating steam, play a dual role in industrial applications by providing heating solutions and powering steam turbines for electricity generation [1]. Historically, boiler operations have predominantly relied on traditional fossil fuels, including natural gas, coal, oil, and diesel, to generate a significant portion of global electricity [2,3]. Despite their widespread use, these traditional fuels have significant limitations in achieving clean combustion. Given that their combustion significantly contributes to global carbon dioxide (CO<sub>2</sub>) and overall greenhouse gas emissions, reducing their carbon intensity is crucial for achieving climate change goals [4–6]. In light of this, the adoption of renewable and clean energy fuels has garnered significant interest in supporting environmental protection efforts. Particularly, transitioning to clean energy fuels such as hydrogen gas (H<sub>2</sub>) is becoming increasingly critical for balancing energy demand with environmental sustainability [7,8].

In recent years, there has been a growing interest in utilizing  $H_2$  to reduce the carbon intensity of industrial boiler operations. Several studies have proven that the use of  $H_2$  as an alternative to fossil fuels for combustion can significantly reduce  $CO_2$  emissions and

enhance environmental sustainability. For instance, Shiro et al. [9] conducted a comparative analysis of the percentage of  $CO_2$  emitted during the combustion of traditional fuels and  $H_2$ . The study demonstrated that the combustion of  $H_2$  and hydrogen-enriched natural gas (HENG) produced the lowest carbon emissions compared to other traditional fuels. A summary of their findings is presented in Figure 1. Shiro et al.'s combustion analysis aligns well with existing literature, confirming the benefits of using  $H_2$  as a substitute for traditional fossil fuels in reducing carbon emissions during combustion [10].

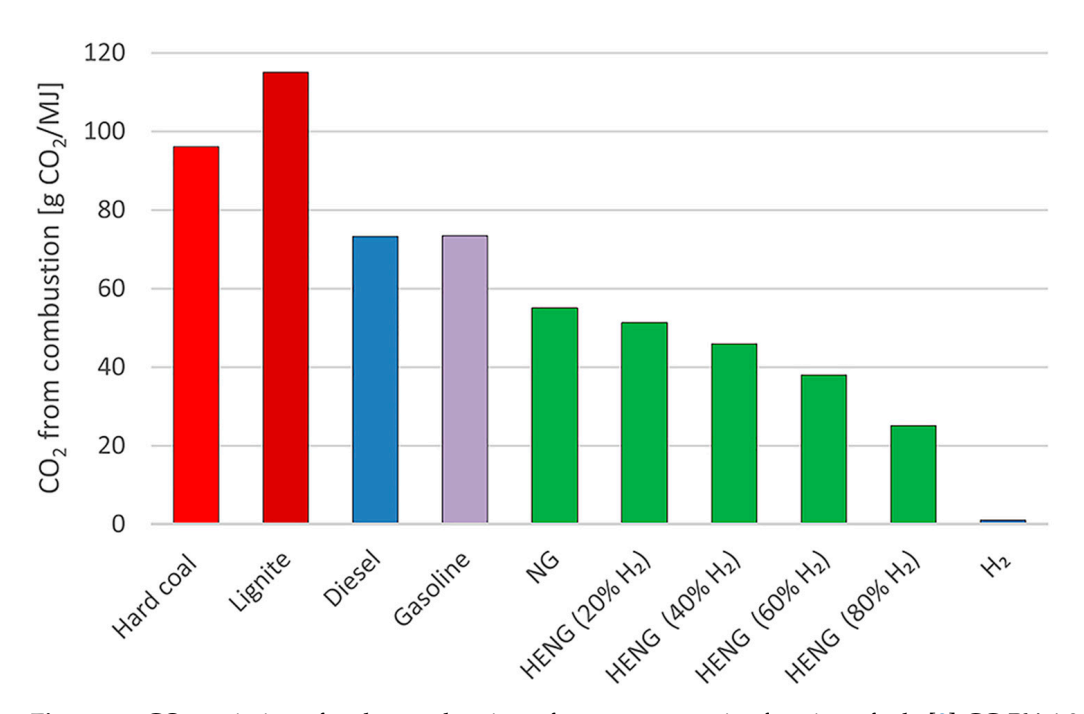


**Figure 1.**  $CO_2$  emissions for the combustion of one energy unit of various fuels [9] CC BY 4.0 (open access).

Some key combustion properties of  $H_2$ , compared with conventional fuels such as methane (CH<sub>4</sub>), were also highlighted in the literature [11,12]. Table 1 compares these key combustion properties of CH<sub>4</sub> and H<sub>2</sub>. For example, H<sub>2</sub> exhibits a wider combustible range, a higher flame temperature, lower spark ignition energy, and a lower autoignition temperature compared to conventional CH<sub>4</sub>. Thus, in addition to its clean burning benefits, these highlighted combustion properties further validate the push for the extensive use of H<sub>2</sub> in industrial boiler operations.

<b>Table 1.</b> Combustion p	properties	of $CH_4$ and $H$	H <sub>2</sub> . Adapted from	Najjar [	[11]	
------------------------------	------------	-------------------	-------------------------------	----------	------	--

Property	$CH_4$	$H_2$
Stoichiometric air/fuel ratio (kg)	17.2	34.3
Combustible range (%)	5–15	6.7–36.0
Flame temperature (°C)	1914	2207
Minimum spark ignition energy (mJ)	0.30	0.017
Autoignition temperature (°C)	600	585

 $\rm H_2$  has also been widely recognized as a high-energy-density fuel and a potential low-cost fuel for future economies [10]. It has been reported that 1 kg (kg) of hydrogen contains 120 megajoules (MJ) or 33 kilowatt-hours (kWh) of energy. This is more than twice the energy density of conventional fuels like natural gas, which can have an energy density of 43 MJ/kg [13–15]. Table 2 corroborates this claim by presenting the comparison between the energy contents of gaseous hydrogen, liquid hydrogen, and conventional fuels [10]. The comparison shows that  $\rm H_2$  has a significantly higher energy density than all traditional

fossil fuels, further emphasizing its potential as an efficient energy solution. Several other studies have also confirmed these benefits and proposed  $H_2$  as an essential solution to the current energy crisis and the threat that global warming poses to environmental safety [16–19]. Thus, overall, the adoption of  $H_2$  has the significant potential to transform the energy sector and promote environmental conservation.

Table 2 Comparison	of some selected energy	contents of fuels l	[10] (with	nermission from F	sevier)
Table 4. Companison	. Of Soffie Selected efferg	Contents of fuels i	I TO I ( WILL)		ISC VICI /.

Fuel	Energy Content [MJ/kg]		
	Lower Heating Value	Higher Heating Value	
Gaseous hydrogen	119.96	141.88	
Liquid hydrogen	120.04	141.77	
Natural gas	47.13	52.21	
Liquified natural gas	48.62	55.19	
Still gas	46.89	50.94	
Crude oil	42.68	45.93	
Liquified petroleum gas (LPG)	46.60	50.14	
Conventional gasoline	43.44	46.52	
Reformulated or Low-sulfur gasoline (RFG)	42.35	45.42	
Conventional diesel	42.78	45.76	
Low-sulfur diesel	42.60	45.56	
Coal (wet basis)	22.73	23.96	
Bituminous coal (wet basis)	26.12	27.26	
Coking coal (wet basis)	28.60	29.86	
Methanol	20.09	22.88	
Ethanol	26.95	29.84	

Despite the benefits of  $H_2$  as a potential combustion fuel for boilers, recent research has been focused on assessing its feasibility for boiler operations. Particular attention has been given to addressing the challenges associated with its use [20–28]. One such challenge would be advancing the technology for  $H_2$  adoption to ensure its safe use and, consequently, reduce the industrial dependence on fossil fuels [29]. Beyond its wide flammability range (between 4% and 75%) and significant explosion potential [12], there are other considerable safety challenges. Currently, these challenges primarily involve understanding the combustion characteristics of  $H_2$  and its impact on materials, industrial components, and the environment. These issues could pose significant obstacles to the widespread adoption of  $H_2$  in industrial boiler operations [9,27,30,31].

The vulnerability of key boiler components to degrade when operating under hydrogenrich conditions could significantly impede overall boiler operation and lead to catastrophic accidents. Critical components such as boiler evaporator tubes, pressure vessels, and fasteners are highly susceptible to a cascade of failure mechanisms under hydrogen-rich, high-temperature, high-pressure conditions. These mechanisms may include hydrogen embrittlement (HE) [21,32,33], high-temperature corrosion failure [34], high-temperature hydrogen attack (HTHA) [35], and high-temperature creep failure [36]. Thus, it is imperative to gain a thorough understanding of these underlying failure mechanisms in hydrogen-rich, high-temperature, and high-pressure operational contexts. This knowledge is crucial for making informed decisions regarding effective mitigation approaches and precise material selection.

Notably, extensive mitigation measures, including material selection studies, have been explored to mitigate the occurrence of both HE and HTHA in industrial boiler components [21,32,33]. Nevertheless, there are significant discrepancies in the extensive body of literature regarding standardized hydrogen-compatible materials that can withstand hydrogen-rich, high-temperature, and high-pressure conditions. Additionally, previous mitigation measures and material selection studies often lack robust, confident validation in specific operational contexts. These unaddressed gaps could result in major equipment

failures in hydrogen-fuel boilers, potentially leading to undesirable incidents. For instance, Djukic et al. [21] and Campari et al. [31] have reported severe hydrogen-induced damage occurrences in boiler evaporator tubes and pressure vessels across numerous industrial boiler plants globally. Most importantly, the literature investigating hydrogen damage of components exposed to H<sub>2</sub> or HENG (with high H<sub>2</sub> percentages) under industrial boiler operation conditions is also obscure and limited [12]. This limitation often arises due to the complexity of experimentally modeling the operating conditions of critical boiler components in industrial power plants.

To address these gaps and facilitate the broader adoption of  $H_2$  in industrial boiler operations, it is essential to develop more effective mitigation strategies and conduct comprehensive material selection studies to tackle the detrimental impacts of  $H_2$  on materials. Therefore, a crucial initial step would be preliminary, detailed assessments, which are vital for identifying and addressing the impact of hydrogen-induced damages on critical boiler components under high-temperature, high-pressure  $H_2$  conditions. Consequently, these assessments would also be indispensable for promoting the wider, more confident application of  $H_2$  in industrial boiler operations.

In this context, essentially, the review study sets out to achieve the following objectives:

- 1. To provide a fundamental understanding of the HE and HTHA phenomena and their potential occurrences in hydrogen-fuel boilers.
- 2. To highlight mitigation measures, hydrogen-compatible materials, and barrier coatings that are feasible under in-service hydrogen boiler operations.
- To discuss advanced computational and data-driven approaches for the simulation and prediction of hydrogen-assisted damages in critical boiler components under varying operational conditions.
- 4. To provide future research directions to guide the advancement of  $H_2$  use in industrial boiler operations.

The remainder of this paper is organized as follows. Section 2 provides an overview of the potential adverse effects of H<sub>2</sub> on critical boiler components. It includes a fundamental discussion of the occurrence of HE and HTHA within specific operational contexts. Section 3 reviews the literature on viable mitigation measures designed to counteract the detrimental effects of H<sub>2</sub> on the boiler components. Section 4 discusses material selection studies for the selection of hydrogen-compatible materials for elevated H<sub>2</sub> conditions. A discussion of the implementation of mitigation measures in an industrial context is also provided. Section 5 highlights both experimental and emerging computational and data-driven approaches for investigating hydrogen-induced damages in boiler components. Section 6 summarizes the key findings of the review and presents future research directions aimed at advancing the use of H<sub>2</sub> in industrial boiler operations.

# 2. Adverse Impacts of the Industrial Use of H<sub>2</sub> in Boiler Operation

 $\rm H_2$  has been gaining increasing attention as an alternative energy source owing to its environmental benefits and high energy density, as formerly discussed. However, the increased use of  $\rm H_2$  in industrial boiler operations could potentially have adverse impacts on critical boiler components and overall boiler operations. In this study, we discussed the detrimental impact of  $\rm H_2$  on critical components in water or fire tube boilers, such as coal-fired and HENG-fired boilers used in thermal power plants. These critical boiler components are typically made of high-strength steels, plain carbon steels, and low-alloy steels and operate under a pressure range of 15.5–27.0 MPa and a temperature range of 300–540 °C [11,21]. However, it is important to note that the combustion of  $\rm H_2$  or HENG (with a high  $\rm H_2$  percentage) is associated with higher operating temperatures, often exceeding 540 °C [11,20]. Hence, investigating novel high-temperature hydrogencompatible materials would be necessary.

As recognized across the literature, the prominent detrimental impacts, potentially on key boiler components in thermal power plants operating under hydrogen-rich elevated conditions, are HE and HTHA [21,26,27,32,33,35,37–39]. For example, earlier investigations

on the effect of H<sub>2</sub> on high-pressure energetic boiler drums for thermal power plants revealed intensive hydrogenation and subsequent embrittlement. This contributed to the development of major corrosion damage, which manifested in the form of linear pits and cracks [37]. Recently, Dwivedi et al. [26] and Venezuela et al. [39] investigated the effect of H<sub>2</sub> on advanced high-strength steel (AHSS) suitable for boilers and pressure vessels under intermediate and moderate temperature conditions. They reported AHSS materials as highly susceptible to HE, with a drastic reduction in ductility without any fracture behavior changes. Djukic et al. [21] also investigated the hydrogen damage of low-carbon steel evaporator tubes in industrial boiler plants through failure and postmortem analysis. Their experimental analysis also demonstrated the drastic decline in steel ductility due to the simultaneous action of active HE mechanisms. In fact, these hydrogen-induced damages (HE and HTHA) continue to be the primary causes of numerous boiler equipment failures and accidents [21,31,40,41].

Despite these challenges, using  $H_2$  as a fuel in boilers has the potential to significantly reduce greenhouse gas emissions, enhance fuel efficiency, and boost overall energy output in industrial operations. Given the growing demand for cleaner energy sources, the potential benefits of using  $H_2$  could outweigh the associated hydrogen-induced damage of components [16–19]. Nonetheless, to address the challenges associated with the extensive use of  $H_2$ , it is essential to implement appropriate mitigation measures and conduct proper material selection studies. These mitigation measures and material selection studies should incorporate emerging computational and data-driven approaches that can confidently inform decisions on enhancing or replacing materials traditionally used for critical boiler components. Therefore, a precise, fundamental understanding of the detrimental hydrogen damages of boiler components exposed to  $H_2$  is crucial. Gaining detailed insights into these hydrogen damages is essential for the development of effective mitigation measures to safeguard critical boiler components, prevent catastrophic failures, and minimize the frequency of power plant shutdowns.

# 2.1. Hydrogen Damage and Simultaneous Embrittlement

Materials used for critical boiler components, particularly steels, exposed to hydrogenrich, high-temperature, and high-pressure conditions tend to be highly susceptible to specific hydrogen-induced damages that can degrade their mechanical performance. Some hydrogen-engendered damages include cracking due to hydride formation, hydrogen-induced fissuring, internal hydrogen precipitation, HTHA, and HE [37,42].

HE is predominantly the hydrogen damage assessed in most materials used for critical boiler components operating under hydrogen-rich conditions [43]. HE is the result of the ingress and trapping of hydrogen atoms in the metal lattice, which leads to the degradation of the mechanical properties of the metal (loss of ductility and impact toughness) and crack initiation under applied loads [32,44]. Under mild to high temperatures, hydrogen atoms can diffuse into the crystalline structure of metals by occupying interstitial sites. Under the influence of external forces, these atoms can also shift and accumulate near grain boundaries or dislocation sites. Due to the inherent instability of hydrogen atoms, they tend to combine rapidly with other hydrogen atoms, leading to an increase in volume and the formation of micro-cracks [45]. Figures 2 and 3 show simplistic schematic depictions of the initiation of the HE mechanism as a result of atomic hydrogen diffusion and segregation. In most cases, an increase in temperature can also lead to increased diffusion of hydrogen atoms. This is simply because the solubility of the hydrogen atoms in certain materials tends to increase at higher temperatures [46]. Moreover, when the concentration of hydrogen outside the material exceeds that which is inside, hydrogen diffusion can also occur even at lower temperatures [40].

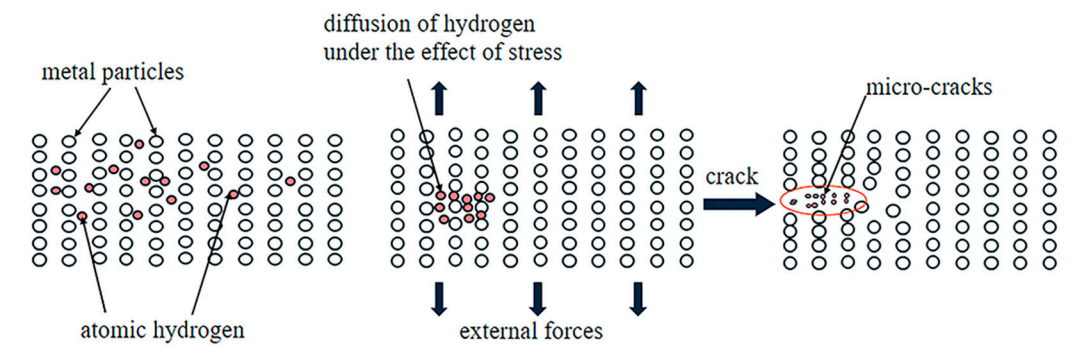


**Figure 2.** The general mechanism of HE is atomic hydrogen diffusion, resulting in microcracks [45] (Figure redrawn from original image).

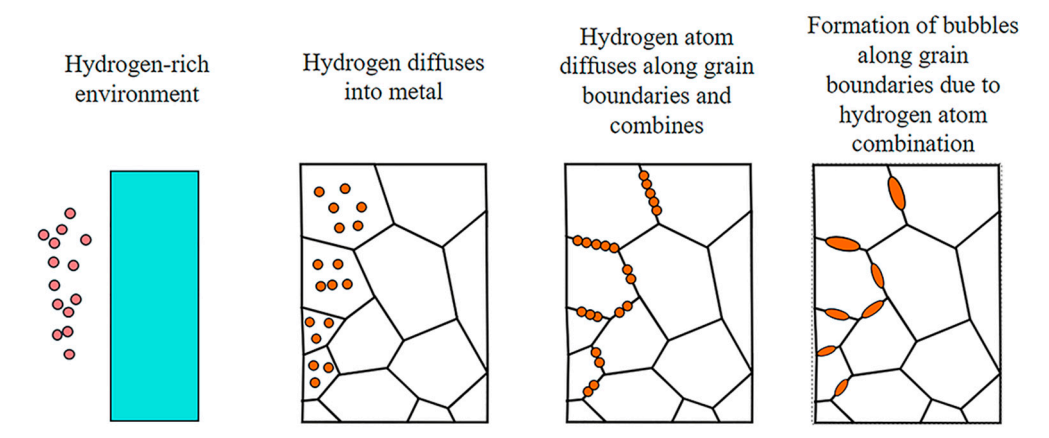


Figure 3. The diffusion of hydrogen atoms along grain boundaries drives the HE occurrence.

The diffusion of hydrogen atoms into a material may occur during fabrication and post-processing. These include casting, carbonizing, surface-chemical cleaning, pickling, electroplating, electrochemical machining, cathodic protection, welding, roll forming, and heat treatment [44]. Moreover, the diffusion of hydrogen atoms into the metal can be further facilitated by environmental exposure during the use of the material. This infiltration could occur owing to various factors such as cathodic electrochemical reactions [44], low-temperature corrosion-induced hydrogen evolution [47], or exposure to gaseous hydrogen at mild to heightened temperatures—a common scenario in most boiler combustion operations [48].

The hydrogen-induced degradation of the mechanical properties of most metallic materials and alloys has been widely studied and confirmed. Essentially, HE reduces the tensile strength, yield strength, hardness, impact strength, fracture toughness, elongation to failure, and fatigue life of affected materials [49-51]. More specifically, several studies have also confirmed the hydrogen-induced mechanical degradation of different grades of steel used for most critical boiler components. These include low-carbon steels [51], mediumstrength steels [52], high-strength steels [53,54], stainless steels [55], ferritic and martensitic steels [37–39], and austenitic steels [56]. However, according to Yamabe et al. [57], the impact of hydrogen on the fatigue crack propagation rate in steels is still a subject of debate and could be dependent on the stress ratio levels. Nonetheless, Pradhan et al. [58] reviewed the impact of HE on fatigue strength in high-strength steels and reported that in intensive hydrogen concentrations, the fatigue crack growth rate increased with increasing stress intensity factors and stress ratios [59]. Additionally, Briotteet et al. [60] revealed that fatigue crack initiation and fatigue crack growth may even occur at ambient temperatures and under an H<sub>2</sub> pressure of 0.5–35 Mpa. They also noted that crack growth was highly dependent on loading frequencies and stress intensity factors.

Murakami et al. [55] identified predominant factors that influence the activation and severity of HE in metals and metallic alloys. These factors include the source of hydrogen

(electrochemical charging or gaseous), global and local hydrogen content in the material, and the hydrogen concentration gradient in the material. For steels and iron, in particular, Djukic et al. [61] also revealed that the HE mechanism is influenced by the microstructure, hydrogen content, and the distribution of hydrogen atoms in the materials. For example, high-strength steels with martensite microstructures can exhibit high susceptibility to HE [26]. Additionally, the environmental and mechanical loading conditions at different scales (macro, micro, and nano) can also play a major role in initiating HE in different grades of steel [61]. Another factor to consider is that the susceptibility of a type of steel to HE is strongly influenced by its strength [44,62]. High-strength steels are generally highly susceptible to HE, while low-strength austenitic steels exhibit relatively low levels of susceptibility compared to ferritic steels [38,44,62].

More generally, factors that could potentially influence HE in metals include material susceptibility, environmental exposure, stresses, quantity of atomic hydrogen diffusion, and micro-hardness of the material [45,63]. Figure 4 depicts the general factors that could influence HE in materials.

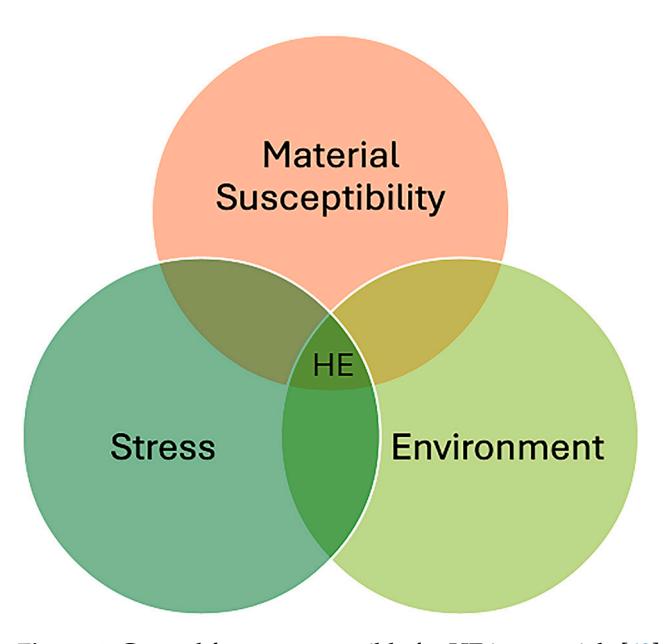


Figure 4. General factors responsible for HE in materials [63] (Redrawn from original image).

#### 2.1.1. Theoretical Modeling of the HE Phenomenon

Although general mechanistic understandings of HE have been held for several decades, many specific details remain obscure. This is often attributed to the challenges associated with detecting hydrogen, given its small size, rapid diffusion, and widespread presence in the environment [64]. Hence, to date, HE remains a complex phenomenon with several underlying mechanisms that can influence material failure [40]. Thus, extensive research has attempted to accurately model this phenomenon and provide a comprehensive theoretical understanding of its occurrence and manifestations in materials [26,65–67]. Conducting theoretical studies would enable more precise modeling and characterization of hydrogen uptake, diffusion, and trapping, as well as a deeper understanding of how these factors influence the kinetics of active HE mechanisms [45]. Such insights are also crucial for making informed decisions regarding advanced material selection and the development of hydrogen-specific components.

Several theoretical models have been formulated to describe the underlying mechanisms that influence the manifestation of HE in materials [26]. The common HE mechanisms highlighted for this study are the hydrogen pressure theory (HPT), hydrogen-enhanced decohesion mechanism (HEDE), hydrogen-enhanced localized plasticity mechanism (HELP), hydrogen-enhanced strain-induced vacancies (HESIV), and absorption-induced dislocation emission theory (AIDE) [26,65–70].

#### HPT Model

For non-austenitic steels, the earliest and most prominent hydrogen-induced defects observed were bright, shiny, and snowflake-like cracks [37,71]. The HPT model, initially proposed by Zapfe et al. [72], provides a more comprehensive description of the development of these defects. The model explains that defect locations in these steels, such as microvoids and inclusion sites, tend to attract hydrogen atoms. The hydrogen atoms tend to accumulate locally to form hydrogen molecules. Over time, the hydrogen molecules in the surrounding area continuously diffuse toward the defect sites, resulting in a buildup of  $H_2$  pressure. If the local  $H_2$  pressure exceeds the material's critical strength, it leads to hydrogen-induced cracking (HIC), which manifests as fisheyes or snowflakes [72].

However, Martin and Sofroni [64] identified a discrepancy in this theoretical modeling of HE. They noted that HE occurs across various metal classes when hydrogen atoms are present within the metal lattice, and its manifestation typically requires an applied force. In contrast, HIC is driven by the accumulation of molecular hydrogen within cracks and is predominantly observed in non-austenitic steels. As a result, the accuracy of the HPT model in broadly characterizing and modeling HE across different metal classes may be questionable.

#### **HESIV Model**

Nagumo [73] proposed the HESIV mechanism to explain HE in relation to the dynamics of dislocation mobility due to the increased density of vacancies. Nagumo reported that the presence of hydrogen in a metal results in the formation of vacancies that can cause premature fracture under strain. The hydrogen atoms can drive the increase in density of vacancies, forming clusters that limit their mobility and stability. Consequently, the agglomeration of vacancies would act as a source of voids and weaken the material's ability to bear stress [73].

# **HEDE** Model

The HEDE model explains the occurrence of HE in the context of interatomic strength and intergranular fractures [66,67]. Essentially, higher hydrogen solubility in materials leads to rapid diffusion of hydrogen atoms in the material. This diffusion weakens the interatomic bonds at the crack tip, ultimately resulting in cleavage-type fractures [58].

For instance, Li et al. [74] conducted a comparative study of HE mechanisms in various high-strength steels and expounded on the HEDE mechanism. They explained that the presence of hydrogen plummets the cohesive interatomic interactions within the metal, making it more susceptible to atomic separation under low tensile stress. The degree of reduction in the metallic interatomic forces increases as the local concentration of hydrogen rises.

Martin et al. [75] also investigated hydrogen-induced intergranular failure in nickel and provided further insights into the HEDE mechanism. They observed that hydrogen atoms, similar to other impurities, accumulate at grain boundaries and reduce cohesive interactions between metal atoms. This ultimately leads to brittle intergranular fractures. Essentially, a decrease in cohesive strength reduces the material's surface energy, leading to a reduction in fracture stress. Consequently, fractures can occur at stress levels below the material's acceptable strength threshold [32].

Kappes et al. [76] investigated HE in magnesium and magnesium alloys, noting that the primary limitation of the HEDE mechanism is the challenge of accurately measuring the cohesive forces of interatomic interactions. This difficulty may hinder a comprehensive understanding of the HE phenomenon. Nonetheless, Dwivedi et al. [32] reported that the HEDE model is one of the simplest theoretical models that can be used to characterize the HE phenomenon.

#### **HELP Model**

The HELP model has been widely accepted as the theoretical framework for characterizing the HE phenomenon [58]. The model is based on the principle that hydrogen atoms facilitate dislocation motion, which results in dislocation coalescence (buildup). Concurrently, the dislocation movement enhances hydrogen transport and increases hydrogen concentration at these dislocation buildups. As a result, localized plastic strain can occur, leading to brittle fractures. In steels, this can manifest as a transformation from ductile fracture modes to transgranular, quasi-cleavage, and intergranular fracture modes [77,78]. Pradhan et al. [58] also revealed that hydrogen atoms tend to accumulate near the crack tip, leading to a reduction in resistance to dislocation movement. As a result, the dislocation motion increases at the crack tip and influences plastic deformation within the metal lattice. The deformation can be further influenced by factors such as hydrogen clustering, microstructure, and stress intensity within the material [42,67].

#### AIDE Model

The AIDE model is employed to explain the HE phenomenon in scenarios where hydrogen atoms are adsorbed near a crack tip. In this context, the model can simultaneously account for the HEDE and HELP theoretical models. The solute hydrogen atoms located near the crack tip induce dislocation motion, which facilitates crack growth through slip and leads to microvoid formation, as described by the HELP model [58,73,76,79,80]. Subsequently, further adsorption of hydrogen at the crack tip weakens the interatomic bonds and cohesive strength of materials, as explained by the HEDE model. Table 3 outlines the general key features, strengths, and limitations of the theoretical models discussed to aid the interested reader.

Table 3. Summary of key features, strengths, and limitations of theoretical models of HE.

Model	Key Features	Strengths	Limitations
НРТ	Hydrogen atoms accumulate at defect sites, forming molecular hydrogen; which leads to increased local pressure and potential cracking.	Provides a clear mechanism for hydrogen-induced cracking (HIC) in non-austenitic steels.	Limited to non-austenitic steels; less applicable to other metal classes; questionable accuracy in general HE characterization.
HESIV	Hydrogen increases vacancy density, causing clusters that limit dislocation mobility and lead to premature fracture.	Highlights the role of vacancies in HE; explains premature fractures under strain.	Focuses on vacancy behavior, which might not capture all aspects of HE, particularly in different metal types.
HEDE	Hydrogen reduces interatomic strength, leading to intergranular fractures.	Provides insight into hydrogen-induced intergranular fracture and interface decohesion; Simple to apply.	Difficulty in measuring cohesive forces; may oversimplify the HE phenomenon.
HELP	Hydrogen facilitates dislocation motion; dislocation buildup at the crack tip leads to brittle fractures.	Widely accepted model; explains hydrogen-induced plastic deformation and brittle fracture.	Highly dependent on microstructure and stress intensity; limited by hydrogen clustering assumptions.
AIDE	Hydrogen adsorption weakens interatomic bonds near crack tips; combines elements of HEDE and HELP.	Integrates aspects of both decohesion and dislocation-based models, providing a more comprehensive view.	Complex mechanism; it may require more experimental validation to fully capture its applicability.

#### Potential Gaps in Theoretical Modeling of HE

Djukic et al. [21,61] investigated hydrogen damage in plain carbon steels and observed that the simultaneous action of both HEDE and HELP mechanisms was responsible for the decline in the ductility of steels. In this context, it is possible for different HE mechanisms to coexist and act synergistically within materials. However, research to investigate such

coexistence is still obscure. Also, identifying the dominant mechanism influencing the HE phenomenon has been a challenging area of research. Nonetheless, Djukic et al. [61] recently proposed the HEDE+HELP model. This model explains that when hydrogen atoms, transported by dislocations through the HELP mechanism, reach a critical concentration at dislocation coalescence sites caused by barriers such as carbides and inclusions, the HEDE mechanism is initiated. This combined effect ultimately leads to an early fracture of the material.

Meanwhile, there is still an ongoing debate regarding the accurate modeling of the micromechanisms that influence the HE phenomenon. In this sense, several other theoretical models are continually being developed for specific materials to account for the precise mechanisms that influence HE. These models were not captured in the present study. Nonetheless, a more comprehensive discussion has been provided elsewhere [26,58,74] for the interested reader. Advancing the theoretical understanding of these mechanisms is crucial for informing precise industrial decisions and developing accurate computational predictive models [21,61].

# 2.2. HTHA under Higher-Temperature H<sub>2</sub> Conditions

There are notable similarities between HE and HTHA, such as the permeation of hydrogen atoms through susceptible materials such as steel, carbon steel, and low-alloy steel. Both hydrogen damages also result in intergranular cracking, a decrease in material ductility, and premature metal failure [81]. This presents a common misconception where some researchers characterize HE as HTHA, particularly under elevated temperature conditions. The primary distinction between HE and HTHA lies in the temperature range in which each phenomenon predominantly occurs. HE is most prevalent at temperatures ranging from ambient to  $\sim$ 149 °C, whereas HTHA dominates within the temperature range of 204 °C to  $\sim$ 800 °C [82–84].

Additionally, the materials susceptible to each mechanism differ significantly. HE can affect high-strength nickel-based alloys, carbon steels, and specific stainless steels, as formerly captured [44,62,75]. In contrast, HTHA mainly affects carbon steels and low-alloy steels [82]. It is crucial to highlight these significant differences in hydrogen-induced damages during material testing, as they can inform the design and tailorability of materials and hydrogen-specific critical boiler components. This insight would also aid in accurately informing appropriate mitigation measures for specific critical components in different operational contexts. An elaborate discussion of the significance of appropriate mitigation measures for tackling hydrogen-induced damages in various operational contexts is presented in Section 3.

HTHA refers to the irreversible degradation of the mechanical properties of carbon steel and low-alloy steels when exposed to H<sub>2</sub> at elevated temperatures [35,85–87]. It is also important to note that while HE can occur during the manufacturing of the material and develop during the service of the material, HTHA occurs and develops only when the material is in service under high-temperature conditions [88]. HTHA has been noted to typically affect boiler tubes and pressure vessels [89].

Essentially, HTHA is the hydrogen damage induced by the reaction or combination of dissolved hydrogen atoms with themselves, impurities, or metal atoms. At elevated temperatures and pressures, atomic hydrogen has the ability to diffuse through steel-based alloys and undergo internal reactions with specific types of solutes (elements and compounds) [35]. One of the most prevalent reactions in steel involves the reaction between hydrogen and iron carbide (Fe<sub>3</sub>C), resulting in the formation of CH<sub>4</sub> [33]. This reaction is shown in Equation (1).

$$Fe_3C + 4H \rightarrow CH_4 + 3Fe \tag{1}$$

Since CH<sub>4</sub> molecules are too large to diffuse out of the steel, they lead to a substantial increase in pressure. This pressure buildup creates cavities or voids, commonly known as CH<sub>4</sub> bubbles, at locations such as grain boundaries or other areas with high interfacial energy, such as inclusion surfaces [90]. The formation and accumulation of CH<sub>4</sub> within the

steel matrix, grain boundaries, and cracks ultimately result in surface decarburization and internal decarburization (fissuring) [35,91,92]. Surface decarburization (or simply decarburization) occurs under a combination of relatively low  $H_2$  pressure and high temperature. The increased temperatures facilitate the diffusion of carbon to the surface, where it forms gases such as  $CH_4$  and  $CO_2$ . On the other hand, fissuring occurs under the combination of relatively high  $H_2$  pressure and low temperature, where atomic hydrogen infiltrates the steel and interacts with carbon in solution. Consequently, the  $CH_4$  produced becomes trapped internally, leading to the formation of micro-fissures along grain boundaries, which eventually result in cracking. [93,94]. Figure 5 shows the manifestation of both decarburization and fissures as a result of HTHA.

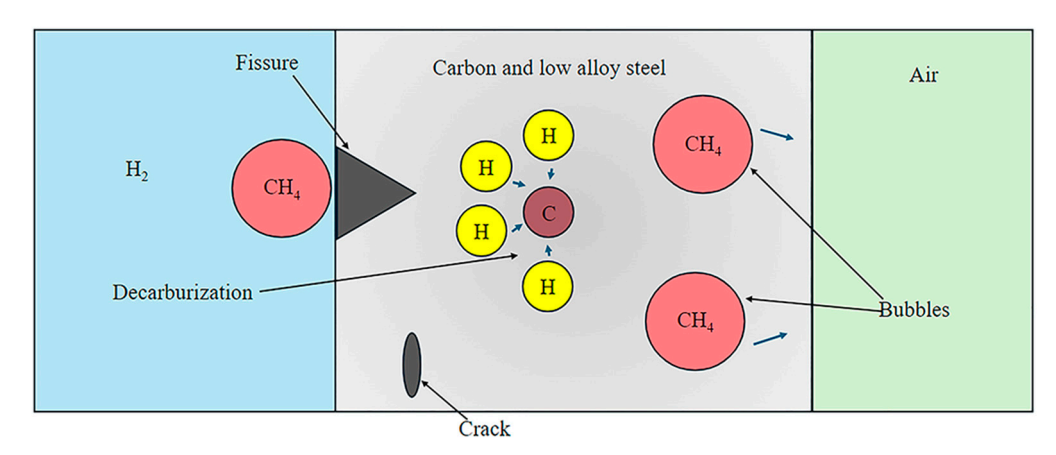


**Figure 5.** Schematic representation of the occurrence of HTHA manifested as decarburization or fissure [94] (Redrawn from the original image).

Based on the above discussion on the manifestation of HTHA damage, HTHA can, to some extent, be characterized as hydrogen reaction embrittlement (HRE). This is because both mechanisms involve the internal reaction of diffused hydrogen with elements or compounds at elevated conditions. However, Lee and Woods [33] noted that HRE could also occur at relatively low temperatures (typical temperatures for HE occurrence) and may involve the reaction of hydrogen atoms with the metal matrix itself to form metallic hydride compounds. In this sense, in addition to iron or steel-based alloys, HRE can manifest in materials such as titanium and zirconium [33].

#### 2.2.1. Factors Influencing HTHA Damages

Temperature, pressure, exposure time, stress, microstructural composition, and the environment are common factors that can influence a material's susceptibility to HTHA [35].

# Temperature

HTHA is highly sensitive to temperature variations, as the severity and rate of damage greatly increase as temperatures rise [92]. For instance, Fletcher and Elsea [95] demonstrated that a temperature increase of 25 °C could transform the condition of a material from minimal to severe HTHA. It is also important to mention that the temperature range of any system to initiate HTHA is approximately between 200 and 800 °C [33,82–84,90,92].

#### Pressure

Compared to temperature, HTHA is less sensitive to pressure variations. However, when the pressure increases, the rate and severity of HTHA damage can be significantly accelerated [35]. For instance, the rupture life of a material under  $H_2$  conditions can decrease by approximately fourfold when the  $H_2$  pressure doubles [96]. Nevertheless, there is a longstanding debate among researchers regarding the minimum  $H_2$  pressure required for HTHA initiation in carbon steels [84,92,97–100].

#### **Exposure Time**

The temperature and pressure thresholds for materials susceptible to HTHA can decrease significantly with prolonged exposure to  $H_2$  [35,101]. Nelson's [97] incubator period curves for carbon steels and Cr-0.5Mo steel have demonstrated a decrease in temperature and pressure limits with increasing exposure time [35]. Although these curves were used to assess the potential for HTHA damage under varying operating conditions, they did not adequately account for all materials and operational scenarios. Notably, Cr-Mo steel and certain material conditions, such as welded but not post-weld heat-treated (PWHT'ed) carbon steel, were initially excluded. Consequently, emerging research has focused on developing precise mechanistic models for HTHA evolution, with the goal of establishing robust time-dependent curves that can be applied to a wide range of steel types and operational conditions [102]. These curves can provide a more rapid and accurate assessment of safe operating parameters, better predicting failure times under specific pressure and temperature conditions [35].

#### Stress

Stress may not play a significant role in influencing HTHA damage in materials, as this factor has not been accounted for in models and curves [35]. However, Woods and Scott [103] investigated the effect of  $H_2$  exposure and applied stresses on 2 1/4 Cr-1 Mo steel (bainitic), which is widely used in high-temperature pressure vessels. In their study, they subjected steel to increasing pressures and temperatures and observed that the temperature threshold for HTHA reduced significantly at high applied stresses. Sakai and Asami [104] similarly observed that applying a stress of 150 MPa (21.8 ksi) to 2.25 Cr-1 Mo steel at 454 °C had an effect comparable to increasing the  $H_2$  pressure by ~5 MPa. The increased applied stress lowered the critical temperature limits of the steel for HTHA occurrence by ~28 °C and ~14 °C at  $H_2$  pressures of 10 and 20 MPa, respectively. Allevato [105] also noted that stresses induced by thermal gradients, commonly encountered during equipment cool-down or start-up procedures, can induce HTHA. This can even occur in equipment that operates within safe operating regimes defined by Nelson curves. Consequently, the high frequency of thermal gradient incidents, such as unplanned shutdowns followed by start-ups, can significantly contribute to the development of HTHA in materials [105].

#### **Material Composition**

The susceptibility of a material to HTHA is highly influenced by its microstructural content and type. In particular, steel such as HTHA is highly dependent on the carbon content, the solubility limit of the carbon in the metal matrix, and the stability of the carbide-rich areas under elevated temperatures [35,101,106]. In this context, carbon steels and Cr-Mo steels have been regarded as being highly susceptible to HTHA. This is because the carbon content in their cementite carbide areas is not thermally stable at elevated temperature conditions and dissolves rapidly upon reaction with atomic hydrogen [35]. For instance, Chiba [106] investigated the impact of carbon content on hydrogen attack in steels and found that increasing the carbon content in 2.25Cr-1Mo steels from 0.05% to 0.17% led to a linear reduction in the time required for HTHA to occur. However, Yokogawa et al. [107] reported that even a small percentage of carbon (0.011%) dissolved in ferrite-induced HTHA in single-phase steels exposed to a temperature of 500 °C and a H<sub>2</sub> pressure of 9.9 MPa. This suggests that steels with extremely low carbon content can also be susceptible to HTHA.

#### 3. General Mitigation Measures for Hydrogen-Induced Damages

Generally, material control measures for mitigating hydrogen-induced damage include but are not limited to: (1) maintaining operating parameters within established safe limits, such as those specified by Nelson curves, to regulate temperature and pressure conditions; (2) employing appropriate thermo-mechanical treatments to enhance material properties and resistance to hydrogen damage; (3) optimizing alloy compositions to improve their

resistance to specific hydrogen damages; (4) the use of liners or surface coatings that can significantly reduce hydrogen permeation or act as insulators to reduce metal surface temperatures; and (5) the appropriate selection of materials [33].

### 3.1. Mitigation Measures to Improve the HE Resistance of Materials

Conventional measures for controlling the manifestation and severity of HE in materials include, but are not limited to (1) the use of appropriate thermomechanical treatments; (2) the use of surface barriers and coatings; (3) the addition of inhibitors to reduce H<sub>2</sub> purity; (4) ensuring proper weld procedures and post-heat treatments; (5) the selection of proper operating temperatures and pressures; and (6) the proper selection of materials.

The selection of thermomechanical treatment can have profound effects on the severity of HE in materials. These effects are often influenced by the evolution of grain structures and phases due to processes such as annealing, solution, and aging heat treatments. The formation of these microstructures and precipitates can either degrade or enhance the HE resistance of a material. For instance, annealed heat-treated steel-based materials with low tensile strengths exhibit better HE resistance than high-strength alloys. Aging heat treatments have also been noted for drastically affecting HE behaviors in iron-based superalloys. This is because aging treatment increases the yield strength and ultimate tensile strength of materials, making them less ductile and highly susceptible to HE. For example, solution treatment of A-286, JBK-75, and Incoloy 903 with aging can drastically decline their HE resistance [33]. On the other hand, solution treatment without aging has been noted to enhance their HE resistance capabilities. Cold-work heat treatment of metallic alloys such as Monel-400 also exhibits lower HE resistance capability compared to annealed Monel-400 [33,35].

The use of gaseous inhibitors can also decrease the severity of HE in some steel-based materials. The addition of gases, such as nitrous oxide ( $N_2O$ ), oxygen ( $O_2$ ), and carbon monoxide (CO), to  $H_2$  has been experimentally shown to inhibit embrittlement. For example, the addition of  $O_2$  to  $H_2$  at a pressure of 7 MPa eliminated the HE effects on the fatigue crack growth of X42 pipeline steel. Similar results have also been demonstrated for gaseous inhibitors such as CO in  $H_2$ . The use of liquid inhibitors such as nitrites, phosphates, chromates, and organic amines can also reduce HE in aqueous, acidic environments [33]. However, to ensure high resistance to HE, it is essential to use the appropriate type and amount of inhibitors when mixing with  $H_2$ . Therefore, it is crucial to thoroughly investigate the efficacy of these inhibitors in preventing HE before their application.

It has also been noted that applying a slow cooling rate to materials exposed to thermal cycling conditions at high temperatures can enhance their HE resistance. However, the rapid cooling of industrial components undergoing thermal cycling can decrease their resistance to HE, even without externally applied stress. This phenomenon occurs because materials exhibit higher hydrogen solubility at elevated temperatures. Hence, as the temperature is rapidly reduced, the material can become supersaturated with hydrogen, thereby increasing the risk of HE [33,105].

As mentioned previously, HE can occur during fabrication, particularly during welding. To mitigate HE induced by welding, it is crucial to employ appropriate measures, such as (1) the use of an inert shielding gas to minimize hydrogen uptake from humidity and air; (2) utilizing dry welding electrodes; and (3) ensuring thorough cleaning and degreasing of welded joints [33]. For some steel-based materials, such as carbon-manganese steels, appropriate post-weld heat treatment (PWHT) would be required to further improve the HE resistance of the material [33,35].

During industrial operations, the selection of appropriate operating conditions is also critical for preventing the manifestation and severity of HE in materials. For instance, for most traditional steel-based materials, HE is severe under ambient temperature conditions. Hence, the selection of a higher or lower operating temperature range for specific material components can reduce HE. Nevertheless, some superalloys, such as nickel-based single-crystal PWA 1480E, can exhibit high HE resistance at high temperatures [33]. This is

because of the enhanced hydrogen mobility and reduction in hydrogen trapping sites within their metal lattice. Meanwhile, it is essential to consider the potential occurrence of HTHA in some steel-based materials at elevated temperatures. Therefore, conducting HE investigations at the intended operating temperatures is crucial for validating the manifestation of specific hydrogen-induced damages.

Increasing  $H_2$  pressure can also result in severe HE effects in materials. At constant operating temperature, an increase in  $H_2$  pressure will increase the amount of atomic hydrogen available per unit volume, thereby enhancing the localized HE effects at dislocation buildups (crack tips). Hence, at constant temperature conditions, by reducing the  $H_2$  pressures, susceptible materials can become less susceptible to HE.

A more comprehensive discussion of mitigation measures for controlling HE in materials can be found elsewhere [9,26,33,35].

# 3.2. Mitigation Measures to Improve the HTHA Resistance of Materials

Numerous studies have investigated the use of alloying elements to enhance the HTHA resistance of materials. These alloying elements are strong carbide formers and can significantly improve the thermal stability of carbide regions [101,108,109]. For instance, Raoff et al. [108] investigated hydrogen attack in 3Cr-1.5Mo steels at high temperatures and reported that by increasing the chromium content in the steels, carbides transitioned to more stable forms, such as  $M_{23}C_7$  (M: metal). However, other studies have also investigated the effect of the reduction of some alloying elements in steels [110–114]. For instance, Imanaka et al. [111] investigated the hydrogen attack in 2.25Cr-1Mo steels and found that reducing the silicon content to 0.15 wt.% and introducing vanadium up to 0.15 wt.% significantly improved the HTHA resistance of the steel. The enhanced HTHA resistance of the steel was attributed to the improved carbide stability [113]. Moreover, Imanaka et al. [114] noted that reducing elements such as sulfur and nitrogen could significantly improve the HTHA resistance of Cr-Mo steel.

The temperature and duration employed for the tempering treatment of certain steel alloys can also enhance carbide stability [35]. For example, Tiejian et al. [115] reported that increasing the tempering temperature of 1.25Cr-0.5Mo steel from 520 °C to 710 °C led to the transformation of  $M_3C$  precipitates into a more stable  $M_{23}C_6$  form with high HTHA resistance. However, Tiejian noted that tempering at 610 °C for 30 min decreased the HTHA resistance of 1.25Cr-0.5Mo steel. Thus, a tempering duration of 30 min may be insufficient to stabilize the carbide regions properly. In this context, other studies have reported that the PWHT of Cr-Mo steels at high tempering temperatures of 690 °C for an extended duration of 16 h is sufficient for enhancing the HTHA resistance [116–118].

Spheroidizing heat treatment has also been noted to improve the HTHA resistance of quenched and tempered carbon steels. This treatment enhances HTHA resistance by coarsening carbide regions and reducing the carbon content in the solution [119,120]. Generally, heat treatment can also be used to recover carbon steels affected by HTHA by repairing hydrogen-induced fissures [35]. For instance, Dong et al. [121] reported that fissures measuring 10 microns ( $\mu$ m) or smaller were completely eliminated after subjecting carbon steels to cyclical heating. The heating was conducted between room temperature and 1000 °C for five cycles over a period of 10 h. However, heat treatment of steels at critical temperatures above 720 °C can drastically alter their microstructure due to austenization and grain enlargement. This can compromise their HTHA resistance and mechanical properties [35].

A comprehensive discussion of measures to improve the HTHA resistance of materials can be found in Poorhaydari's review [35] for the interested reader.

# 3.3. The Importance of Controlling HE and HTHA under Different Operational Contexts

As previously established, damage from HE may occur during material fabrication and also while the material is in service in the lower-temperature regions of the boiler system [89]. Conversely, damage induced by HTHA manifests only during the service of

the material in relatively high-temperature regions of the boiler system. These damage phenomena can manifest individually or collectively in specific critical components. Therefore, mitigation measures, such as material selection for critical boiler components, must be precise and specific.

From this perspective, when exploring mitigation measures, it is crucial to consider the specific operational environments of the critical components and the potential hydrogeninduced damage mechanisms (HE or HTHA) that may affect them in their respective applications. In fact, Shiro et al. [9] reported that critical components exposed to HENGs (with high H<sub>2</sub> percentages) can experience varying temperatures due to changes in combustion properties, including heat exchange mechanisms, flame temperature, and flame shape [30]. Additionally, they noted that the geometric and material characteristics of a component can have a significant effect on the combustion conditions (mainly varying temperature levels). In this context, material selection criteria for critical components such as burners, boiler tubes, heat exchanger tubes, pressure vessels, valves, flanges, pipelines, hoses, storage tanks, and fasteners may vary significantly. For instance, boiler evaporator tubes located in the high-temperature regions of the boiler system are particularly vulnerable to HTHA damage [21]. Conversely, fasteners, such as bolts, which are often made of high-strength steel [26,39], are more susceptible to HE. Consequently, for each case, it is crucial to conduct specific and rigorous material selection studies and safety analyses to mitigate the distinct damage mechanisms accordingly.

Marchi et al. [122] further corroborated this logic, emphasizing the importance of a twostep process during material selection and qualification for  $H_2$ -service conditions. The two steps include (1) hydrogen compatibility (material evaluation); and (2) hydrogen suitability (component evaluation). Hydrogen compatibility tests typically involve the investigation of material properties and performance in  $H_2$  environments. These compatibility tests must be followed by hydrogen suitability tests. These tests involve further detailed engineering analysis to assess the appropriateness of a compatible material in specific applications or an intended service condition [122].

#### 4. Material Selection of Hydrogen-Compatible Materials

4.1. Technical Databases, Standards, and Charts for Selecting Hydrogen-Compatible Materials

Several organizations, such as the National Aeronautics and Space Administration (NASA), Sandia National Laboratories, the American Society of Mechanical Engineers (ASME), and the American Petroleum Institute (API), have developed hydrogen-specific material databases, standards, and charts. These resources are readily available to assist in the selection of hydrogen-compatible materials and the design of hydrogen-specific components, including piping, pipelines, valves, flanges, fittings, storage tanks, and boiler vessels [33,123–129].

For example, the ASME Boiler and Pressure Vessel Code (BPVC) VIII.3, Article KD-10 outlines specific requirements for designing pressure vessels used for high-pressure hydrogen transport and storage [127]. ASME B31.12, a recent addition to the ASME code for pressure piping, also provides prescriptive design codes and standards for hydrogen-specific pipelines [125]. The American Petroleum Institute Recommended Practice (API RP) 941 [124] provides a comprehensive discussion on hydrogen-compatible steels designed for elevated temperature and pressure applications. It includes revised Nelson curves, which are essential for selecting materials for new equipment and determining the operating limits of steels for elevated H<sub>2</sub> service to mitigate HTHA [123,124]. Additionally, the "Technical Reference for Hydrogen Compatibility of Materials" developed by Sandia National Laboratories and the "Hydrogen Embrittlement" document reported by NASA provide laboratory-scale mechanical testing data for various materials under different H<sub>2</sub> conditions [33,129].

#### 4.2. General Material Selection of Hydrogen-Compatible Materials

Metallic materials, including austenitic stainless steel, aluminum alloys, copper, and copper alloys, have been commonly explored as feasible materials for  $H_2$ -service conditions to withstand HE [9,130]. For example, austenitic stainless steels with more than 7% nickel content (such as 304, 304L, 308, 316, 321, and 347 stainless steels) have been regarded as suitable for elevated  $H_2$  applications [131]. Superalloys such as JBK-75 stainless steel, A286 stainless steel, A216 stainless steel, A310 stainless steel, A286 stainless steel, nitronic 10 stainless steel, and 18-3-Mn stainless steel have also exhibited remarkable HE-resistant capabilities under high  $H_2$  pressure conditions [33]. In particular, some nickel-based superalloys have been recognized for their low susceptibility to HE under high-pressure, high-temperature  $H_2$  conditions. For example, single-crystal PWA 1480E superalloys exhibited remarkable HE resistance when exposed to high  $H_2$  pressure (34.5 MPa) and high temperature (870 °C) [33]. Similarly, nickel-based superalloys such as Inconel 625 and Hastelloy X exhibited a high resistance to HE when subjected to an  $H_2$  pressure of 34.5 MPa and a high temperature of 678 °C [129].

The addition of alloying elements such as chromium and molybdenum to carbon and low-alloy steels is also beneficial for preventing HTHA [132]. Thus, under elevated H<sub>2</sub> conditions, alloy steels such as 5Cr-0.5Mo or 9Cr-1Mo have been noted as suitable steel candidates for withstanding HTHA [33]. Cr-Mo steels with higher chromium contents generally exhibit high HTHA resistance because of their ability to form more stable carbides [108]. High-strength micro-alloyed steels, such as those containing 0.02–0.14% niobium, can also exhibit greater resistance to HTHA when compared to Cr-0.5Mo steel alloys. This is because of their ability to form stable MC-type carbides [133]. A detailed discussion of material selection studies for HTHA can be found in Poorhayadi's review [35].

Machi and Somerday [129] have developed a comprehensive database to assist in selecting materials compatible with H<sub>2</sub> under various conditions. Their technical references reported the literature on mechanical testing data used to assess the susceptibility of structural materials to HE. Similarly, Lee and Woods [33] have reviewed studies over the past five decades on the susceptibility of metallic materials to hydrogen-induced damage. Although the present study refrained from comprehensively discussing these existing databases, a wealth of information is readily available for interested readers in the "Hydrogen Embrittlement" and "Technical Reference for Hydrogen Compatibility of Materials" documents provided in the references [33,129]. Although these reviews may offer a thorough analysis of hydrogen-compatible materials, they lack detailed information on rigorous fracture mechanics tests, such as fatigue and creep failure tests, for the majority of the materials examined. Moreover, most of the materials discussed in their study were investigated under high pressure and constant ambient temperature conditions. Consequently, the existing technical databases may not provide definitive recommendations for materials suitable for use in elevated H<sub>2</sub> environments.

However, currently, aside from the Nelson curves, there is limited comprehensive data available for material selection under high-pressure, high-temperature  $H_2$  conditions. Therefore, the highlighted material selection databases should be used primarily for initial qualitative assessments of material susceptibility to hydrogen-induced damage. Following this screening phase, conducting more rigorous fracture-mechanics analyses is advisable to ensure material suitability for specific applications.

# The Emergence of High-Entropy Alloys

High-entropy alloys (HEAs), an emerging concept of metallic alloys based on multiprincipal alloy systems, have gained significant attention in the hydrogen economy, particularly for hydrogen storage applications [134–136]. Unlike traditional alloys, which display complex intermetallic phases with one or two principal elements, HEAs can consist of five or more principal elements. These elements can be present in ratios ranging from 5 to 35 at.%, showcasing simple solid solution phases such as body-centered cubic (BCC), face-centered cubic (FCC), and hexagonal close-packed (HCP) [134]. HEAs have been noted

to exhibit outstanding physicochemical properties, including high ductility, high strength (at elevated temperatures), and high resistance to wear, oxidation, and corrosion [137–139].

Although HEAs development research for hydrogen is in its nascent stages, HEAs have been noted to have shown promising capabilities for hydrogen storage [134]. For example, Shahi et al. [134] highlighted the four core effects of HEAs development that influence their enhanced capabilities in remarkable hydrogen storage applications. These effects include the high-entropy effect, sluggish-diffusion effect, severe-lattice-distortion effect, and cocktail effects. The high-entropy effect of HEAs provides an increased number of void spaces for hydrogen atoms by the formation of BCC and FCC solid solution phases. The sluggish-diffusion effect also enhances the hydrogen absorption and desorption kinetics in HEAs by the formation of nanograins. The severe-lattice-distortion effect also improves accommodation in HEAs by providing more interstitial sites for hydrogen atoms. Finally, the cocktail effects allow tailoring of the physical and chemical properties of HEAs by the selection and control of specific principal alloying elements.

Moreover, Marques et al. [136] noted that HEAs with BCC structures possess excellent hydrogen storage capabilities because of their high hydrogen-to-metal ratio. This allows alloys such as refractory BCC HEAs to absorb up to 4 wt% of  $\rm H_2$ . Recent studies have also shown that BCC HEAs exhibit remarkable hydrogen storage potential because of the ability of hydrogen atoms to undergo crystallization in BCC structures. For instance, titanium-and vanadium-rich BCC HEAs have shown remarkable hydrogen storage capacities of 3.67 wt% and 2.75 wt%, respectively. In particular,  $\rm TiZrNbTa$ ,  $\rm TiVZrNb$ , and  $\rm TiVZrHfNb$  HEAs have been extensively studied for their potential hydrogen storage capabilities.

The advanced properties associated with the core effects of HEAs and their physicochemical characteristics make them well-suited for extensive hydrogen applications, such as industrial boiler operations. To the best of our knowledge, there is a lack of literature investigating the feasibility of HEAs for critical boiler components and their ability to withstand hydrogen-induced damage in high-pressure, high-temperature boiler operations. Thus, rigorous fracture mechanics investigations are required to verify their viability as hydrogen-compatible materials and to advance their application in industrial boiler operations.

#### 4.3. Nelson Curves for Material Selection

Nelson curves were progressively developed based on past equipment failures and are primarily based on empirical observations accumulated over several years [140]. Consequently, they may not fully account for factors such as the material microstructure, carbide stability, and underlying failure mechanisms of HTHA. However, they remain the predominant tool used by industries and researchers for material selection and design practices against HTHA [97,141–144]. These curves, constructed using data from past HTHA failures, outline safe operational regimes for materials on a temperature and hydrogen partial pressure diagram [145]. In view of this, Nelson curves have been widely used by designers to select the appropriate type of steel for specific operating conditions, such as temperature and pressure [102].

The Nelson curves are fundamentally defined by four key variables: temperature (ranging from 204 to 800 °C), hydrogen partial pressure (ranging from 0 to ~90 MPa), steel-based material of interest, and specific type of HTHA damage mechanism. For HTHA damage, the curves are distinguished to represent either surface decarburization or fissuring [93]. When a steel-based material operates below the designated limiting curves, it is considered within a safe zone with no susceptibility to surface decarburization or fissuring. Conversely, if the material operates above the curve, the region is deemed unsafe, and the material becomes prone to a specific type of HTHA failure [81].

Steel-based materials typically represented under these curves include carbon steel, 0.5 Mo steel, 1Cr-0.5Mo steel, 2Cr-0.5Mo steel, 3Cr-0.5Mo steel, and 6Cr-0.5Mo steel [93]. Nelson curves have undergone major revisions over the years since the first set of curves for carbon steel and low-alloy chromium steel (1, 2, 3, and 6% chromium) was published

by Naumann [35,101,108,109]. For example, the curves were revised to differentiate between non-PWHT'ed and PWHT'ed carbon steels. This revision was necessary because of a series of reported failures involving carbon steels without PWHT. These steels were operating in regions previously considered safe according to the Nelson curves [93,146,147]. Additionally, several reported failures of C-0.5Mo steel occurred even within the region deemed safe by Nelson curves. These failures persisted despite subsequent revisions that lowered the curve by ~30 °C [97,113,148]. Connor [81] also observed that several instances of HTHA damage were reported for C-0.5Mo carbon steels under temperature and pressure conditions of 442 °C and 3.07 MPa, respectively, despite operating within the safe zone of the Nelson curves. Consequently, these accidents and failures have led to the removal of C-0.5Mo steels from the Nelson curve diagrams. Consequently, this material is no longer considered suitable for high-temperature, high-pressure hydrogen services, and designers should exercise additional caution when considering its use [148].

Evidently, equipment failures may still occur within designated safe zones. This may be because the actual operating conditions exceeded the designated nominal values [35,146,149]. In this context, the API RP 941 industry code recommends that end users or designers establish a safety factor below the curves [124]. This precaution is recommended because operating the equipment very close to the curves may render it vulnerable to HTHA [93]. Figure 6 illustrates typical Nelson curves depicting the safe operational regimes for selected steels under high-temperature and high-pressure conditions.

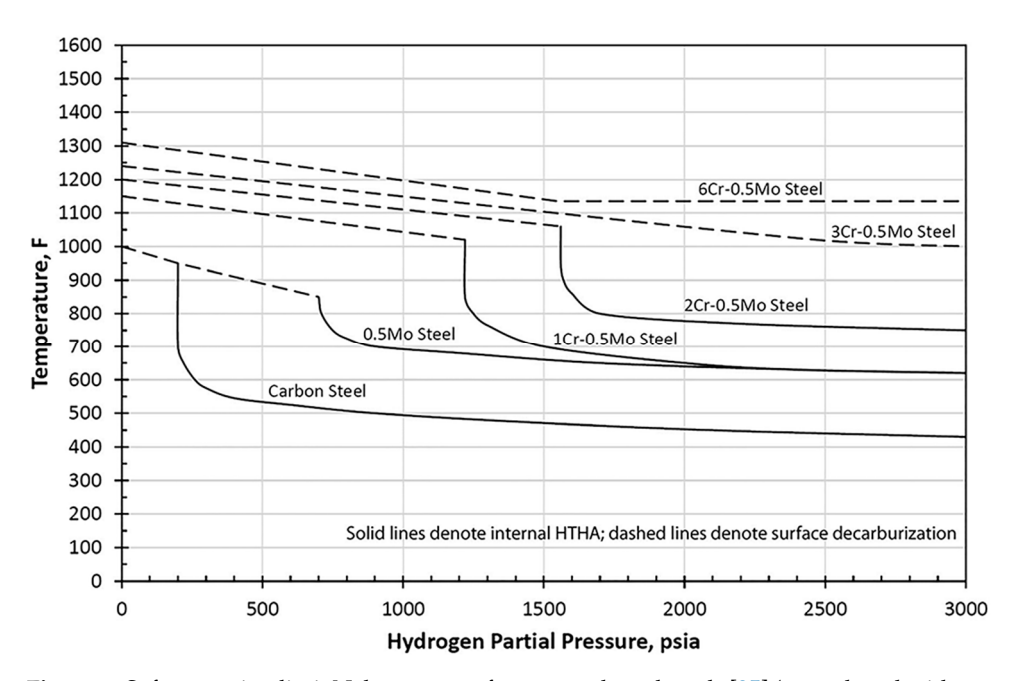


**Figure 6.** Safe operating limit Nelson curves for some selected steels [35] (reproduced with permission from Springer Nature).

# Enhancement of Nelson Curves to Mitigate HTHA Damages

Clearly, significant discrepancies exist in the application of Nelson curves when selecting appropriate steel materials for elevated H<sub>2</sub> applications. Designers have criticized the extensive use of these curves because they have found them to be too optimistic and significantly lacking because of their simplicity [150]. This is primarily due to the inability of the curves to account for additional critical variables, such as the state of working stress, carbide stability, chemical composition, grain size, type of weld, duration of operation, and operating conditions such as low-cycle fatigue [81,150,151]. In response to these limitations, several studies have attempted to improve or replace the Nelson curves. For instance, Prager curves were recently introduced as time-dependent curves to better assess safe zone regions. Unlike conventional Nelson curves, which do not account for time, Prager curves

are based on multiple curves for different time periods established using the Monte Carlo analysis approach [35].

Hattori and Aikawa [102] also introduced the hydrogen attack tendency (HAT) chart as an additional tool to incorporate specific hydrogen conditions and time exposure variables in determining the probability of HTHA damage. A HAT chart typically consists of two diagrams. The upper diagram consists of Nelson curves for carbon, C-0.5Mo, and 1Cr-0.5Mo steels. The lower diagram shows hydrogen exposure conditions determined quantitatively based on the H<sub>2</sub> pressure, temperature, and service duration. By pairing the hydrogen condition with the exposure times, the chart can predict four distinct zones where equipment may be operating. These zones are safe, unsafe for the as-welded heat-affected zone (HAZ), unsafe for PWHT HAZ, and unsafe for normalized-and-tempered base metal [152]. The original HAT charts were updated to include a carbide morphology zone. This zone considers the influence of carbide stability on the transition between zones, resulting in a more precise representation of the structural integrity of a material against HTHA. A more detailed description of HAT charts can be found elsewhere [35,102].

Dewees et al. [153] also identified significant gaps in the current application of Nelson curves for equipment life management. These gaps include failure to account for time to failure, variability in operational data, and treatment of welds. To address these gaps, they utilized existing HTHA mechanistic models to recreate Nelson curves for varying operational histories and work durations. This study was further validated using advanced non-destructive examination (NDE) models to promote judicious equipment management.

In a subsequent study, Dewees et al. [154] further enhanced time-based Nelson curves [153]. They reintroduced C-0.5Mo steel, which had previously been omitted from standard Nelson curves [81,148]. They also accounted for additional factors, such as residual weld stress and nucleation effects in the materials. The enhanced model demonstrated remarkable capabilities for correlating HTHA damage with the remaining useful life of a component. Moreover, it provides capabilities for detecting and sizing HTHA flaws to prolong equipment life spans [154].

# 4.4. Defining the HEE Index for Evaluating Material Susceptibility to Hydrogen-Induced Damages

To facilitate rapid and informed decisions in material selection studies, it is essential to develop a reliable tool to characterize the susceptibility of materials to hydrogen-induced damage. The hydrogen environmental embrittlement (HEE) index was formulated to address this requirement. This index serves as a screening and quantitative rating tool, allowing for quick experimental evaluation of the severity of environmental hydrogen damage in materials [33,155,156]. To quantitatively assess the effects of HEE on the mechanical properties of a material, changes in the HEE index, ranging from 0 to 1, were monitored under varying hydrogen conditions. Materials that are less susceptible to HE have HEE index values closer to 1 [33]. The HEE index is typically determined experimentally by comparing the mechanical property ratios of notched tensile stress (NTS), reduction in area (RA), and plastic elongation (EL) in an H<sub>2</sub> environment to those in helium or air [33].

Marchi et al. [122] later introduced a logic diagram for the rapid screening and qualification of materials for  $H_2$  applications. This diagram, as shown in Figure 7, is based on the concept of HEE indexing. Essentially, the diagram indicates that materials with a notched tensile strength ratio (RNTS) or a reduction in the area ratio (RRA) of 90% or higher are compatible with  $H_2$ . However, materials with RNTS values of at least 50% may require additional validation to confirm their suitability for specific  $H_2$  applications. These compatibility tests should involve rigorous fatigue testing in a gaseous hydrogen environment [33,122,129]. Materials such as austenitic stainless steel and aluminum alloys, which are widely accepted for hydrogen service applications, should be included in these tests to ensure confident validation of their suitability.

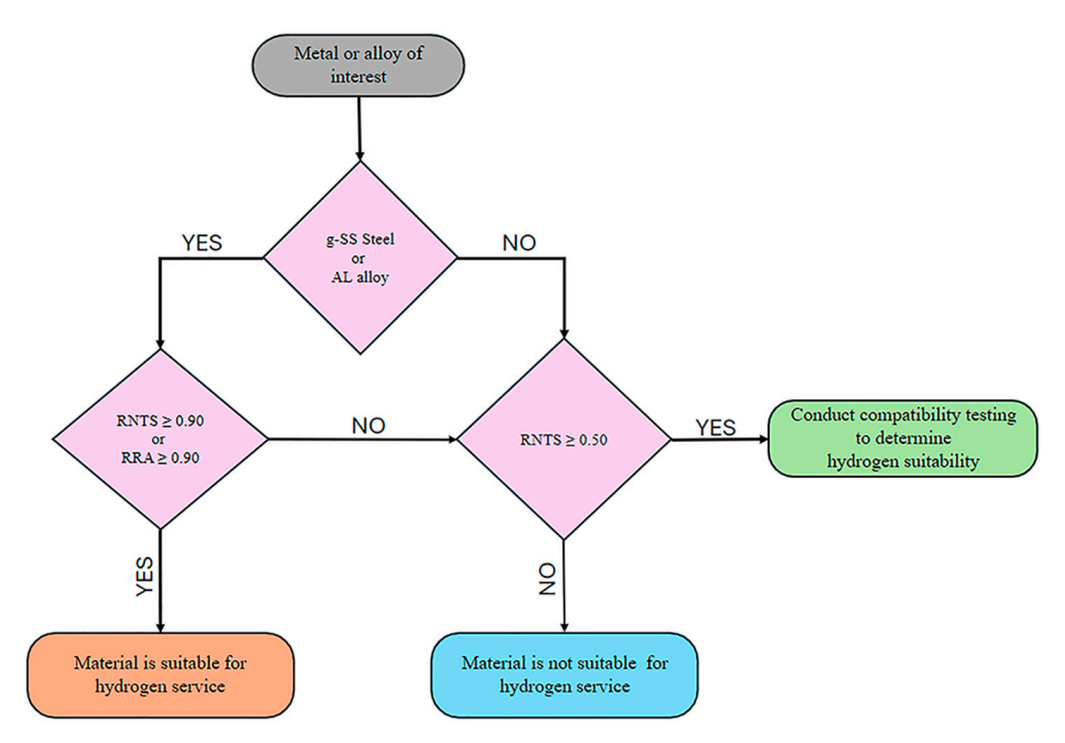


**Figure 7.** Standard logic flow diagram for qualifying hydrogen-compatible materials [122] (Redrawn from the original image).

It is important to mention that the HEE index is based on accelerated laboratory tests and serves primarily as a screening method for material selection in hydrogen-rich services. Consequently, this approach alone is insufficient for designing hydrogen-specific critical boiler components, and further comprehensive fracture mechanics analysis is necessary to ensure the suitability of material in elevated hydrogen environments.

#### 4.5. Defining a Hydrogen Safety Factor in Material Selection Studies

The material selection technical references and approaches reviewed thus far do not offer definite recommendations for feasible hydrogen-compatible materials under elevated H<sub>2</sub> conditions. This is because the compatibility of a given material with H<sub>2</sub> is highly dependent on the complex interplay of factors, including intrinsic material properties, hydrogen concentration, and environmental loading conditions, which is difficult to model [129]. Therefore, to address this complexity during material selection and the design of hydrogen-specific components, it is essential to establish a specific hydrogen safety factor that considers the mechanical properties of the material and relevant environmental conditions [157].

Fortunately, the CSA group has produced the *Compressed Hydrogen Materials Compatibility* (CHMC1) reports approved by the American National Standard Institute (ANSI) to establish such a safety factor. The documents provide standard test procedures (tensile, fracture, and fatigue) for evaluating metals under high-pressure  $H_2$  conditions with specific equipment and environmental requirements [122]. In particular, the reports outline a safety factor multiplier approach (based on fatigue testing) for qualifying materials for specific  $H_2$  service applications. This approach considers that different components may have varying design requirements and applications [9,158].

The stress-based safety factor approach involves determining a safety factor multiplier from fatigue life tests of notched specimens in both gaseous hydrogen and a reference environment, such as air. This multiplier is the largest ratio obtained from the RNTS and fatigue stress ratios of the specimens in these environments at several fatigue cycle numbers. It is then used to adjust the standard stress-based safety factor in the design of hydrogen service components by multiplying it with other safety factors. Further details on the

protocol for establishing the hydrogen safety factor through fatigue testing can be found in other sources [122,158].

Nonetheless, general experimental fatigue tests performed below the fatigue limits of materials or advanced computational fatigue tests conducted in accordance with the CHMC1 standards can serve as viable alternatives for establishing hydrogen safety factors. This can ensure the safe application of materials under elevated gaseous hydrogen conditions [33,122,129].

# 4.6. Hydrogen Permeation Barriers

It has become economically viable to investigate accelerated mitigation approaches centered on surface barrier coatings (SBCs) or thermal barrier coatings (TBCs) during material selection studies. SBCs can provide a temporary and limited solution for mitigating the effects of  $\rm H_2$  on critical boiler components. This approach is essential to avoid the need for a complex overhaul of boiler infrastructure. This is also because novel studies on hydrogen-compatible metallic alloys are still being validated and standardized [33,129]. The primary purpose of SBCs is to protect the components from harsh environmental conditions and corrosion, thereby improving the durability of the underlying substrate material [159–161]. SBCs can modify the adsorption properties of a surface to reduce the absorption rate of atomic hydrogen and subsequent hydrogen attacks [33,159–161].

Lee and Woods [33] observed that in aqueous environments, stable SBCs can be applied to metal surfaces to protect against corrosion and limit hydrogen absorption. However, in high-temperature, high-pressure  $H_2$  environments, these coatings may not be effective for long-term use. This is because  $H_2$  has a high diffusion rate, which allows atomic hydrogen to permeate most metallic materials easily. Nonetheless, extensive studies have investigated the efficacy of hydrogen permeation barriers (HPBs) designed particularly for low-alloy steels, high-strength steels, and other metallic alloys [162,163]. The efficiencies of several HPBs, mostly dielectric materials such as oxides, carbides, and nitrides, have been reported [162]. These materials were evaluated based on their hydrogen permeabilities over the temperature range of 400–600 °C [163].

Oxides have been noted as compelling candidates for HPBs because of their minimal inherent hydrogen permeability and their capacity to coat uneven geometrical shapes at elevated temperatures [162–165]. The most widely studied oxides for HPB applications are aluminum oxide or alumina ( $Al_2O_3$ ), chromium oxide ( $Cr_2O_3$ ), erbium oxide or erbia ( $Er_2O_3$ ), and silicon oxide or silica [165–168].

Al $_2O_3$  has proven to be a stable, suitable oxide for high-temperature hydrogen conditions, capable of achieving permeation reduction factor (PRF) values of ~1000 for temperatures up to 800 °C [163]. PRF is defined as the steady-state ratio of the permeation rate through the uncoated membrane to the permeation rate through the coated membrane. PRF values much greater than 1 (>>1) are usually desired to characterize viable HPBs. However, because hydrogen permeation through a coated membrane may involve the interplay of various processes, the PRF value may be insufficient to accurately characterize the permeation properties of HPBs [163]. For a 1  $\mu$ m thick Al $_2O_3$  coating, the lowest hydrogen permeability reported in the literature is  $25.9 \times 10^{-18} \, \text{mol} \cdot \text{s}^{-1} \cdot \text{m}^{-1} \cdot (\sqrt{\text{Pa}})^{-1}$  [164]. It is important to note that this was achieved using the filtered arc discharge disposition technique. However, Serra et al. [165] reported that using a commercial alumina tube for disposition, a bulk permeability value of  $9 \times 10^{-17} \, \text{mol} \cdot \text{s}^{-1} \cdot \text{m}^{-1} \cdot (\sqrt{\text{Pa}})^{-1}$  could also be achieved.

 $Cr_2O_3$  has also demonstrated high anti-permeation efficiency. These HPBs can achieve PRF values of ~1000 within an operational temperature range of 700 to 800 °C. Other studies have also highlighted the promising performance of Al-Cr-O, which is a composite mixture of  $Al_2O_3$  and  $Cr_2O_3$ . Al-Cr-O can exhibit high PRF values ranging from ~2000 to 3500 at an elevated temperature of 700 °C [169].  $Er_2O_3$  has also been recognized as a good candidate for HPBs. However, its bulk hydrogen properties are still not well established [163]. A 1  $\mu$ m layer of  $Er_2O_3$ , deposited using a filtered arc discharge technique, can achieve PRF values

of ~800–1000 at temperatures between 600 and 800 °C [167]. Silica is widely recognized for its protection against oxidation. However, its PRF values have not been easily evaluated and validated [170]. Consequently, silica has not yet been considered a viable candidate for HPB applications [168].

Nitrides such as boron nitride (BN) [171], titanium nitride (TiN) [172], and silicon nitride (SiN) [163] have also been recognized as viable candidates for HPB applications. However, some experimental evaluations have not been confidently validated [163]. Therefore, other studies have attempted to optimize and validate their performance. For instance, Tamura et al. [171] reported the improved performance of BN HPBs within a temperature range of 300–500 °C. Notably, combining TiN and AlN to form TiAlN coatings can achieve the most promising permeability values of the order of  $10^{-18}$  mol·s<sup>-1</sup>·m<sup>-1</sup>·( $\sqrt{Pa}$ )<sup>-1</sup> [95].

Carbides have not garnered significant interest in HPB applications [162]. However, permeability values of  $2.8 \times 10^{-15} \, \mathrm{mol \cdot s^{-1} \cdot m^{-1} \cdot (\sqrt{Pa})^{-1}}$  and  $1.5 \times 10^{-15} \, \mathrm{mol \cdot s^{-1} \cdot m^{-1} \cdot (\sqrt{Pa})^{-1}}$  have been reported for titanium carbides (TiC) and silicon carbides (SiC), respectively [173,174]. TiC can also be used as a bilayer in combination with other barrier coatings to reduce permeability. Promising permeability values ranging from  $3 \times 10^{-13} \, \mathrm{mol \cdot s^{-1} \cdot m^{-1} \cdot (\sqrt{Pa})^{-1}}$  to  $3.2 \times 10^{-16} \, \mathrm{mol \cdot s^{-1} \cdot m^{-1} \cdot (\sqrt{Pa})^{-1}}$  can be achievable with this design [175]. A summary of the efficiencies of dielectrics suitable for HPBs at 400 °C is presented in Table 4. Where Ds and Df represent the diameters of the substrate and HPB film, respectively, and Ps and Pf represent the permeabilities of the substrate and HPB film, respectively.

Dielectrics	PRF	D <sub>s</sub> (mm)	D <sub>f</sub> (μm)	$\begin{array}{c} P_s \\ \times 10^{-11} mol H_2 \\ \cdot s^{-1} \cdot m^{-1} \cdot (\sqrt{Pa})^{-1} \end{array}$	$\begin{array}{c} P_f \\ \times 10^{-11} mol H_2 \\ \cdot s^{-1} \cdot m^{-1} \cdot (\sqrt{Pa})^{-1} \end{array}$
$Al_2O_3$	1000	0.5	1	1.30	25.9
$Cr_2O_3$	1000	1.6	$10^{\ 1}$	0.017	$0.72^{\ 1}$
$Cr_2O_3/Al_2O$	3500	0.5	1	1.30	7.41
$Er_2O_3$	1000	0.5	1	1.30	25.9
$Er_2O_3$	1000	0.5	1.3	1.30	33.7
$SiO_2$	1	0.15	0.2	0.13	1711
BN	100	0.1	1.5	0.13	193
TiN	100	0.1	1.5	0.13	193
TiN	1100	0.35	1.7	0.13	5.7
TiN	1000	0.1	1.7	0.13	21.8
TiAlN	6800	0.35	1.7	0.13	0.92
TiAlN	20,000	0.5	5	1.30	6.5
SiN	2000	0.5	0.5	1.30	6.5
WN	38	0.5	2.3	1.30	1570
CrWN	100	0.5	4.4	1.30	1140
CrN	117	0.5	2.6	1.30	576
$Cr_2N$	286	0.5	2.2	1.30	241
ALCrN	350	0.5	4.5	1.30	333
ZrN	4600	0.5	1.4	1.30	7.9
TiC	10	0.1	1	0.27	2750
TiN+TiC	100	0.5	1 + 0.25	1.30	324

Nemanic [163] assumed Cr<sub>2</sub>O<sub>3</sub> thickness for calculations as it was not captured in the literature.

HTHA resistance cladding has also been identified as an efficient permeation-barrier solution. The liner materials used in cladding exhibit low hydrogen permeabilities, significantly reducing the amount of hydrogen that diffuses into susceptible materials [176]. For instance, metallurgically bonded austenitic stainless steel liners are highly efficient for lining carbon steel vessels because of their lower hydrogen diffusivity than ferritic steel liners [177].

Nonetheless, the efficacy of cladding liners in restricting hydrogen diffusion and mitigating hydrogen-induced attacks is questionable. For instance, Fletcher and Elsea [95]

observed that hydrogen molecules tend to accumulate at the interface between the liners and metal substrate, eventually diffusing through the liners. Consequently, this accumulation can lead to the swelling and detachment of the liner or cladding material, thereby undermining its protective capabilities. Eventually, this can facilitate the occurrence of HTHA in affected regions. Nonetheless, an effective approach to address this issue is to create small "weep holes" in the material to alleviate the buildup of hydrogen pressure at the interface [141,142].

# 4.7. Implementation of General Mitigation Measures in an Industrial Context

The effective implementation of mitigation measures in the design of hydrogen-specific engineering components is crucial, as significant and fatal hydrogen-induced damage accidents continue to occur in hydrogen-related industrial operations. For instance, one of the major fatal incidents was the 2010 fatal incident at the Tesoro Anacortes Refinery in Washington [151]. The incident was caused by HTHA in a carbon steel heat exchanger, which led to its rupture. Interestingly, this heat exchanger component operated within the safe zone limits as defined by the Nelson curves [124].

The Hydrogen Incidents and Accidents Database (version 2.0) (HIAD 2.0) also revealed that HE and HTHA were responsible for 20 of 24 recorded failures of industrial equipment [31]. These hydrogen-induced damages caused major failures in critical components, such as evaporator tubes, hydrogen tanks, high-pressure vessels, and high-pressure cylinders. HIAD 2.0 identified the following as the primary root causes of hydrogen-induced damages leading to equipment failures: (1) improper material selection; (2) lack of PWHT; (3) severe operating conditions; (4) off-design operating conditions (such as high pressure and near-room temperature, which facilitated HE occurrence); and (5) undetected hydrogen-induced fractures in the HAZ. A detailed discussion of the accident report of hydrogen-induced material failures in industrial equipment is available elsewhere [31].

Campari et al. [31] emphasized that welded regions of industrial components were highly prone to HE occurrence, as 51.1% of industrial equipment failures caused by HE were in the proximity of welded joints. The lack of PWHT at the HAZ and an extensive understanding of the susceptibility of the HAZ microstructures of the welds to HE have led to other major, undesired, and fatal industrial incidents. From this perspective, optimal preventive mitigation measures to address the occurrence of hydrogen-induced damage in industrial boiler components may include, but are not limited to (1) proper PWHT on welds and HAZs; (2) generic component replacement and precise material selection through rigorous fracture mechanics analysis; (3) precise implementation of standards and codes for material testing and component design; and (4) implementation of state-of-the-art inspection methods for the accurate and rapid detection of hydrogen-induced damage.

It is important to mention that the implementation of these mitigation measures, along with recent standards and codes such as ASME B31.12 and CHMC1 reports, has significantly improved the design of new hydrogen-specific critical components [33,122,124,129]. However, most existing industrial boiler infrastructures were designed before the introduction of these mitigation measures and hydrogen-specific standards. Hence, applying these measures to older boiler infrastructure may be ineffective, and critical components may not comply with the updated guidelines.

In this context, it is essential to conduct rigorous inspection procedures regularly to minimize the occurrence of hydrogen-induced damage to equipment. In addition to visual inspection, advanced techniques such as liquid penetrant testing (LPT), phased-array ultrasonic testing (PAUT), shear-wave ultrasonic testing (SWUT), and magnetic particle testing (MPT) have been recommended. These techniques are effective for detecting surface cracking, internal damage, microvoids, microfissures, and the depth of cracks. The implementation of these preventive inspection techniques can enable timely decision-making to prevent further material degradation and potential equipment failure. For a more detailed discussion of NDE techniques for the rapid detection of hydrogen-induced damage in industrial equipment, refer to the literature [35].

# 5. Experimental and Computational Modeling of Hydrogen-Induced Damages

#### 5.1. Experimental Investigation of Hydrogen-Induced Damages

Experimental investigations of hydrogen-induced damage usually focus on hydrogen charging, diffusible hydrogen measurements (e.g., the mercury method), thermal desorption spectroscopy (TDS) analysis, mechanical testing, corrosion testing, microstructural characterization, and chemical composition analysis. These approaches are favored because investigating the effects of hydrogen damage mechanisms in materials under natural (in-service) conditions is time-consuming and has proven to be a challenging area of research [58].

Investigations typically involve the use of hydrogen-enriched materials, either extracted from failed industrial components affected by hydrogen damage or prepared through the hydrogen charging of specimens. These materials are then analyzed to measure the hydrogen concentration levels contributing to the severity of failure. Subsequently, microstructural and fractographic analyses are conducted to examine the microstructure and fracture surfaces of the material, thereby providing insights into the active damage mechanisms responsible for failure. Finally, standard mechanical tests are conducted to correlate the mechanical performance of the material with its microstructural properties and the identified damage mechanisms [21,26,58,178–181]. In this section, we highlight the experimental investigations conducted by Djukic et al. [21], which assessed hydrogen damage in plain carbon steel. In addition, we discuss the challenges associated with the experimental investigation of hydrogen-induced damage.

# 5.1.1. Experimental Investigation of Hydrogen Damage in Plain Carbon Steels

Djukic et al. [21] investigated the active HE mechanisms responsible for hydrogen damage in plain carbon steel (St.20) evaporator tubes in industrial thermal powerplant boilers. They conducted failure and postmortem analyses on samples extracted from coal-fired boiler evaporator tubes (enriched with hydrogen) that failed after 73,000 h of operation.

The initial failure analyses utilized conventional experimental methods to identify the root causes of the boiler tube fractures. These traditional experimental methods included visual inspection, tube-wall thickness measurements, chemical composition analysis, macroscopic mechanical testing (such as hardness and tensile testing), metallographic analysis, and corrosion testing in the vicinity of the fracture. Subsequently, post-mortem analyses were conducted using a specially applied experimental concept. This specialized experimental approach was employed to investigate the active HE mechanisms contributing to the failure of St.20 steel owing to local hydrogenation of the tube metal during boiler operations. This investigation established a structure-property relationship by correlating scanning electron microscopy (SEM) micrographs of fracture surfaces from Charpy samples with macromechanical testing characteristics (impact strength values).

The failure analyses revealed that local hydrogen enrichment in the evaporator tubes induced HTHA in the vicinity of welded joints, which manifested as "window"-type fractures. The analyses also indicated that localized hydrogen enrichment caused under-deposit corrosion of the tube metal during the boiler operation. This hydrogen-induced corrosion was exacerbated by the thermal cycling experienced by the tube metal during operation. Figure 8a depicts the representation of the "window"-type fracture and the underdeposit corrosion formed on the inner surface of the tube. From Figure 8b, one can observe the formation of corrosion products on the inner surface of the tube near the "window"-type fracture. The corrosion products were characterized using energy-dispersive X-ray spectroscopy (EDS), atomic absorption spectroscopy (AAS), and Zimmermann–Reinhardt (Z–R) methods.

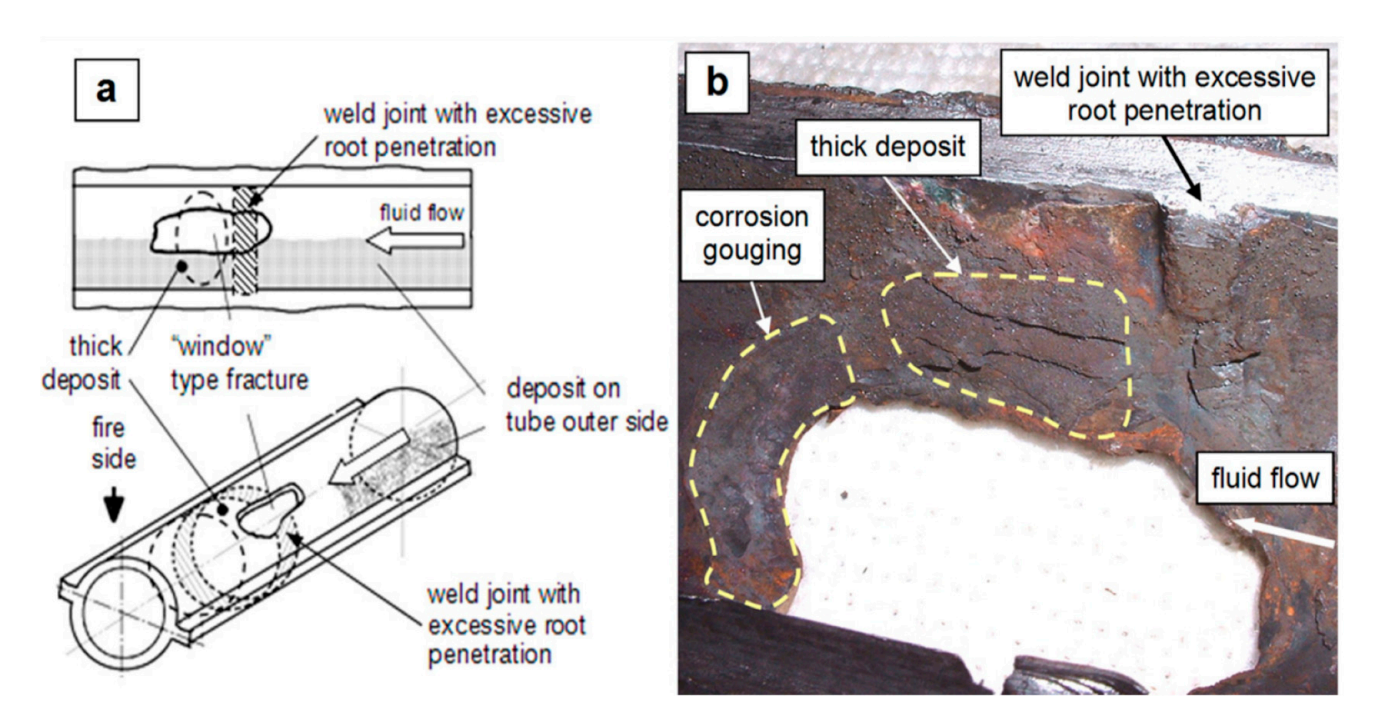


**Figure 8.** Fractured evaporator tube: (a) schematic representation of the "window" type fracture; (b) corrosion on the tube's inner surface in the vicinity of the fracture [21] (reprinted with permission from Elsevier).

Subsequent post-mortem analysis confirmed that both the HELP and HEDE mechanisms were active in the steel, with their relative dominance dependent on the local hydrogen concentration. The macrohardness of the specimens was strongly correlated with the measured hydrogen concentration levels. Specifically, macrohardness increased with higher hydrogen concentrations, regardless of the predominant embrittlement mechanism. At lower hydrogen concentrations, the HELP mechanism was predominant, leading to ductile fracture features. This also resulted in a modest increase in hardness without a substantial loss in ductility. However, as the hydrogen concentration increased, the HEDE mechanism prevailed, causing a transition from ductile to brittle fracture and a significant reduction in the impact strength.

However, the coexistence of HELP and HEDE mechanisms led to reduced ductility in the steel, although the precise critical hydrogen concentration at which this transition occurs was not determined. The experimental approaches effectively detected both HTHA and HE mechanisms and assessed their impacts on the macroscopic mechanical properties of steel. Nonetheless, further research is required to fully understand the coexistence and dominance of active HE mechanisms under varying operating conditions, which remains a challenging area of study. Djukic et al. also observed that SEM fractography analysis of fracture surfaces was insufficient to fully understand the deformation and fracture mechanisms in the hydrogen-enriched steels.

# 5.1.2. Challenges Associated with Experimental Modeling of Hydrogen-Induced Damages

Dwivedi et al. [26] reviewed the effects of hydrogen on the mechanical and microstructural properties of AHSS. They reported that experimental investigations typically involve diffusible hydrogen measurements, strength degradation tests, fractography, and microstructural analyses. Diffusible hydrogen measurements were conducted using several techniques to determine the hydrogen content in the materials that contributed to the failure. These methods include the glycerin method, vacuum hot extraction, the mercury method, and gas chromatography. Among these, the mercury method was particularly noted for its effectiveness in measuring the diffusible hydrogen content, especially when the hydrogen concentration was very low. Mechanical testing involved linearly increasing

stress tests (load control testing) and slow stress rate tests (strain control rate testing) to determine key properties, such as yield strength, ultimate tensile strength, percentage elongation, and percentage reduction in the area of damaged steels. Fractographic analysis was also conducted to examine the transition of the fracture surface from ductile to brittle features as a result of increased hydrogen content in the material. A microstructural analysis was conducted using SEM to examine the austenite and martensite microstructures that developed during mechanical degradation and fracture.

They revealed that the effect of hydrogen on specific AHSSs, such as twinning-induced plasticity (TWIP) steels, remains a subject of ongoing debate. While some studies have suggested that hydrogen does not significantly impact the mechanical and microstructural properties of these steels, others have reported notable degradation in their mechanical performance due to hydrogen exposure. However, the properties of other AHSSs, such as transformation-induced plasticity (TRIP), exposed to hydrogen conditions have been well established, as their properties are severely affected by HE. When TRIP steels undergo HE, the austenite phase transforms into the martensite phase, which releases excess hydrogen to the crack tip. The accumulation of hydrogen at the crack tip substantially reduces the ductility of the material through the HELP mechanism. Fractography analysis also confirmed that cracks were initiated in the martensite regions, which then grew toward the ferrite regions.

Nonetheless, Dwivedi et al. [26] noted that investigations into the effects of hydrogen on AHSS were typically conducted under controlled laboratory-scale testing conditions, which may not accurately reflect the complexities of the actual operating environments. Hence, the correlation between the actual operating condition results and the experimental results remains unclear. Fagnon et al. [180] also noted that the use of advanced techniques, such as TDS, to measure the hydrogen concentration in high-strength steels necessitates immediate measurement following material fracture. This requirement poses significant challenges for accurately assessing the hydrogen concentration in steel, which may fail during service.

Clearly, these experimental methods would require accurate validation under actual in-service hydrogen conditions. The impact of hydrogen-induced damage on material properties can vary significantly owing to differences in hydrogen concentration levels and the specific locations of atomic hydrogen diffusion within the materials [178,180]. Hydrogen atoms can diffuse not only to the interstitial lattice sites of the material but also to carbide-rich areas, inclusions, dislocation cores, and along the grain boundaries [26,182,183]. Consequently, if these specific changes are not adequately accounted for and monitored, accelerated laboratory assessments of hydrogen damage may lack accuracy.

Despite the extensive development of experimental setups and methodologies over the years to simulate hydrogen-induced damage in metals, these setups still fail to accurately characterize hydrogen uptake, diffusion, concentration, and defect severity [26,184–186]. These macroscale assessments might also not define and predict actual in-service conditions such as hydrostatic pressure, temperature, and local hydrogen content distribution in the material over extended periods of time [21,58]. Hence, overall, the ability to predict hydrogen content and the severity of damage based on service conditions remains limited and substandard [180].

However, computational and numerical investigations conducted at multiple scales can offer a precise assessment and mechanistic understanding of hydrogen-induced damage phenomena, as well as their true impact on the mechanical properties of materials. Although research into these advanced assessments remains limited, they have garnered significant attention from experts in the field. These approaches are crucial for advancing the current understanding of damage mechanisms as well as their impact and manifestation in materials [57].

# 5.2. Emerging Computational Models for Simulating Hydrogen-Induced Damages

Computational modeling and simulations have proven valuable in structural analysis, failure analysis, and material selection studies. They have allowed for the assessment of material performance and viability in varying operational contexts, as well as the identification of the root causes of component failures [187–189]. Given that the physical experimental assessment of hydrogen-induced damage and its impact on materials is often challenging, time-consuming, and costly, it would be more practical to rely on computational modeling. These approaches can allow for the simulation of relevant inservice boiler conditions and provide accurate predictions of the damage mechanisms in the boiler materials. Models such as density functional theory (DFT), molecular dynamic (MD) models, and continuum approaches based on finite element modeling (FEM) have been well utilized for the simulation of damage mechanisms [81,190–194]. These models have proven promising for predicting hydrogen diffusion and the intricate and extricate factors that influence hydrogen damage in steels and other susceptible materials across multiple scales [191].

For example, Chavoshi et al. [195] utilized FEM with commercial Abaqus 2019 software to evaluate the service lifetime of C-0.5Mo steel exposed to  $\rm H_2$  pressures of 4–6.48 MPa at high temperatures of 350–500 °C over a period of 80,000 h. They implemented a coupled Fick's diffusion law and a multiaxial creep ductility model to simulate the combined effects of creep and HTHA on a C-0.5Mo steel inlet nozzle in service. Their simulation results successfully predicted safe operational regimes for an in-service nozzle based on the following findings: (1) nozzle operating at temperatures and  $\rm H_2$  pressures below 300 °C and 4.0 MPa, respectively, for 100,000 h experienced no damage; (2) increasing the operating temperatures from 400 °C to 500 °C at a  $\rm H_2$  pressure of 4 MPa resulted in ~88% increase in damage depth; and (3) increasing the  $\rm H_2$  pressure to 6.48 MPa while increasing the operating temperature from 400 °C to 500 °C led to significant damage due to creep or the combined effects of creep and HTHA, which can potentially cause premature nozzle failures. Figure 9 shows the evolution of the total damage of the nozzle owing to the combined effect of creep and HTHA with increasing exposure time. This simulation was performed at a temperature of 400 °C and a  $\rm H_2$  pressure of 4.0 Mpa.

Connor [81] also utilized MD to provide an atomistic perspective on the occurrence of HTHA in susceptible materials such as those with Fe<sub>3</sub>C structures. The MD model was used to simulate atomistic-scale mechanisms that influenced the formation of HTHA, such as (1) how hydrogen atoms migrate from the surface to a cementite structure (fissuring occurrence); (2) how the hydrogen atom takes carbon out of a cementite structure; and (3) the rate of formation of CH<sub>4</sub> at different operating temperatures and void sizes. The simulation results demonstrated that the formation of CH<sub>4</sub> on a surface was considerably more difficult, requiring twice as much energy as the formation of CH<sub>4</sub> inside a void. This result corroborated Poorhaydari's [35] prior review, which identified fissuring as the primary HTHA damage mechanism observed in materials rather than surface decarburization. Fissuring, which is commonly observed in steels, often leads to catastrophic hydrogen-induced damage.

Computational models based on extended finite element modeling (XFEM), damage modeling, decohesion zone modeling, and remeshing have been extensively explored to simulate crack propagation and general mechanical damage failures in materials. However, these conventional computational models face significant limitations that can hinder their widespread application in accurately simulating hydrogen-assisted cracks and other complex crack topologies. These models typically rely on the sharp interface (discrete) approach to simulate crack evolution in materials, making it challenging to account for complex features, such as microcracks, microvoids, and branching. The sharp-interface approach assumes that cracks propagate only between two discrete elements, necessitating additional ad hoc criteria and sophisticated computational coding to account for the behavior of microcracks and branching, which may contribute to material deformation. Additionally, in these conventional computational predictive models, it is necessary to

assume the potential location of the crack formation and perform fine meshing in that region accordingly. Clearly, this approach is not ideal for simulating crack evolution, as it limits the flexibility and accuracy of the model in capturing the unstable and unpredictable nature of crack propagation.

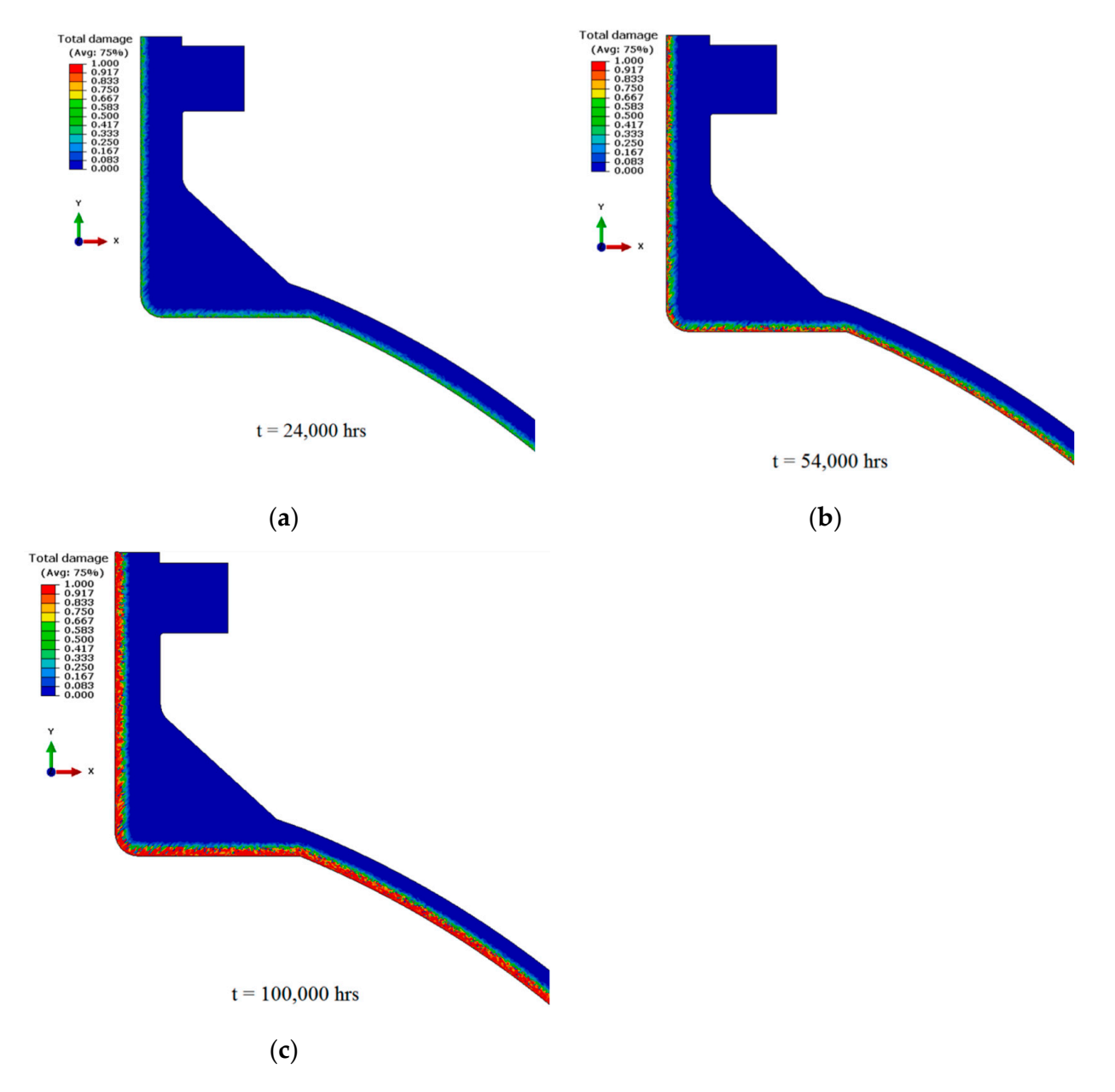


**Figure 9.** (a–c) Total damage evolution of the C-0.5Mo inlet nozzle due to creep and HTHA at a temperature of 400 °C and a H<sub>2</sub> pressure of 4.0 MPa with increasing H<sub>2</sub> exposure times [195] (reprinted with permission from Elsevier).

However, on the other hand, phase-field modeling has garnered significant attention as a powerful computational tool, providing a diffuse-interface approach for simulating complex crack topologies [196–199]. This method excels at accurately simulating phenomena such as crack branching and microcracks, thereby addressing the shortcomings of discontinuity-based methods that rely on conventional discrete FEMs [199]. It employs a variational mathematical approach by extending Griffith's formulation of crack formation [197]. This continuum-based damage mechanics model has shown great promise for modeling hydrogen-assisted fractures, showing remarkable agreement with experimental data.

For example, Martinez-Paneda et al. [197] successfully developed a robust phase-field model framework for predicting hydrogen-assisted cracking that can be adapted for a wide range of engineering conditions. In their study, the material surface and diffuse crack topology were numerically modeled in terms of the phase field and displacement variables. Similarly, the governing balanced equations regarding the bulk stored and surface energies of the material were also modeled as functions of the displacement variable and phase field parameter. Fick's diffusion law was also extended to model hydrogen diffusion into the material. Subsequently, the mechanical deformation, phase-field fracture, and hydrogen transport problems were weakly coupled and solved. The model was implemented using the Abaqus user element (UEL) and user material (UMAT) subroutines written in Fortran, which allow one to define materials, properties, loads, and elements that are not available in commercial Abaqus built-in models. The model successfully predicted unstable crack growth due to hydrogen and internal hydrogen-assisted fractures under specific conditions of increasing hydrogen concentration. These predictions showed remarkable agreement with experimental results [200–203].

Figures 10–12 present the results of their benchmark studies on a simple 2D-notched square plate subjected to uniaxial tension. The load is applied by prescribing a constant total displacement of 0.01 mm, as done in experimental uniaxial tensile testing. Considering high-carbon steel (an iron-based material typically used for boiler drums), the following material properties were chosen: Young's modulus of E = 200 GPa, Poisson's ratio of  $\nu$  = 0.3, and critical energy release rate of Gc = 27 MPa·mm. An initial hydrogen concentration (C) (in wt ppm) was prescribed and kept constant along the boundaries of the plate to mimic laboratory-scale testing.

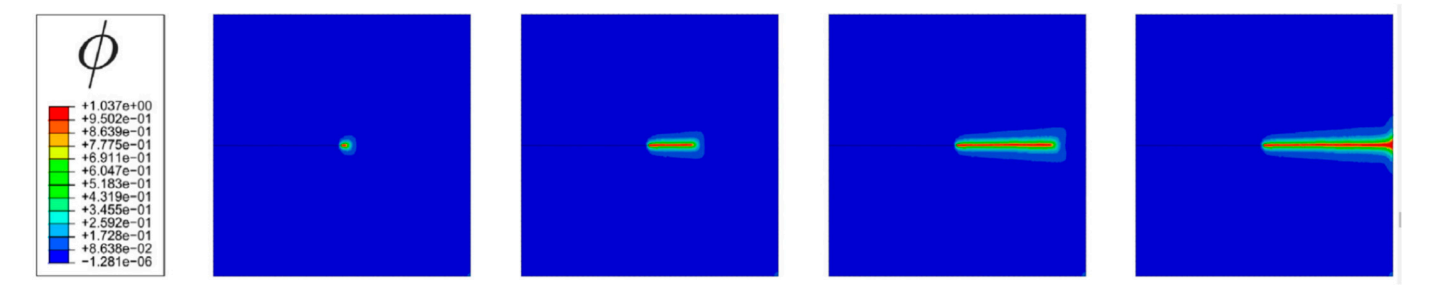


**Figure 10.** Phase field crack growth contours at varying displacements for an initial hydrogen concentration ( $C_0$ ) of 0 wt ppm of a square plate under tension [197] (reprinted with permission from Elsevier).

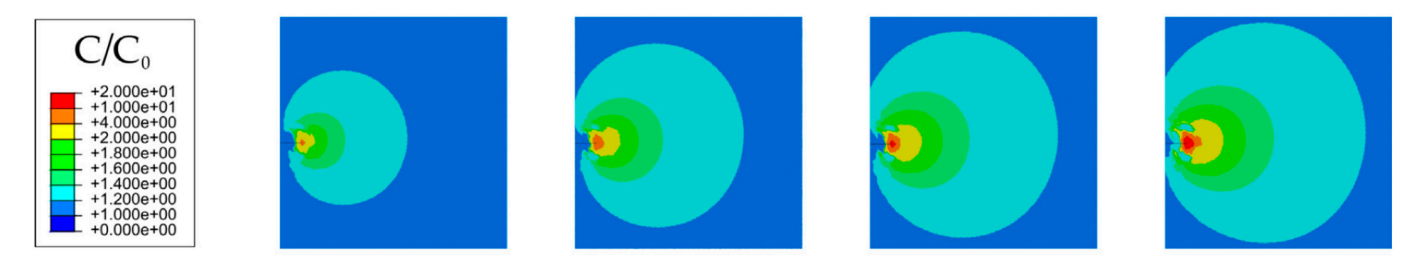


**Figure 11.** Hydrogen concentration buildup in the horizontal crack region of a square plate under tension at varying displacements for  $C_0$  of 0.5 wt ppm [197] (reprinted with permission from Elsevier).

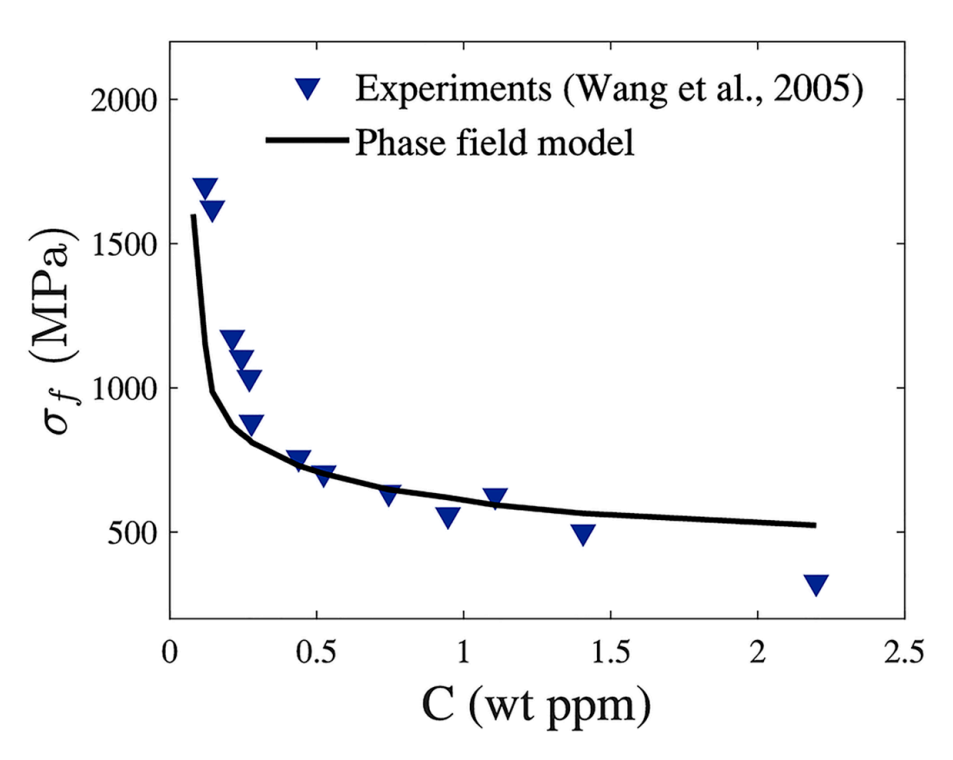


**Figure 12.** Net section strength ( $\sigma$ f) of a notched AISI 4135 steel bar under tension as a function of hydrogen concentration, showing good consistency with the prior experimental work of Wang et al. [197] (reprinted with permission from Elsevier).

Figure 10 shows the phase-field fracture evolution of the notched square plate at different load steps and displacements. The red contour regions depict a fully cracked state represented by a phase-field damage parameter ( $\phi$ ) of 1, whereas the blue contour regions depict a fully intact state with a  $\phi$  of 0. One can observe diffuse crack growth rather than sharp crack growth, as shown in the fracture process zone, because of the definition of a length scale parameter. The length scale parameter defines the smoothness of the crack surface and accounts for other microcracks and branching that may contribute to crack growth. A length scale parameter that is 10 times larger than the finite element size is usually chosen to resolve the solution at the fracture process zone by ensuring a sufficient number of elements within the process zone. Moreover, the model demonstrated mesh independence by accurately predicting the crack growth location without relying on ad hoc criteria or remeshing along the fracture process zone.

Figure 11 also shows the hydrogen concentration contours at the onset of crack growth in the fracture process zone. The red and blue contours represent the highest and lowest hydrogen concentration levels in the material, respectively. The highest hydrogen accumulation was observed at the crack tip, where the hydrostatic stresses were high. This observation is consistent with the widely accepted HELP theoretical model, which postulates that hydrogen atoms tend to accumulate near dislocation buildup (crack tip), leading to reduced resistance to dislocation movement [21,58]. To investigate the level of agreement of the phase-field model with prior experimental investigations of hydrogeninduced damage in steels, Martinez-Paneda et al. mimicked laboratory-scale testing of hydrogen-enriched notched AISI 4135 steel. Figure 12 demonstrates the remarkable consistency of the phase-field formulation with prior experimental work by Wang et al. [199], who experimentally investigated the influence of hydrogen concentration on the NTS of AISI 4135 steel. It is evident that the strength of the steel material significantly decreases at lower hydrogen concentrations. However, beyond a hydrogen concentration of 0.5 wt ppm, the strength stabilizes, with minimal changes in failure stress observed. This evolution may be attributed to the saturation of hydrogen concentration at the lattice or microstructural traps within the material, a behavior commonly observed in most low-alloy steels.

Valverde-Gonzalez et al. [204] also integrated the phase-field approach with a decohesion zone formulation to predict HE in polycrystalline materials, including Ni-Cu superalloys. It is worth noting that the model also showed good agreement with Harris et al.'s [205] prior experimental work on hydrogen-induced intergranular cracking in polycrystalline nickel. Valverde-Gonzalez et al. observed that the combined model effectively predicted the crack evolution without convergence issues.

In practical applications, most industrial boiler components may be subjected to cyclic mechanical loading during operation. Therefore, extending the phase-field model to simulate hydrogen-assisted fatigue crack growth is highly beneficial. In view of this, Cui et al. [206] have recently developed an extended and robust phase-field model for predicting hydrogen-assisted fatigue crack growth. The model combined the phase field description of fracture and fatigue, stress-assisted hydrogen diffusion, and the toughness degradation formulation with cyclic and hydrogen concentration contributions.

The model was capable of predicting the influence of H<sub>2</sub> pressure, loading frequencies, and loading ratios on hydrogen-assisted fatigue crack propagation. The hydrogen-assisted fatigue crack growth predictions also showed excellent agreement with experimental fatigue data, showing remarkable predictive capabilities and the ability to map safe regimes of loading frequencies in pressure vessel steels. The robustness of the model also allowed for the simulation of both laboratory-scale samples and large industrial-scale critical engineering components such as pressure vessels and tubes.

Benchmark simulation results captured from their work are shown in Figures 13–15. Figure 13 shows the phase-field fatigue crack contours, describing the evolution of fatigue crack growth under representative conditions of  $H_2$  pressure, loading frequency, and loading ratio. Likewise, Figure 14 also depicts the hydrogen concentration contours, showing the accumulation of hydrogen at the moving crack tip, which is a high hydrostatic stress location. The predictions of hydrogen-assisted crack growth and hydrogen concentration evolution are consistent with the findings of Martinez-Paneda et al. [197] under static loading conditions. Figure 15 shows the influence of  $H_2$  pressure on fatigue crack growth (based on the Paul Paris rule), showing remarkable agreement with experimental data. Observing closely, the model adequately predicted the experimental data for both  $H_2$  pressures of 55 MPa and 106 MPa.

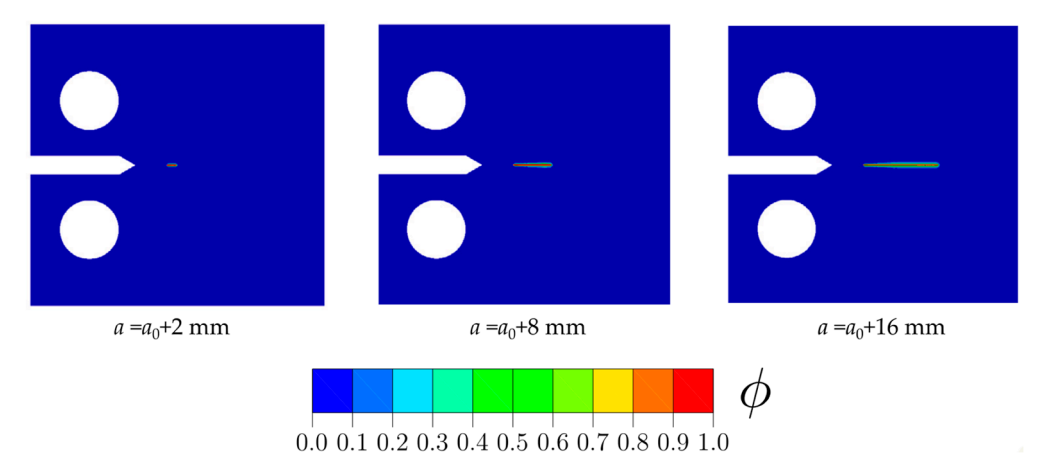


**Figure 13.** The contour of phase field fatigue crack growth at different stages ( $a = a_0 + 2$  mm,  $a = a_0 + 8$  mm, and  $a = a_0 + 16$  mm), where a represents the crack size, and  $a_0$  represents that initial crack size. The simulation contour was obtained under the following conditions:  $H_2$  precharged samples under an  $H_2$  pressure of  $pH_2 = 106$  Mpa, loading frequency of f = 1 Hz, and a loading ratio of f = 0.1. [206]. CC BY 4.0 (open access).

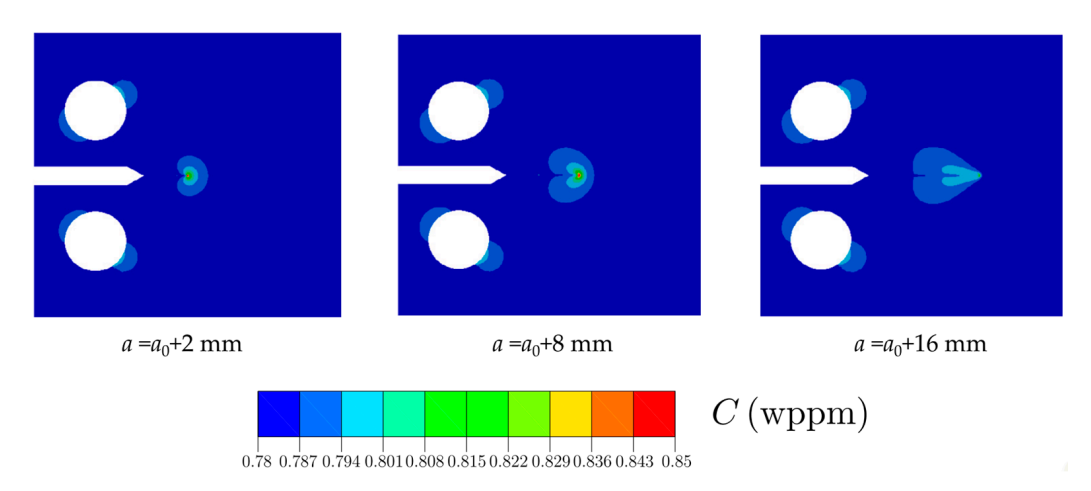


**Figure 14.** The contour of hydrogen concentration evolution at different stages of crack growth:  $a = a_0 + 2$  mm,  $a = a_0 + 8$  mm, and  $a = a_0 + 16$  mm. The simulation contour was obtained under the following conditions: H<sub>2</sub> precharged samples under an H<sub>2</sub> pressure of pH<sub>2</sub> = 106 Mpa, loading frequency of f = 1 Hz, and a loading ratio of R = 0.1. [206]. CC BY 4.0 (open access).

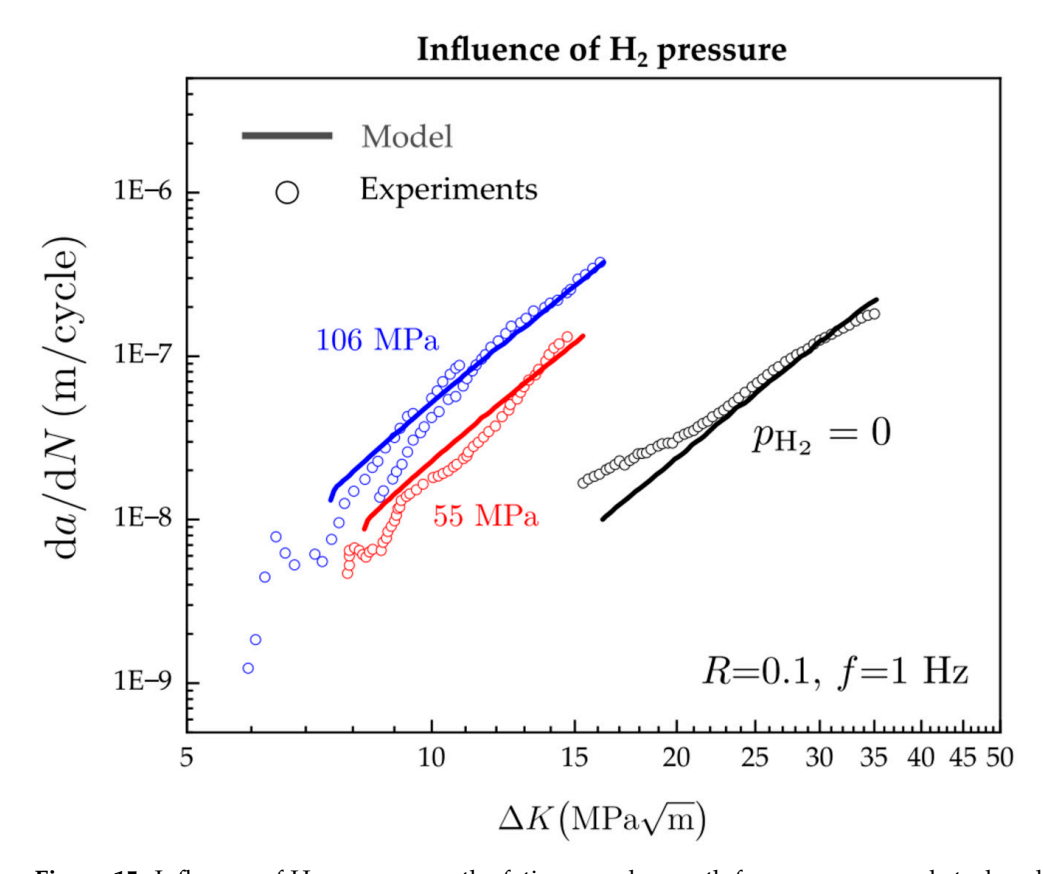


**Figure 15.** Influence of  $H_2$  pressure on the fatigue crack growth for pressure vessel steels, where a = crack size, N = fatigue cycle,  $pH_2 = H_2$  pressure, R = loading ratio, and f = loading frequency [206]. CC BY 4.0 (open access).

However, the model developed by Cui et al. [206] was only capable of predicting the degradation of fracture toughness owing to increasing hydrogen content. In this context, it was assumed that the hydrogen content only affected the reduction in fracture toughness and did not influence fatigue crack growth. This assumption may be acceptable, as fatigue crack growth is usually sensitive to enhanced fatigue crack growth rates, loading frequencies, and stress intensity factors rather than hydrogen concentration [58–60]. However, other experimental studies have also reported changes in the fatigue curve (S-N curve)

behavior owing to the increasing hydrogen content in the materials [57]. This implies that the nucleation and growth of fatigue cracks are also highly sensitive to hydrogen content. Therefore, to achieve a more accurate and robust assessment, it is essential to extend the present model to account for the synergistic interplay between hydrogen concentration and fatigue crack growth. The present phase-field model should be extended to incorporate additional material parameters in  $H_2$  environments and simulate their impact on fatigue crack growth behavior [206].

Nonetheless, the phase-field frameworks presented by both Martinez-Paneda et al. [197] and Cui et al. [206] have shown remarkable capabilities for qualitative and quantitative predictions of hydrogen-assisted fracture and fatigue behaviors under various static and cyclic H<sub>2</sub> pressure conditions. These models have sufficiently facilitated rapid and cost-effective numerical investigations beyond the limitations of accelerated laboratory-scale test conditions. Additionally, the models are capable of handling complex 2D and 3D geometries, allowing one to perform advanced virtual testing of industrial engineering components. Hence, these computational tests can offer a significant advantage in simulating complex practical scenarios with minimal challenges, such as critical boiler components operating under elevated H<sub>2</sub> conditions. They also show promise for the evaluation and validation of novel hydrogen-compatible materials. More comprehensive documentation of general phase-field modeling of fractures or phase-field formulation of hydrogen-assisted fracture and fatigue with several benchmark studies can be found elsewhere [195,197,198,206].

Going forward, subsequent studies focusing on multiscale material characterization are necessary. These studies should explore the accurate implementation and integration of theoretical models, micro- and macro-scale experimental models, and computational fracture mechanics models, such as phase-field models and MD. Additionally, employing advanced high-computing visualization techniques, such as atomic probe tomography (APT), to visualize hydrogen distribution is worthwhile. This can assist in resolving discrepancies and challenges in accurately analyzing the location of atomic hydrogen within materials [180,207]. The insights and knowledge gained from these advanced studies will aid in efficient material selection and validation studies. These can also assist in defining safe operational regimes where critical boiler components can adequately perform.

#### 5.3. Data-Driven Approaches for the Prediction of Material Susceptibility and Compatibility

It is also important to highlight the current state-of-the-art, where both advanced and traditional machine learning (ML) data-driven models have been utilized for the rapid prediction of material susceptibility and compatibility under specific H<sub>2</sub> conditions. Advanced ML algorithms, such as neural networks, along with traditional methods, such as support vector machines (SVM) and extreme gradient boosting (XGBoost), have demonstrated remarkable capabilities for the design of novel metallic materials and the prediction of defects and mechanical properties [208–211]. By training these models on extensive datasets that include features such as mechanical performance, environmental stresses, material composition, hydrogen concentration, hydrogen solubility, and hydrogen diffusivity, material designers can develop robust predictive models. These predictive models can rapidly and accurately estimate material susceptibility to hydrogen-induced damage, greatly enhancing the reliability of material selection studies and designs. Moreover, by analyzing various specific material properties, environmental factors, and their synergistic influence, these models can provide valuable insights into the compatibility of boiler materials with specific H<sub>2</sub> boiler conditions.

The use of traditional ML models and artificial neural networks (ANNs) for evaluating material susceptibility to hydrogen-induced damage and their compatibility with  $H_2$  is an emerging field that is steadily gaining traction. Consequently, to the best of our knowledge, there is limited research on this topic. Nonetheless, it is pertinent to acknowledge the few existing studies in this data-driven field that have investigated the prediction of hydrogen-induced damage.

For instance, Campari et al. [212] employed a traditional supervised ML approach to predict material susceptibility to HE using data from the "Technical Reference for Hydrogen Compatibility of Materials" [129]. In their study, they developed a gradient boosting (GB) classification model to evaluate material susceptibility to HE, categorizing susceptibility into two distinct classes: "small/medium/high" (SMH) and "extreme" (E). The GB model demonstrated an accuracy of 88.6% for predicting the severity of HE in metals under specific environmental and loading conditions. However, they noted that the model has the tendency to mislabel an E susceptibility as an SMH susceptibility, which is more critical than vice versa. Such inaccurate predictions could result in erroneous assessments of the susceptibility of a metal to HE. Consequently, this may lead to improper material selection for specific working conditions and a higher risk of component failure during service.

Following this work, Subedi et al. [213] also applied a classical supervised ML model to assess factors influencing HE in pipeline steels. Similarly, their study relied on data sourced primarily from industrial reports, such as the "Technical Reference for Hydrogen Compatibility of Materials" [129], with input features, including environmental conditions, material properties, and mechanical loading parameters. They also trained a decision tree classifier (DTC) model, which achieved an accuracy of 82.5% in predicting HE severity in pipeline steels. It is important to note that the synergistic interplay of various factors, such as environmental conditions, material properties, and loading conditions, in driving HE remains a complex concept to model. Failure to account for this complexity can affect the prediction accuracy of the traditional ML models discussed. Campari et al. [212] and Subedi et al. [213] recognized this limitation, highlighting that expanding datasets and utilizing more advanced ML algorithms have significant potential to enhance the accuracy and performance of models in predicting and classifying HE severity in materials.

Kim et al. [214] also evaluated the performance of four traditional ML models: random forest (RF), linear regression (LR), bayesian regression (BR), and SVM in predicting the influence of alloying elements, environmental conditions, and experimental variables on the HEE index of austenitic steels, specifically in terms of RRA. Their dataset included ten input features: environmental and experimental variables (such as H<sub>2</sub> pressure and strain rate) and alloying elements (including nickel, molybdenum, chromium, manganese, silicon, carbon, nitrogen, and copper).

They employed Pearson's correlation coefficient (PCC) and maximum information coefficient (MIC) to quantitatively investigate the correlations between these input features and the HEE index. From the correlation analysis, both PCC and MIC identified nickel and molybdenum as the strongest features influencing the HEE index in austenitic stainless steels. The correlation analysis was consistent with the existing literature, identifying nickel and molybdenum as significant alloying elements affecting the HEE index in austenitic stainless steel [33,129]. Additionally, the analysis revealed a negative correlation with H<sub>2</sub> pressure, indicating that a higher H<sub>2</sub> pressure, which influences higher hydrogen concentrations in materials, can adversely affect the HEE. This correlation analysis also resonated with prior experimental and computational studies on the effect of hydrogen concentration on the HE of steels [33,129,197,206].

Figure 16 depicts the prediction accuracy of the HEE index using the four ML models: LR, BR, RF, and SVM. By calculating the coefficient of determination (R²), the RF model, with an accuracy of ~82%, outperformed the other models in predicting the HEE index of austenitic steels. In contrast, LR, BR, and SVM showed significant errors when compared with the RF model. The prediction of the RF model also showed remarkable agreement with the experimentally reported HEE indices of austenitic steels [33,129]. However, Kim et al. noted limitations in ML models despite their high prediction accuracy. These limitations were attributed to factors such as the small size of the dataset (57) and variations in the surface roughness and geometry of the samples considered for the dataset.

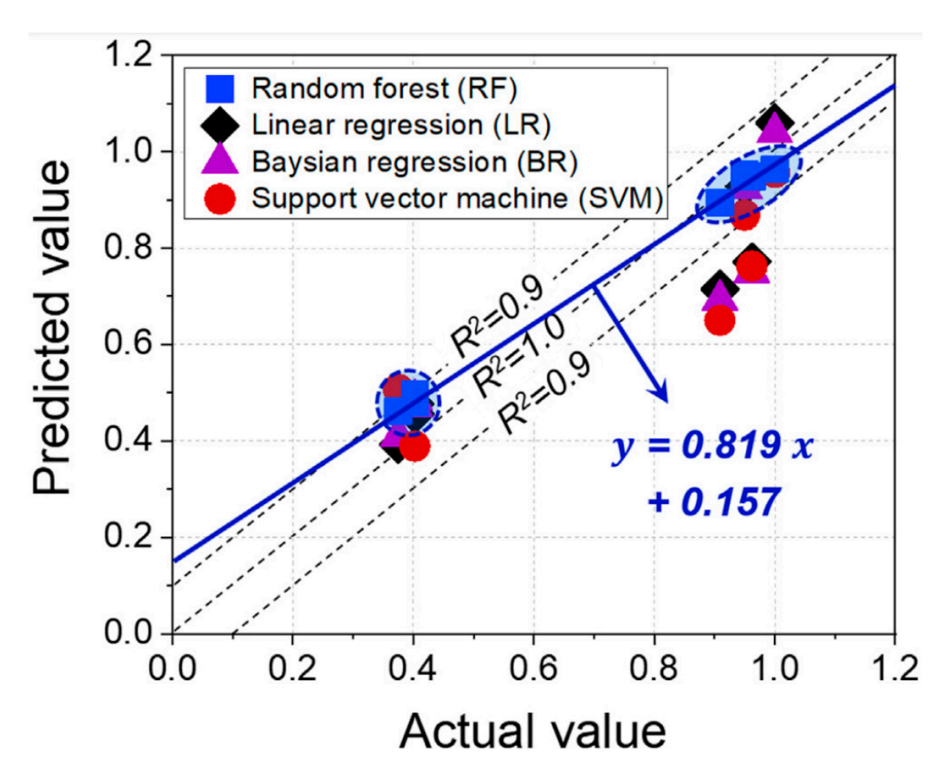


**Figure 16.** Predicted values versus actual values of RRA for new test data. The dashed lines represent the 100% and 90% accuracy intervals, respectively, and the blue line indicates the result of linear fitting of the RF model expressed as slope and y-intercept [214]. CC BY 4.0 (open access).

The application of other advanced ML algorithms to investigate the effects of hydrogen on mechanical properties and the severity of damage to materials has also been reported. For example, Fagnon et al. [180] developed two ANNs to predict the influence of hydrogen concentration levels on the evolution of hydrogen-induced failures in martensitic ultrahigh-strength steels. The two ANN models, Model I and Model II, exhibited identical architectures. However, the topology of these models varied in terms of the size of the input features. Model I had an input layer of 12 nodes, while Model II had an input layer of 14 nodes, corresponding to their feature sizes. The input layers of both models were followed by four hidden, densely connected layers with node configurations of 7, 5, 3, and 2, respectively. These hidden layers were then summed up with a single-node output layer. Hence, the topologies of Model I and Model II can be summarized as follows: 12-7-5-3-2-1 and 14-7-5-3-2-1, respectively.

Their dataset included input features such as the mechanical properties of the tested steels (both in air and under continuous hydrogen charging), hydrogen charging parameters, and hydrogen concentration levels determined through TDS analysis. The models were designed to receive input from these features and predict a target output of the total hydrogen concentration influencing mechanical property degradation for a specific data sample. Both ANN models demonstrated comparable hydrogen concentration prediction capabilities with remarkable accuracy despite variations in mechanical responses due to different prior austenite grain (PAG) morphologies. However, they noted that these models might be less effective in predicting the hydrogen concentration levels at fracture for high-strength steels with ferritic or austenitic microstructures. This limitation arises because these high-strength steels respond differently to hydrogen-induced fracture when compared to the tested steels. To address this limitation, an extensive dataset that considers the unique responses of other high-strength steels is required.

Other studies have also evaluated the performance of both traditional and advanced ML models in predicting the severity of hydrogen-induced damage to materials. For example, Ahmed et al. [211] comparatively studied the use of seven traditional and advanced

ML models: RF, DTC, XGBoost, GB, Adaptive Boosting (AdaBoost), Categorical Boosting (CatBoost), and ANN, to predict neck reduction of areas in low-carbon and low-alloy steels due to HE. They obtained data from laboratory-scale tensile testing of low-carbon and low-alloy steels subjected to pressurized H<sub>2</sub> conditions.

The prediction results indicated that the CatBoost model outperformed the other models in predicting neck reduction in the area of steel exposed to H<sub>2</sub>, achieving a testing accuracy of 72.50%. Additionally, feature importance analysis identified H<sub>2</sub> pressure, the ultimate tensile strength of the material, and iron percentage weight composition as the most significant factors influencing the prediction of HE. Subsequently, a sensitivity analysis of the CatBoost model was conducted based on these three key parameters and validated against the existing literature. By examining these critical input features, the sensitivity of the model was found to be in good agreement with the existing literature.

For instance, the sensitivity analysis of H<sub>2</sub> pressure revealed that an increase in H<sub>2</sub> pressure resulted in a significant decrease in the neck area reduction of the steels. This observation validated the capability of the model to accurately predict the decline in the ductility of steel due to an increase in  $H_2$  pressure, as reported in the literature [197,215]. Observing Figure 17a closely, one can notice an initial sharp decline in ductility, followed by a plateau steady-state progression beyond the saturation limit. The authors attributed this evolution to the fact that the lattice traps in the material attained a hydrogen concentration saturation point. Previous studies corroborated this observation, indicating that for lowcarbon and low-alloy steels, the neck area reduction plateaued at an H<sub>2</sub> pressure of 6.9 MPa, with a hydrogen saturation point being attained at pressures exceeding 13.8 MPa [215]. Similarly, the sensitivity analysis of the ultimate tensile strength demonstrated a linear decrease in ductility with increasing strength, as shown in Figure 17b. This trend also agrees remarkably with the established literature, which postulates that as the strength of steel increases, its susceptibility to HE is heightened [33,129,180]. Figure 17c shows the sensitivity analysis of the iron weight composition. Observing closely, one can notice a consequent linear decrease in ductility with increasing iron content. The amplification of HE with an increase in iron composition is also consistent with previous studies, further validating the model's predictive capabilities [33,129]. Overall, the accurate prediction of HE using the CatBoost model, coupled with feature importance analysis, provides a valuable industrial tool for material scientists and designers. This tool can assist in optimizing H<sub>2</sub> pressure elemental composition and the selection of appropriate materials for hydrogen pipelines, potentially reducing the risk of hydrogen-induced fractures in practical applications.

Subedi et al. [216] demonstrated a more practical application of ML for the advancement of H<sub>2</sub> utilization in industrial applications. They evaluated the performance of traditional and advanced ML approaches in assessing the safety of hydrogen pipeline transport. In their study, three ML models (RF, AdaBoost, and ANN) were comparatively analyzed to evaluate the HE susceptibility of pipeline steels. Their dataset was curated from in situ tensile test results conducted in hydrogenated environments. Comparative analysis identified RF and AdaBoost as the most effective models for predicting HE susceptibility (based on an embrittlement index). RF and Adaboost achieved prediction accuracies of 84% and 84.5%, respectively. Based on the embrittlement index, they ranked the HE susceptibility of various pipeline materials, as well as their compatibility with H<sub>2</sub>. The study highlighted X100 as the pipeline material with the highest susceptibility to hydrogen-induced degradation, whereas X120 pipeline steel was identified as the most suitable low-alloy steel for hydrogen pipeline applications. These models were also able to predict the H<sub>2</sub> compatibility of the pipeline network connecting Norway and other European countries.

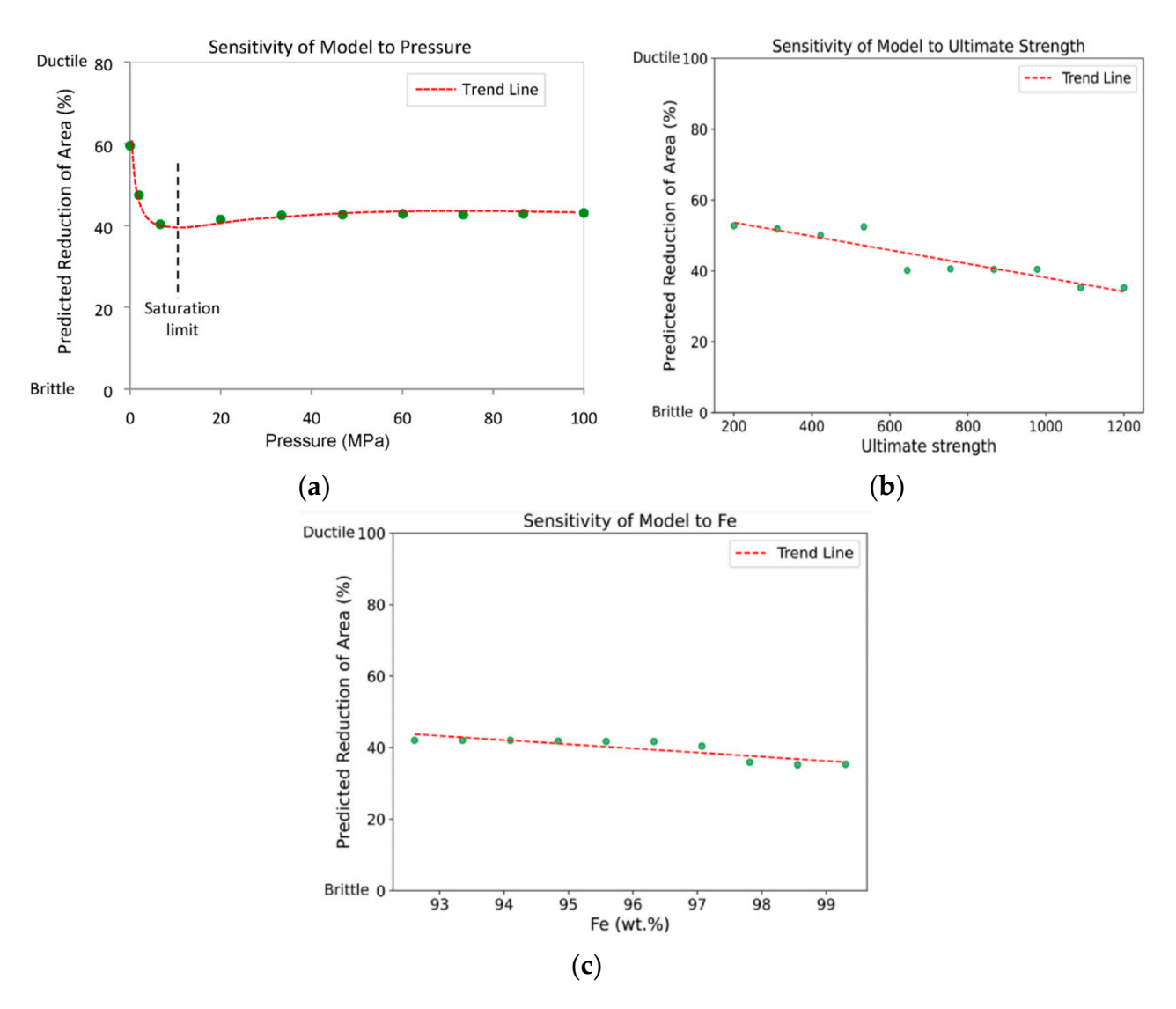


**Figure 17.** Sensitivity analysis of (a) H<sub>2</sub> pressure, (b) ultimate strength, and (c) Fe weight composition in the CatBoost model [211] (reprinted with permission from Elsevier).

### Limitations of Data-Driven Approaches

Clearly, the limited availability of extensive training datasets and lack of a precise mechanistic understanding of the interplay between several input features can significantly affect the predictive performance of these models. As observed, the prediction accuracies for most of the models discussed were generally below 90%, which may be insufficient for making confident decisions regarding material selection studies. The datasets used for training most of the ML models are typically curated from accelerated laboratory test settings. These tests often focus on high-pressure, ambient-temperature conditions (~22 °C) and are conducted in the absence of gaseous inhibitors and impurities [33,129,212]. These laboratory-scale assumptions are based on the justifications that the severity of HE in metals, particularly ferritic steels, is most pronounced near room temperature and that the pure hydrogen concentration within a metal lattice is directly proportional to the hydrogen partial pressure, as described by Sievert's law, as shown in Equation (2) [33,212]. Moreover, it has been argued that hydrogen atoms exhibit increased mobility at elevated temperatures and are easily detrapped from the metal lattice. In contrast, at relatively low temperatures, hydrogen diffusion through the lattice requires longer exposure times to reach critical local concentrations. This accumulation of hydrogen leads to embrittlement, particularly when combined with localized stress conditions [212].

$$C = S\sqrt{p(H_2)} \tag{2}$$

where C, S, and p(H<sub>2</sub>) represent hydrogen concentration, solubility, and H<sub>2</sub> partial pressure, respectively.

Nonetheless, expanding the datasets to encompass measurements obtained under a broader range of testing conditions, including high temperatures, varying H<sub>2</sub> pressures, different loading frequencies, and gaseous impurity conditions, would be valuable. This comprehensive dataset is essential for enhancing the prediction accuracy of these models and extending their capability to also predict additional damage occurrences, including HTHA and hydrogen-assisted fatigue. Meanwhile, meticulous data collection is crucial to avoid inhomogeneous or irrelevant data, which can negatively impact both the prediction accuracy and validation efficiency of the models. In this context, it is essential to develop a consistent and high-quality database that encompasses diverse boiler operating conditions. This comprehensive dataset is crucial for training robust ML algorithms capable of making rapid and accurate material selection decisions under elevated hydrogen boiler conditions.

However, creating such a standardized and robust database poses a significant challenge because of the broad range of operational scenarios that must be considered in boiler systems during data collection. Inconsistencies in data collection may arise owing to variations in testing techniques, equipment failures, and environmental conditions. Currently, the "Technical References for Hydrogen Compatibility of Materials" document [129] remains the primary material selection database for curating data. However, the report provides a limited, inconsistent amount of experimental (slow-strain rate tensile testing) data, and certain data, such as fatigue testing results for most materials, have not been reported. Therefore, expanding such a database and developing standardized data collection procedures in elevated hydrogen environments beyond laboratory-scale testing would be highly beneficial.

Nonetheless, incorporating ML techniques, or more broadly, artificial intelligence (AI), into the study and selection of materials for critical boiler components holds significant promise. This can revolutionize the evaluation and prediction of material performance under high-temperature, high-pressure H<sub>2</sub> conditions. In fact, engineers can accelerate the material assessment process by leveraging computational fracture mechanics for confident data curation and validation alongside data-driven approaches. This integrated strategy can facilitate the rapid identification of materials with superior resistance to hydrogen-induced damage, thereby enhancing the efficacy of material selection studies. Consequently, this approach can reduce the overreliance on conventional materials such as austenitic stainless steel and aluminum for hydrogen-service applications. The insights gained from this approach can inform the design of new hydrogen-specific boiler materials and critical components and guide risk-informed strategies for the inspection of existing boiler components [213].

#### 6. Conclusions and Future Studies

#### 6.1. Conclusions

This critical review has highlighted the significant potential of  $H_2$  as a sustainable alternative in industrial boiler operations. This is an important step towards advancing the hydrogen economy and achieving global decarbonization goals. Among its key advantageous findings,  $H_2$ 's high heating value, high energy content, and near-zero carbon emissions stand out, promising a substantial reduction in greenhouse gas emissions. However, the gradual transition to extensive use of  $H_2$  in industrial boiler operations presents significant challenges. The effects of damage mechanisms such as HE and HTHA on critical boiler components under elevated conditions present a crucial gap that must be addressed to enable the widespread adoption of  $H_2$  in these systems. Based on this review, the following key conclusions were drawn:

Over the years, the HE and HTHA phenomena have been complex damage mechanisms to understand and daunting research hurdles for material designers and engineers. Nonetheless, significant experimental, theoretical, and computational advancements have been made to substantially bridge these gaps. These advancements have yielded satisfactory accuracy in characterizing hydrogen diffusion into materials and assessing the subsequent effects of hydrogen-assisted damage. Nevertheless, significant challenges remain as the acceptance of the most accurate theoretical model for driving the HE mechanism in materials continues to be a major point of debate among experts. Establishing a standard theoretical model for defining HE manifestations could enhance the precision of numerical modeling and simulations of hydrogen-assisted fractures, thereby supporting the development of novel hydrogen-specific materials and components.

- 2. To reduce the occurrence of HE and HTHA in boiler components, general mitigation measures that could be explored include proper thermomechanical treatments, the use of HPBs, the addition of inhibitors to reduce H<sub>2</sub> purity, proper weld procedures and post-heat treatments, the selection of proper operating temperatures and pressures, the introduction and reduction of alloying elements, and the proper selection of materials. In an industrial context, visual and advanced inspection procedures using sophisticated inspection techniques such as LPT, PAUT, SWUT, and MPT can also be utilized for rapid failure detection to inform decisions to prevent potential equipment failure. However, when exploring mitigation measures, it is important to consider the specific operational contexts of the critical components and the potential hydrogen-induced damage mechanisms (HE or HTHA) that may affect them.
- 3. Numerous studies and technical references have identified several prominent metals and metallic alloys, such as aluminum, austenitic stainless steel alloys, and superalloys, as promising candidates for H<sub>2</sub> boiler applications. In particular, superalloys such as single-crystal PWA 1480E, Inconel 625, and Hastelloy X exhibit promising HE-resistant capabilities under high-pressure, high-temperature H<sub>2</sub> conditions. However, the material selection for both traditional and emerging alloys, such as BCC HEAs, must be validated through rigorous fracture mechanics analysis to establish hydrogen safety factors and confirm their suitability as hydrogen-compatible materials for elevated hydrogen boiler operations.
- 4. Metallurgically bonded austenitic stainless steel liners and dielectrics, such as oxides, carbides, and nitrides, have been considered promising candidates for HPB coating applications. Notably, the TiAlN HPBs exhibit the most promising HPB coating characteristics, with permeabilities on the order of  $10^{-18}$  mol·s<sup>-1</sup>·m<sup>-1</sup>·( $\sqrt{\text{Pa}}$ )<sup>-1</sup>. Therefore, TiAlN coatings can be further explored for use in coating boiler components. However, extensive investigation of these coatings beyond laboratory-scale conditions would be valuable for validating their effectiveness in industrial hydrogen boiler operations.
- 5. Emerging numerical and computational models, such as MD and phase-field models, have proven to be efficient tools for modeling and predicting HE, HTHA, and complex crack morphologies in materials subjected to H<sub>2</sub> conditions. In particular, phase-field modeling of hydrogen-assisted fracture or hydrogen-assisted fatigue crack growth can allow sophisticated *virtual testing* of hydrogen-specific critical boiler components. In the future, computational modeling of hydrogen-assisted damage in hydrogen boiler materials can assist in: (1) confident validation of material selection studies; (2) informing major material development decisions of hydrogen-specific engineering components; and (3) mapping out safe regimes of operations for materials working under elevated H<sub>2</sub> boiler conditions to ensure good performance.
- 6. Data-driven machine learning (ML) models, such as DTC, have shown significant potential for the rapid prediction of material susceptibility to hydrogen-induced damage and their compatibility with H<sub>2</sub> under specific loading conditions. These models were validated against experimental and theoretical studies and demonstrated remarkable agreement with the observed data. However, limitations such as small

datasets and a lack of consistent, standardized databases can significantly impact the prediction accuracy and validation of these models in a practical context. In the future, the development of more sophisticated ML algorithms and the creation of exhaustive material testing databases using advanced computational modeling can offer valuable insights into the design of novel, advanced hydrogen-compatible materials and infrastructure for  $H_2$  boiler operation.

### 6.2. Future Research Roadmap

To facilitate the gradual widespread adoption of  $H_2$  in industrial boilers, future research should focus on, but not be limited to, the following:

- Implementation of hydrogen-specific standards and codes for rigorous fracture mechanics investigations into the feasibility of traditional alloys, superalloys, and novel materials, such as BCC HEAs, for the design of hydrogen-specific boiler components.
- 2. Extensive investigations into the viability of HPBs and liners on critical boiler components under actual H<sub>2</sub> conditions beyond laboratory-scale testing.
- 3. Employing phase-field modeling to conduct rigorous *virtual testing* of hydrogen-specific components to assess their suitability for specific H<sub>2</sub> conditions and industrial-scale applications. Additionally, these models should be employed to design safe operational regimes for conventional components and old boiler infrastructures.
- 4. Development of robust ML algorithms and standardized, extensive mechanical testing databases to ensure remarkable prediction accuracy of a material's susceptibility to hydrogen-induced damages and its compatibility with H<sub>2</sub>. As previously mentioned, phase-field modeling of hydrogen-assisted fracture and fatigue crack growth enables efficient and cost-effective numerical testing, extending beyond laboratory-scale conditions. Thus, phase-field modeling can be instrumental in developing a comprehensive, standardized ML database. This approach can guide industrial decision-making in selecting materials and designing components specifically for hydrogen-fuel boilers.

**Author Contributions:** Conceptualization, E.H., C.Z., S.R., S.G. and P.M.; Visualization, E.H.; Writing—original draft, E.H.; Investigation, E.H., C.Z., S.R. and P.M.; Writing—review and editing, C.Z., S.R., P.M. and S.G.; Supervision, C.Z., P.M. and S.G.; Funding acquisition, C.Z., P.M. and S.G. All authors have read and agreed to the published version of the manuscript.

**Funding:** This work was supported by the US National Science Foundation under Grant OIA-2118756 RII Track-2 FEC: Rapid Qualification for Additively Manufactured Safety-Critical Components (CAMQ); Louisiana NASA EPSCoR Research Awards Program (RAP) under the contract number of LEQSF-EPS (2023)-RAP-45; Louisiana NASA EPSCoR Research Enhancement Award (REA) Program under the contract number of PO-0000245417. The research was also partially supported by the US National Science Foundation under grant number OIA 1946231 and the Louisiana Board of Regents for the Louisiana Materials Design Alliance (LAMDA).

**Data Availability Statement:** The raw data supporting the conclusions of this article will be made available by the authors, without undue reservation, to any qualified researcher. For additional information on the datasets, please contact the corresponding author.

**Acknowledgments:** The authors would like to acknowledge Eric A.K Fagnon (VTT, Finland) for his insights and discussions. Also, the authors are sincerely grateful to Ama Agyapomaa Darkwah (University of Washington, Seattle, USA) for her help in visualization and image reproduction.

**Conflicts of Interest:** The authors declare that they do not have any recognized competing financial interests or personal relationships that might be perceived as having an influence on the work presented in this paper.

## Nomenclature, Subscripts, Superscripts, Acronyms, and Abbreviations

CO<sub>2</sub> Carbon dioxide H<sub>2</sub> Hydrogen gas

HENG Hydrogen-enriched natural gas

CH<sub>4</sub> Methane kg Kilogram MJ Megajoules kWh Kilowatt-hours

LPG Liquified petroleum gas RFG Reformulated gasoline HE Hydrogen embrittlement

HTHA High-temperature hydrogen attack **AHSS** Advanced high-strength steel HIC Hydrogen-induced cracking **HPT** Hydrogen pressure theory **HEDE** Hydrogen-enhanced decohesion **HELP** Hydrogen-enhanced localized plasticity **HESIV** Hydrogen-enhanced strain-induced vacancies **AIDE** Absorption-induced dislocation emission theory

HRE Hydrogen reaction embrittlement

 $\begin{array}{cc} N_2O & \text{Nitrous oxide} \\ O_2 & \text{Oxygen} \end{array}$ 

CO Carbon monoxide
PWHT'ed Post-weld heat treated
PWHT Post-weld heat treatment

API RP American Petroleum Institute Recommended Practice

HAT Hydrogen attack tendency

HAZ Heat-affected zone

NDE Non-destructive examination

NASA National Aeronautics and Space Administration ASME American Society of Mechanical Engineers

BPVC Boiler and pressure vessel codes

HEAs High-entropy alloys BCC Body-centered cubic FCC Face-centered cubic

HEE Hydrogen environment embrittlement

NTS Notched tensile strength RA Reduction in area

EL Elongation RNTS Notched tensile str

RNTS Notched tensile strength ratio RRA Reduction in area ratio

ANSI American National Standard Institute

CHMCI Compressed Hydrogen Materials Compatibility

SBCs Surface barrier coatings
TBCs Thermal barrier coatings
HPBs Hydrogen permeation barriers

 $Al_2O_3$  Aluminum oxide  $Cr_2O_3$  Chromium oxide  $Er_2O_3$  Erbium oxide

PRF Permeation reduction factor

 $\begin{array}{lll} BN & Boron nitride \\ TiN & Titanium nitride \\ SiN & Silicon nitride \\ TiC & Titanium carbide \\ SiC & Silicon carbide \\ D_s & Substrate diameter \\ D_f & Film diameter \\ \end{array}$ 

P<sub>s</sub> Substrate permeability value

P<sub>f</sub> Film permeability value

HIAD Hydrogen Incidents and Accidents Database

LPT Liquid penetrant testing
PAUT Phased array ultrasonic testing
SWUT Shear wave ultrasonic testing
MPT Magnetic particle testing

TDS Thermal desorption spectroscopy
SEM Scanning electron microscopy
EDS Energy-dispersive X-ray spectroscopy

Transformation-induced plasticity

AAS Atomic absorption spectroscopy
Z–R Zimmermann–Reinhardt
AHSS Advanced high-strength steel
TWIP Twinning-induced plasticity

DFT Density functional theory MD Molecular dynamic FEA Finite element analysis

UEL User element UMAT User material

TRIP

 $\phi$  Phase-field parameter

C Initial hydrogen concentration C Hydrogen concentration

a Crack size
 a<sub>0</sub> Initial crack size
 K Stress intensity factor

N Fatigue cycle
 R Loading ratio
 f Loading frequency
 Fe<sub>3</sub>C Iron carbide

APT Atomic probe tomography

ML Machine learning **SVM** Support vector machine **PAG** Prior austenite grain XGBoost Extreme gradient boosting **ANN** Artificial neural network GB Gradient boosting DTC Decision tree classifier RF Random Forest LR Linear regression

PCC Pearson's correlation coefficient
MIC Maximum information coefficient
R<sup>2</sup> Coefficient of determination

Bayesian regression

AdaBoost Adaptive Boosting
CatBoost Categorical Boosting

S Solubility

BR

p(H<sub>2</sub>) Hydrogen partial pressure AI Artificial intelligence

# References

1. Jayamaha, D.L. Energy-Efficient Building Systems; Mcgraw-Hill Publishing Company: New York, NY, USA, 2007.

- 2. Total Energy Annual Data—U.S. Energy Information Administration (EIA). Available online: https://www.eia.gov/totalenergy/data/annual/index.php (accessed on 30 December 2023).
- 3. Barma, M.C.; Saidur, R.; Rahman, S.M.A.; Allouhi, A.; Akash, B.A.; Sait, S.M. A review on boilers energy use, energy savings, and emissions reductions. *Renew. Sustain. Energy Rev.* **2017**, *79*, 970–983. [CrossRef]
- 4. Jorgenson, D.W.; Wilcoxen, P.J. Reducing U.S. carbon dioxide emissions: An assessment of different instruments. *J. Policy Model.* **1993**, *15*, 491–520. [CrossRef]

5. Jorgenson, D.W.; Wilcoxen, P.J. Reducing US carbon emissions: An econometric general equilibrium assessment. *Resour. Energy Econ.* **1993**, *15*, 7–25. [CrossRef]

- 6. Glaeser, E.L.; Kahn, M.E. The greenness of cities: Carbon dioxide emissions and urban development. *J. Urban. Econ.* **2010**, *67*, 404–418. [CrossRef]
- 7. Qazi, A.; Hussain, F.; Rahim, N.A.; Hardaker, G.; Alghazzawi, D.; Shaban, K.; Haruna, K. Towards Sustainable Energy: A Systematic Review of Renewable Energy Sources, Technologies, and Public Opinions. *IEEE Access* **2019**, *7*, 63837–63851. [CrossRef]
- Uney, M.S.; Cetinkaya, N. Comparison of CO<sub>2</sub> emissions fossil fuel based energy generation plants and plants with Renewable Energy Source. In Proceedings of the 2014 6th International Conference on Electronics, Computers and Artificial Intelligence (ECAI), Bucharest, Romania, 23–25 October 2014; IEEE: Piscataway, NJ, USA, 2014; pp. 29–34. [CrossRef]
- 9. Schiro, F.; Stoppato, A.; Benato, A. Modelling and analyzing the impact of hydrogen enriched natural gas on domestic gas boilers in a decarbonization perspective. *Carbon Resour. Convers.* **2020**, *3*, 122–129. [CrossRef]
- 10. Abe, J.O.; Popoola, A.P.I.; Ajenifuja, E.; Popoola, O.M. Hydrogen energy, economy and storage: Review and recommendation. *Int. J. Hydrogen Energy* **2019**, *44*, 15072–15086. [CrossRef]
- 11. Najjar, Y.S.H. Hydrogen safety: The road toward green technology. Int. J. Hydrogen Energy 2013, 38, 10716–10728. [CrossRef]
- 12. Hodges, J.P.; Geary, W.; Graham, S.; Hooker, P.; Goff, R. Injecting Hydrogen into the Gas Network—A Literature Search. 1 January 2015. Available online: https://www.h2knowledgecentre.com/content/policypaper1193 (accessed on 19 March 2023).
- 13. Hwang, H.T.; Varma, A. Hydrogen storage for fuel cell vehicles. Curr. Opin. Chem. Eng. 2014, 5, 42-48. [CrossRef]
- 14. Becherif, M.; Ramadan, H.S.; Cabaret, K.; Picard, F.; Simoncini, N.; Bethoux, O. Hydrogen Energy Storage: New Techno-Economic Emergence Solution Analysis. *Energy Procedia* **2015**, *74*, 371–380. [CrossRef]
- 15. Colozza, A.J.; Kohout, L. Hydrogen Storage for Aircraft Applications Overview. E-13540. 1 September 2002. Available online: https://ntrs.nasa.gov/citations/20020085127 (accessed on 20 March 2023).
- 16. de Jongh, P.E.; Adelhelm, P. Nanosizing and Nanoconfinement: New Strategies Towards Meeting Hydrogen Storage Goals. *ChemSusChem* **2010**, *3*, 1332–1348. [CrossRef]
- 17. Sherif, S.A.; Goswami, D.Y.; (Lee) Stefanakos, E.K.; Steinfeld, A. *Handbook of Hydrogen Energy*; CRC Press: Boca Raton, FL, USA, 2014.
- 18. Sadhasivam, T.; Kim, H.-T.; Jung, S.; Roh, S.-H.; Park, J.-H.; Jung, H.-Y. Dimensional effects of nanostructured Mg/MgH<sub>2</sub> for hydrogen storage applications: A review. *Renew. Sustain. Energy Rev.* **2017**, 72, 523–534. [CrossRef]
- 19. In-Depth Analysis in Support on the COM(2018) 773: A Clean Planet for All—A European Strategic Long-Term Vision for a Prosperous, Modern, Competitive and Climate Neutral Economy | Knowledge for Policy. Available online: https://knowledge4policy.ec.europa.eu/publication/depth-analysis-support-com2018-773-clean-planet-all-european-strategic-long-term-vision\_en (accessed on 15 February 2024).
- 20. Gersena, S.; Slima, B.; Zeijlmakera, R.; Van Essena, M.; Tichelaarb, R. The Development of a Natural Gas/Hydrogen Boiler System. In *Proceedings of the International Gas Union Research Conference*; Muscat, Oman, 24–26 February 2020, pp. 1–8. Available online: https://www.researchgate.net/publication/339899796\_The\_Development\_of\_a\_Natural\_GasHydrogen\_Boiler\_System (accessed on 13 March 2023).
- 21. Djukic, M.B.; Zeravcic, V.S.; Bakic, G.M.; Sedmak, A.; Rajicic, B. Hydrogen damage of steels: A case study and hydrogen embrittlement model. *Eng. Fail. Anal.* **2015**, *58*, 485–498. [CrossRef]
- 22. Lamioni, R.; Bronzoni, C.; Folli, M.; Tognotti, L.; Galletti, C. Impact of H<sub>2</sub>-enriched natural gas on pollutant emissions from domestic condensing boilers: Numerical simulations of the combustion chamber. *Int. J. Hydrogen Energy* **2023**, *48*, 19686–19699. [CrossRef]
- 23. Skalska, K.; Miller, J.S.; Ledakowicz, S. Trends in NOx abatement: A review. Sci. Total Environ. 2010, 408, 3976–3989. [CrossRef]
- 24. Gómez-García, M.A.; Pitchon, V.; Kiennemann, A. Pollution by nitrogen oxides: An approach to NOx abatement by using sorbing catalytic materials. *Environ. Int.* **2005**, *31*, 445–467. [CrossRef]
- 25. Yu, B.; Lee, S.; Lee, C.-E. Study of NOx emission characteristics in CH<sub>4</sub>/air non-premixed flames with exhaust gas recirculation. *Energy* **2015**, *91*, 119–127. [CrossRef]
- 26. Dwivedi, S.K.; Vishwakarma, M. Effect of hydrogen in advanced high strength steel materials. *Int. J. Hydrogen Energy* **2019**, *44*, 28007–28030. [CrossRef]
- 27. Ichihara, T.; Koike, R.; Watanabe, Y.; Amano, Y.; Machida, M. Hydrogen damage in a power boiler: Correlations between damage distribution and thermal-hydraulic properties. *Eng. Fail. Anal.* **2023**, *146*, 107120. [CrossRef]
- 28. Yan, F.; Xu, L.; Wang, Y. Application of hydrogen enriched natural gas in spark ignition IC engines: From fundamental fuel properties to engine performances and emissions. *Renew. Sustain. Energy Rev.* **2018**, *82*, 1457–1488. [CrossRef]
- 29. Regulagadda, P.; Dincer, I.; Naterer, G.F. Exergy analysis of a thermal power plant with measured boiler and turbine losses. *Appl. Therm. Eng.* **2010**, *30*, 970–976. [CrossRef]
- 30. Sánchez, A.L.; Williams, F.A. Recent advances in understanding of flammability characteristics of hydrogen. *Prog. Energy Combust. Sci.* **2014**, *41*, 1–55. [CrossRef]
- 31. Campari, A.; Akel, A.J.N.; Ustolin, F.; Alvaro, A.; Ledda, A.; Agnello, P.; Moretto, P.; Patriarca, R.; Paltrinieri, N. Lessons learned from HIAD 2.0: Inspection and maintenance to avoid hydrogen-induced material failures. *Comput. Chem. Eng.* **2023**, 173, 108199. [CrossRef]

32. Dwivedi, S.K.; Vishwakarma, M. Hydrogen embrittlement in different materials: A review. *Int. J. Hydrogen Energy* **2018**, 43, 21603–21616. [CrossRef]

- 33. Lee, J.A.; Woods, S. Hydrogen Embrittlement. 2016. Available online: https://ntrs.nasa.gov/api/citations/20160005654/downloads/20160005654.pdf (accessed on 5 March 2023).
- 34. Yang, G.; Gou, Y.; Liu, X.; Zhang, X.; Zhang, T. Failure Analysis of the Corroded Water Wall Tube in a 50MW Thermal Power Plant. *High Temp. Mater. Process.* **2018**, *37*, 995–999. [CrossRef]
- 35. Poorhaydari, K. A Comprehensive Examination of High-Temperature Hydrogen Attack—A Review of over a Century of Investigations. *J. Mater. Eng. Perform.* **2021**, *30*, 7875–7908. [CrossRef]
- 36. Subramanian, C. Reducing the Risk of High Temperature Creep Failures in Refinery Service Component and Equipment. *J. Press. Vessel. Technol.* **2019**, *141*, 064501. [CrossRef]
- 37. Smiyan, O.D.; Grigorenko, G.M.; Vainman, A.B. Effect of hydrogen on corrosion damage of metal of the high-pressure energetic boiler drum. *Int. J. Hydrogen Energy* **2002**, 27, 801–812. [CrossRef]
- 38. Marchetti, L.; Herms, E.; Laghoutaris, P.; Chêne, J. Hydrogen embrittlement susceptibility of tempered 9%Cr–1%Mo steel. *Int. J. Hydrogen Energy* **2011**, *36*, 15880–15887. [CrossRef]
- 39. Venezuela, J.; Zhou, Q.; Liu, Q.; Li, H.; Zhang, M.; Dargusch, M.S.; Atrens, A. The influence of microstructure on the hydrogen embrittlement susceptibility of martensitic advanced high strength steels. *Mater. Today Commun.* **2018**, *17*, 1–14. [CrossRef]
- 40. Khare, A.; Vishwakarma, M.; Parashar, V. A review on failures of industrial components due to hydrogen embrittlement & techniques for damage prevention. *Int. J. Appl. Eng. Res.* **2017**, *12*, 1784–1792.
- 41. Abohamzeh, E.; Salehi, F.; Sheikholeslami, M.; Abbassi, R.; Khan, F. Review of hydrogen safety during storage, transmission, and applications processes. *J. Loss Prev. Process Ind.* **2021**, 72, 104569. [CrossRef]
- 42. Lynch, S.P. 2—Hydrogen embrittlement (HE) phenomena and mechanisms. In *Stress Corrosion Cracking*; Woodhead Publishing Series in Metals and Surface Engineering; Raja, V.S., Shoji, T., Eds.; Woodhead Publishing: Sawston, UK, 2011; pp. 90–130. [CrossRef]
- 43. Thomas, S.; Ott, N.; Schaller, R.F.; Yuwono, J.A.; Volovitch, P.; Sundararajan, G.; Medhekar, N.V.; Ogle, K.; Scully, J.R.; Birbilis, N. The effect of absorbed hydrogen on the dissolution of steel. *Heliyon* **2016**, 2, e00209. [CrossRef] [PubMed]
- 44. Popov, B.N.; Lee, J.-W.; Djukic, M.B. Chapter 7—Hydrogen Permeation and Hydrogen-Induced Cracking. In *Handbook of Environmental Degradation of Materials*, 3rd ed.; Kutz, M., Ed.; William Andrew Publishing: Amsterdam, The Netherlands, 2018; pp. 133–162. [CrossRef]
- 45. Wróbel, I.; Sikora, K. Simulation of a System for Controlling Atmosphere in Furnace Used to Heating of Blanks. In Proceedings of the 14th International Scientific Conference: Computer Aided Engineering; Lecture Notes in Mechanical Engineering. Rusiński, E., Pietrusiak, D., Eds.; Springer International Publishing: Cham, Switzerland, 2019; pp. 829–835. [CrossRef]
- 46. Stahle, R.W.; Hochmann, J.; McCright, R.D.; Slater, J.E.; Shatynski, S.R. Stress Corrosion Cracking and Hydrogen Embrittlement of Iron Base Alloys. *J. Electrochem. Soc.* **1979**, 126, 215C. [CrossRef]
- 47. Kim, S.J.; Park, J.S.; Jung, S.-P. Corrosion-induced hydrogen evolution, absorption, and cracking behaviors of ultra-high-strength galvanized and galvannealed steel sheets. *NPJ Mater. Degrad.* **2022**, *6*, 31. [CrossRef]
- 48. Turnbull, A. 4—Hydrogen diffusion and trapping in metals. In *Gaseous Hydrogen Embrittlement of Materials in Energy Technologies*; Woodhead Publishing Series in Metals and Surface Engineering; Gangloff, R.P., Somerday, B.P., Eds.; Woodhead Publishing: Sawston, UK, 2012; Volume 1, pp. 89–128. [CrossRef]
- 49. Bhadeshia, H.K.D.H. Prevention of Hydrogen Embrittlement in Steels. ISIJ Int. 2016, 56, 24–36. [CrossRef]
- 50. Lynch, S. Hydrogen embrittlement phenomena and mechanisms. Corros. Rev. 2012, 30, 105–123. [CrossRef]
- 51. Djukic, M.B.; Bakic, G.M.; Zeravcic, V.S.; Sedmak, A.; Rajicic, B. Hydrogen embrittlement of industrial components: Prediction, prevention, and models. *Corrosion* **2016**, 72, 943–961. [CrossRef]
- 52. Liu, Q.; Atrens, A. A critical review of the influence of hydrogen on the mechanical properties of medium-strength steels. *Corros. Rev.* **2013**, *31*, 85–103. [CrossRef]
- 53. Garrison, W.M.; Moody, N.R. 12—Hydrogen embrittlement of high strength steels. In *Gaseous Hydrogen Embrittlement of Materials in Energy Technologies*; Woodhead Publishing Series in Metals and Surface Engineering; Gangloff, R.P., Somerday, B.P., Eds.; Woodhead Publishing: Sawston, UK, 2012; Volume 2, pp. 421–492. [CrossRef]
- 54. Sun, B.; Wang, D.; Lu, X.; Wan, D.; Ponge, D.; Zhang, X. Current Challenges and Opportunities Toward Understanding Hydrogen Embrittlement Mechanisms in Advanced High-Strength Steels: A Review. *Acta Metall. Sin. Engl. Lett.* **2021**, 34, 741–754. [CrossRef]
- 55. Murakami, Y.; Kanezaki, T.; Mine, Y. Hydrogen Effect against Hydrogen Embrittlement. *Metall. Mater. Trans. A* **2010**, *41*, 2548–2562. [CrossRef]
- 56. Takakuwa, O.; Mano, Y.; Soyama, H. Increase in the local yield stress near surface of austenitic stainless steel due to invasion by hydrogen. *Int. J. Hydrogen Energy* **2014**, *39*, 6095–6103. [CrossRef]
- 57. Yamabe, J.; Yoshikawa, M.; Matsunaga, H.; Matsuoka, S. Hydrogen trapping and fatigue crack growth property of low-carbon steel in hydrogen-gas environment. *Int. J. Fatigue* **2017**, *102*, 202–213. [CrossRef]
- 58. Pradhan, A.; Vishwakarma, M.; Dwivedi, S.K. A review: The impact of hydrogen embrittlement on the fatigue strength of high strength steel. *Mater. Today Proc.* **2020**, *26*, 3015–3019. [CrossRef]

59. Chen, T.C.; Chen, S.T.; Kai, W.; Tsay, L.W. The effect of phase transformation in the plastic zone on the hydrogen-assisted fatigue crack growth of 301 stainless steel. *Mater. Charact.* **2016**, *112*, 134–141. [CrossRef]

- 60. Briottet, L.; Moro, I.; Escot, M.; Furtado, J.; Bortot, P.; Tamponi, G.; Solin, J.; Odemer, G.; Blanc, C.; Andrieu, E. Fatigue crack initiation and growth in a CrMo steel under hydrogen pressure. *Int. J. Hydrogen Energy* **2015**, *40*, 17021–17030. [CrossRef]
- 61. Djukic, M.B.; Bakic, G.M.; Zeravcic, V.S.; Sedmak, A.; Rajicic, B. The synergistic action and interplay of hydrogen embrittlement mechanisms in steels and iron: Localized plasticity and decohesion. *Eng. Fract. Mech.* **2019**, *216*, 106528. [CrossRef]
- 62. Al-Anezi, M.A.; Frankel, G.S.; Agrawal, A.K. Susceptibility of Conventional Pressure Vessel Steel to Hydrogen-Induced Cracking and Stress-Oriented Hydrogen-Induced Cracking in Hydrogen Sulfide-Containing Diglycolamine Solutions. *Corrosion* 1999, 55, 1101–1109. [CrossRef]
- 63. Herring, D.H. Hydroqen embrittlement. Wire Form. Technol. Int. 2010, 13, 24–27.
- 64. Martin, M.L.; Sofronis, P. Hydrogen-induced cracking and blistering in steels: A review. *J. Nat. Gas Sci. Eng.* **2022**, 101, 104547. [CrossRef]
- 65. McMahon, C.J. Hydrogen-induced intergranular fracture of steels. Eng. Fract. Mech. 2001, 68, 773–788. [CrossRef]
- 66. Song, J.; Curtin, W.A. Atomic mechanism and prediction of hydrogen embrittlement in iron. *Nat. Mater.* **2013**, *12*, 145–151. [CrossRef]
- 67. Khare, A.; Dwivedi, S.K.; Vishwakarma, M.; Ahmed, S. Experimental Investigation of Hydrogen Embrittlement during Coating Process and Effect on Mechanical Properties of High Strength Steel used for Fasteners. *Mater. Today Proc.* **2018**, *5*, 18707–18715. [CrossRef]
- 68. Li, X.; Ma, X.; Zhang, J.; Akiyama, E.; Wang, Y.; Song, X. Review of hydrogen embrittlement in metals: Hydrogen diffusion, hydrogen characterization, hydrogen embrittlement mechanism and prevention. *Acta Metall. Sin. Engl. Lett.* **2020**, *33*, 759–773. [CrossRef]
- 69. Nagumo, M. Manifestations of Hydrogen Embrittlement. In *Fundamentals of Hydrogen Embrittlement*; Nagumo, M., Ed.; Springer: Singapore, 2016; pp. 103–135. [CrossRef]
- 70. Nagumo, M. Fundamentals of Hydrogen Embrittlement; Springer: Singapore, 2016. [CrossRef]
- 71. Ren, X.; Chu, W.; Su, Y.; Li, J.; Qiao, L. Effects of atomic hydrogen and flaking on mechanical properties of wheel steel. *ACTA Metall. Sin.-Chin. Ed.* **2006**, 42, 153.
- 72. Zappfe, C.A.; Sims, C.E. Hydrogen embrittlement, internal stress and defects in steel. Trans. Metall. Soc. AIME 1941, 145, 225–271.
- 73. Nagumo, M. Hydrogen related failure of steels-a new aspect. Mater. Sci. Technol. 2004, 20, 940-950. [CrossRef]
- 74. Li, X.; Zhang, J.; Fu, Q.; Song, X.; Shen, S.; Li, Q. A comparative study of hydrogen embrittlement of 20SiMn2CrNiMo, PSB1080 and PH13-8Mo high strength steels. *Mater. Sci. Eng. A* **2018**, 724, 518–528. [CrossRef]
- 75. Martin, M.L.; Somerday, B.P.; Ritchie, R.O.; Sofronis, P.; Robertson, I.M. Hydrogen-induced intergranular failure in nickel revisited. *Acta Mater.* **2012**, *60*, 2739–2745. [CrossRef]
- 76. Kappes, M.; Iannuzzi, M.; Carranza, R.M. Hydrogen Embrittlement of Magnesium and Magnesium Alloys: A Review. *J. Electrochem. Soc.* **2013**, *160*, C168. [CrossRef]
- 77. Sofronis, P.; Birnbaum, H.K. Mechanics of the hydrogendashdislocationdashimpurity interactions—I. Increasing shear modulus. *J. Mech. Phys. Solids* **1995**, 43, 49–90. [CrossRef]
- 78. Robertson, I.M.; Sofronis, P.; Nagao, A.; Martin, M.L.; Wang, S.; Gross, D.W.; Nygren, K.E. Hydrogen Embrittlement Understood. *Metall. Mater. Trans. A* **2015**, *46*, 2323–2341. [CrossRef]
- 79. Lynch, S.P. Mechanisms of hydrogen assisted cracking—A review. In *Hydrogen Effects on Material Behaviour and Corrosion Deformation Interactions*; The Minerals, Metals & Materials Society: Pittsburgh, PA, USA, 2003; pp. 449–466.
- 80. Nibur, K.A.; Bahr, D.F.; Somerday, B.P. Hydrogen effects on dislocation activity in austenitic stainless steel. *Acta Mater.* **2006**, *54*, 2677–2684. [CrossRef]
- 81. Connor, M.B. Molecular Dynamics of High Temperature Hydrogen Attack. Ph.D Thesis, Mississippi State University, Starkville, MS, USA, 2022. Available online: https://scholarsjunction.msstate.edu/td/5702 (accessed on 7 February 2024).
- 82. Sabine, M.; Der Giessen, V. Micromechanics of high temperature hydrogen attack. Int. J. Numer. Methods Eng. 2001, 52, 559–567.
- 83. Shewmon, P.G. Hydrogen attack of carbon steel. Metall. Trans. A 1976, 7, 279–286. [CrossRef]
- 84. Shewmon, P.G. Hydrogen attack of pressure-vessel steels. Mater. Sci. Technol. 1985, 1, 2–11. [CrossRef]
- 85. Eliezer, D. High-temperature hydrogen attack of carbon steel. J. Mater. Sci. 1981, 16, 2962–2966. [CrossRef]
- 86. Benac, D.J.; McAndrew, P. Reducing the risk of high temperature hydrogen attack (HTHA) failures. *J. Fail. Anal. Prev.* **2012**, 12, 624–627. [CrossRef]
- 87. Martin, M.L.; Dadfarnia, M.; Orwig, S.; Moore, D.; Sofronis, P. A microstructure-based mechanism of cracking in high temperature hydrogen attack. *Acta Mater.* **2017**, *140*, 300–304. [CrossRef]
- 88. Becker, W.T. ASM Handbook: Failure Analysis and Prevention; ASM International: Almere, The Netherlands, 2002.
- 89. Hadzihafizovic, D. API 571 Damage Mechanisms. 15 April 2023. Available online: https://zenodo.org/records/10391499 (accessed on 29 January 2024).
- 90. Allen, R.E.; Jansen, R.J.; Rosenthal, P.C.; Vitovec, F.H. Analysis of probable mechanisms of high-temperature hydrogen attack of steel. *Proc. API* **1962**, 42, 452–462.

91. Krynicki, J.; Bagnoli, K.; McLaughlin, J.E. Probabilistic Risk Based Approach for Performing an Onstream High Temperature Hydrogen Attack Inspection. In *NACE CORROSION*; NACE, OnePetro: Richardson, TX, USA, 2006; p. NACE-06580. Available online: https://onepetro.org/NACECORR/proceedings-abstract/CORR06/All-CORR06/121255 (accessed on 25 January 2024).

- 92. Sagüés, A.A.; Okray Hall, B.; Wiedersich, H. On the mechanisms of hydrogen attack. Scr. Metall. 1978, 12, 319–326. [CrossRef]
- 93. American Petroleum Institute, Division of Refining. Steels for Hydrogen Service at Elevated Temperatures and Pressures in Petroleum Refineries and Petrochemical Plants; American Petroleum Institute: Washington, DC, USA, 1970.
- 94. Ustolin, F.; Paltrinieri, N.; Berto, F. Loss of integrity of hydrogen technologies: A critical review. *Int. J. Hydrogen Energy* **2020**, 45, 23809–23840. [CrossRef]
- 95. Fletcher, E.E.; Elsea, A.R. The Effects of High Pressure, High Temperature Hydrogen on Steel; Defense Metals Information Center, Battelle Memorial Institute, Columbus, Ohio, USA 1964; Volume 202. Available online: https://books.google.com/books?hl=en&lr=&id=TvAQh9s6tV4C&oi=fnd&pg=PA1&dq=+E.E.+Fletcher+and+A.R.+Elsea,+The+Effects+of+High-Pressure+HighTemperature+Hydrogen+on+Steel,+Defense+Metals+Information+Center,+Columbus,+Ohio,+1964&ots=\_X6 RWkGHQq&sig=7MODWSSfa3jhY5hy90VvBUI5vdg (accessed on 25 January 2024).
- 96. Prager, M. A Worldwide Look at Hot Hydrogen Attack; ASME-Publ.-PVP: New York, NY, USA, 2000; Volume 411, pp. 65–76.
- 97. Nelson, G.A. Use curves to predict steel life. Hydrocarb. Process. 1965, 44, 185–188.
- 98. Parthasarathy, T.A. Mechanisms of Hydrogen Attack of carbon and 214Cr-1Mo steels. Acta Metall. 1985, 33, 1673–1681. [CrossRef]
- 99. Thygeson, J.R.; Molstad, M.C. High Pressure Hydrogen Attack of Steel. J. Chem. Eng. Data 1964, 9, 309–315. [CrossRef]
- 100. Looney, L.; Hurst, R.C.; Taylor, D. The effect of high pressure hydrogen on the creep fracture of notched ferritic-steel components. *J. Mater. Process. Technol.* **1998**, *77*, 25–31. [CrossRef]
- 101. Naumann, F.K. Der Einfluß von Legierungszusätzen auf die Beständigkeit von Stahl Gegen Wasserstoff unter Hohem Druck. No Title. 1938. Available online: https://cir.nii.ac.jp/crid/1130000795045189760 (accessed on 29 January 2024).
- 102. Hattori, K.; Aikawa, S. Scheduling and planning inspection of C-1/2Mo equipment using the new hydrogen attack tendency chart. *Am. Soc. Mech. Eng. Press. Vessel. Pip. Div.* **1992**, 239, 121–128.
- 103. Woods, C.M.; Scott, T.E. *Hydrogen Attack of Bainitic 2 1/4 Cr-1 Mo Steel*; Mound Facility: Miamisburg, OH, USA, 1982. Available online: https://www.osti.gov/biblio/5228194 (accessed on 29 January 2024).
- 104. Sakai, T.; Asami, K. Effect of Applied Stress on Hydrogen Attack of 2 1/4 Cr-1Mo Steel. Tetsu Hagane 1987, 73, 551–557. [CrossRef] [PubMed]
- 105. Allevato, C. Utilizing acoustic emission testing to detect high-temperature hydrogen attack (HTHA) in Cr-Mo reformer reactors and piping during thermal gradients. *Procedia Eng.* **2011**, *10*, 3552–3560. [CrossRef]
- 106. Chiba, R. Effect of Carbon on Hydrogen Attack of 21/4Cr-1Mo Steels. Tetsu Hagane 1985, 71, 1639–1646. [CrossRef]
- 107. Yokogawa, K.; Fukuyama, S.; Kudo, K.; Shewmon, P.G. Effect of hydrogen attack on tensile and creep properties of low carbon steel. *Int. J. Press. Vessels Pip.* **1989**, *37*, 365–385. [CrossRef]
- 108. Ruoff, S.; Stone, D.; Li, C.-Y. Hydrogen attack in a 3Cr-1.5 Mo steel at elevated temperatures. Mater. Sci. Eng. 1987, 93, 217–225.
- 109. der Burg, M.V.; der Giessen, E.V.; Brouwer, R.C. Investigation of hydrogen attack in 2.25 Cr-1Mo steels with a high-triaxiality void growth model. *Acta Mater.* 1996; 44, 505–518.
- 110. Imanaka, T.; Shimomura, J.I. Temper Embrittlement and Hydrogen Attack on 2 1/4 Cr-1Mo Steels in High Pressure and High Temperature Hydrogen Atmosphers. In Proceedings of the 5th International Conference on Pressure Vessel Technology, San Francisco, CA, USA, 9–14 September 1984.
- 111. Imanaka, T.; Shimomura, J.I.; Nakano, S.; Yasuda, K. Hydrogen Attack in Cr–Mo Steels and Disbonding of Austenitic Stainless Weld Overlay. *Kawasaki Steel Tech. Rep.* **1985**, *13*, 109–119.
- 112. Sakai, T.; Kaji, H. Effects of P, Sn, As, Sb, Si, and Cu on the Formation of Bubbles by Hydrogen Attack in 2.25 Cr-1Mo Steel. *Tetsu Hagané* **1980**, *66*, 1133–1141.
- 113. Shimomura, J.; Imanaka, T. Decomposition of carbides in 2 1/4Cr 1Mo steels during hydrogen attack. *Scr. Metall.* **1985**, 19, 1507–1511. [CrossRef]
- 114. Imanaka, T.; Sato, S.; Aso, K.; Shimomura, J.; Ueda, S.; Ejima, A.; Ohashi, N. Improvement in elevated temperature strength, hydrogen attack resistivity and stress relief cracking susceptibility of Cr-Mo steels. *Nucl. Eng. Des.* 1986, 96, 195–207. [CrossRef]
- 115. Tiejian, S.U.; Xinghong, L.U.O.; Cungan, F.A.N.; Yiyi, L.I.; Xiao, C.; Aimin, G.U.O. Tempering Precipitates of Steel 1.25 Cr-0.5 Mo and Their Effects on Its Hydrogen Attack Resistance. *Acta Met. Sin.* **1998**, *34*, 393–399.
- 116. Chiba, R.; Ohnishi, K.; Ishii, K.; Maeda, K. Effect of Heat Treatment on Hydrogen Attack Resistance of C-0.5 Mo Steels for Pressure Vessels, Heat Exchangers, and Piping. *Corrosion* **1985**, *41*, 415–426.
- 117. Chiba, R.; Ohnishi, K.; Ishii, K.; Maeda, K. Effect of Postweld Heat Treatment on Critical Temperature in Hydrogen Attack of 1/2 Mo Steel Welds. *Tetsu Hagane* **1987**, 73, 175–182. [CrossRef]
- 118. Prager, M. Hydrogen Attack Susceptibility of Chrome-Moly Steels and Weldments. In *American Society of Mechanical Engineers, Pressure Vessels and Piping Division (Publication) PVP*; American Society of Mechanical Engineers: New York, NY, USA, 1992; Volume 239.
- 119. Soleimani, M.; Mirzadeh, H.; Dehghanian, C. Effects of spheroidization heat treatment and intercritical annealing on mechanical properties and corrosion resistance of medium carbon dual phase steel. *Mater. Chem. Phys.* **2021**, 257, 123721. [CrossRef]
- 120. López, H.F. Effect of deoxidation practice and heat treatment on the hydrogen attack of carbon steels. *Metall. Trans. A* **1987**, *18*, 1971–1977. [CrossRef]

121. Dong, C.F.; Li, X.G.; Shen, Z.S.; Chu, W.Y. Study on crack healing of hydrogen attack in carbon steel by heat treatment. *Corrosion* **2003**, *59*, 401–406. [CrossRef]

- 122. Marchi, C.S.; Somerday, B.P.; Nibur, K.A. Development of methods for evaluating hydrogen compatibility and suitability. *Int. J. Hydrogen Energy* **2014**, *39*, 20434–20439. [CrossRef]
- 123. Nelson, G.A.; Effinger, R.T. *Blistering and Embrittlement of Pressure Vessel Steels by Hydrogen*; Weld. J (NY); U.S. Department of Energy, Office of Scientific and Technical Information: Washington, DC, USA, 1955; Volume 34. Available online: https://www.osti.gov/biblio/4401716 (accessed on 17 February 2024).
- 124. *API RP 941*; Steels for Hydrogen Service at Elevated Temperatures and Pressures in Petroleum Refineries and Petrochemical Plants. 8th ed. American Petroleum Institute: Washington, DC, USA, 2016.
- 125. Hayden, L.E.; Stalheim, D. ASME B31.12 Hydrogen Piping and Pipeline Code Design Rules and Their Interaction With Pipeline Materials Concerns, Issues and Research. In Proceedings of the ASME 2009 Pressure Vessels and Piping Conference, Prague, Czech Republic, 26–30 July 2009; American Society of Mechanical Engineers Digital Collection; ASME: New York, NY, USA, 2010; pp. 355–361. [CrossRef]
- 126. ASME BPVC Sec VIII-3 Alt Rules Construction High Pressure Vessels—ASME. Available online: https://www.asme.org/codes-standards/find-codes-standards/bpvc-viii-3-bpvc-section-viii-rules-construction-pressure-vessels-division-3-alternative-rules-construction-high-pressure-vessels/2021/print-book (accessed on 18 February 2024).
- 127. Rana, M.D.; Rawls, G.B.; Sims, J.R.; Upitis, E. Technical Basis and Application of New Rules on Fracture Control of high Pressure Hydrogen Vessel in ASME Section VIII, Division 3 Code. 2008. Available online: https://asmedigitalcollection.asme.org/pressurevesseltech/article-abstract/130/2/021101/442772 (accessed on 18 February 2024).
- 128. Rivkin, C.; Blake, C.; Burgess, R.; Buttner, W.J.; Post, M.B. A national set of hydrogen codes and standards for the United States. *Int. J. Hydrogen Energy* **2011**, *36*, 2736–2741. [CrossRef]
- 129. Marchi, C.S.; Somerday, B. *Technical Reference for Hydrogen Compatibility of Materials*; SAND2012-7321; Sandia National Laboratories (SNL): Albuquerque, NM, USA; Livermore, CA, USA, 2012. [CrossRef]
- 130. Safety Standard for Hydrogen and Hydrogen Systems: Guidelines for Hydrogen System Design, Materials Selection, Operations, Storage and Transportation. NASA-TM-112540. 1 January 1997. Available online: https://ntrs.nasa.gov/citations/19970033338 (accessed on 3 May 2023).
- 131. NASA: SAFETY Standard for Hydrogen and Hydrogen Systems. Available online: https://www.energy.gov/sites/prod/files/20 14/03/f11/871916.pdf (accessed on 5 February 2024).
- 132. Nelson, G.A. Operating limits and incubation times for steels in hydrogen Service. *Am. Pet. Inst. Proc. Sect.* 111 Refin. 1965, 45, 190–195.
- 133. Sundararajan, G.; Shewmon, P.G. The hydrogen attack of HSLA steels. Metall. Trans. A 1980, 11, 509–516. [CrossRef]
- 134. Shahi, R.R.; Gupta, A.K.; Kumari, P. Perspectives of high entropy alloys as hydrogen storage materials. *Int. J. Hydrogen Energy* **2023**, *48*, 21412–21428. [CrossRef]
- 135. Miracle, D.B.; Senkov, O.N. A critical review of high entropy alloys and related concepts. *Acta Mater.* **2017**, 122, 448–511. [CrossRef]
- 136. Marques, F.; Balcerzak, M.; Winkelmann, F.; Zepon, G.; Felderhoff, M. Review and outlook on high-entropy alloys for hydrogen storage. *Energy Environ. Sci.* **2021**, *14*, 5191–5227. [CrossRef]
- 137. Xin, Y.; Li, S.; Qian, Y.; Zhu, W.; Yuan, H.; Jiang, P.; Guo, R.; Wang, L. High-Entropy Alloys as a Platform for Catalysis: Progress, Challenges, and Opportunities. *ACS Catal.* **2020**, *10*, 11280–11306. [CrossRef]
- 138. Ye, Y.F.; Wang, Q.; Lu, J.; Liu, C.T.; Yang, Y. High-entropy alloy: Challenges and prospects. *Mater. Today* **2016**, 19, 349–362. [CrossRef]
- 139. Wang, X.; Guo, W.; Fu, Y. High-entropy alloys: Emerging materials for advanced functional applications. *J. Mater. Chem. A* **2021**, 9, 663–701. [CrossRef]
- 140. Brear, J.M.; Church, J.M. TECHNICAL BASIS FOR API PUBLICATION 941 (NELSON CURVES). 1996. Available online: https://www.researchgate.net/profile/John-Brear/publication/303919409\_Technical\_basis\_for\_API\_Publication\_RP941 \_Nelson\_Curves/links/575db5ba08aed88462166d52/Technical-basis-for-API-Publication-RP941-Nelson-Curves.pdf (accessed on 10 February 2024).
- 141. Nelson, G.A. Hydrogenation plant steels. Proc. API M 1949, 29, 163.
- 142. Decker, S.; Hynes, T.; Buchheim, G. Safe Operation of a High Temperature Hydrogen Attack Affected DHT Reactor. In *NACE CORROSION*; NACE, OnePetro: Richardson, Texas, USA, 2009; p. NACE-09339. Available online: https://onepetro.org/NACECORR/proceedings-abstract/CORR09/All-CORR09/128742 (accessed on 21 February 2024).
- 143. Nelson, G.A. Metals for high-pressure hydrogenation plants. Trans. Am. Soc. Mech. Eng. 1951, 73, 205–211. [CrossRef]
- 144. Cramer, S.D.; Covino, B.S., Jr. *ASM Handbook*; ASM International Materials Park: Novelty, OH, USA, 2003; Volume 13, Available online: https://www.asminternational.org/wp-content/uploads/files/06494G-toc.pdf (accessed on 6 February 2024).
- 145. Vijayvargia, K.; Dadfarnia, M.; Sofronis, P.; Kubota, M.; Staykov, A.; Wada, K.; Nguyen, T.; Pugh, J.; Eason, T. A Combined Micromechanics/Materials Science Approach to Understanding High Temperature Hydrogen Attack. 2023. Available online: https://dc.engconfintl.org/cgi/viewcontent.cgi?filename=0&article=1099&context=hydrogen&type=additional (accessed on 5 February 2024).

146. McLaughlin, J.; Krynicki, J.; Bruno, T. Cracking of Non-PWHT'd Carbon Steel Operating at Conditions Immediately Below the Nelson Curve. In Proceedings of the Pressure Vessels and Piping Conference, Bellevu, WA, USA, 18–22 July 2010; pp. 919–930. Available online: https://asmedigitalcollection.asme.org/PVP/proceedings-abstract/PVP2010/919/342781 (accessed on 13 February 2024).

- 147. De Marco, M.; Mannello, G. A Novel Approach for Risk Ranking, NDT Priorities and Damage Mitigation of TIP Units Piping Systems in High Temperature Hydrogen Service. In *NACE CORROSION*; NACE, OnePetro: Richardson, TX, USA, 2013; p. NACE-2013. Available online: https://onepetro.org/NACECORR/proceedings-abstract/CORR13/All-CORR13/121568 (accessed on 13 February 2024).
- 148. Cantwell, J.E. High-Temperature Hydrogen Attack. *Mater. Perform.* **1994**, *33*, 7052013. Available online: https://www.osti.gov/biblio/7052013 (accessed on 25 January 2024).
- 149. Rothwell, J. Maintaining the Integrity of Process Plant Susceptible to High Temperature Hydrogen Attack. Part 2: Factors Affecting Carbon Steel; Health and Safety Executive (HSE): London, UK, 2018.
- 150. Van Der Burg, M.W.D.; Van der Giessen, E.; Tvergaard, V. A continuum damage analysis of hydrogen attack in a 2.25 Cr–1Mo pressure vessel. *Mater. Sci. Eng. A* 1998, 241, 1–13.
- 151. Catastrophic Rupture of Heat Exchanger: Seven Fatalities; Investigation Report, no. Report no. 2010-08-I-WA; Chemical Safety and Hazard Investigation Board: Washington, DC, USA, 2010.
- 152. Hattori, K. An Advanced Hydrogen Attack Tendency Chart as a Life Assessment Strategy for C-0.5 Mo Equipment. ASME-Publ.-PVP: New York, NY, USA, 1997; Volume 359, pp. 333–338.
- 153. High Temperature Hydrogen Attack Method Using Time-Based Nelson Curves. Available online: https://inspectioneering.com/journal/2020-04-30/9160/practical-htha-experience-and-time-based-nelson-curves-for-improved-equipment-li (accessed on 13 February 2024).
- 154. HTHA Time Dependent Nelson Curves and Inspection Planning Enhancements. Available online: https://inspectioneering.com/journal/2022-02-24/10019/breakthroughs-in-predictive-htha-life-assessment-time-dependent-nelson-curves-a (accessed on 13 February 2024).
- 155. Harris, J.A.; Van Wanderham, M.C. Properties of Materials in High Pressure Hydrogen at Cryogenic, Room, and Elevated Temperatures Annual Report. PWA-FR-4566. 30 June 1971. Available online: https://ntrs.nasa.gov/citations/19710024252 (accessed on 4 May 2023).
- 156. Jewett, R.P.; Walter, R.J.; Chandler, W.T.; Frohmberg, R.P. Hydrogen Environment Embrittlement of Metals. NASA-CR-2163. 1 March 1973. Available online: https://ntrs.nasa.gov/citations/19730012717 (accessed on 4 May 2023).
- 157. Report on Hydrogen Tanks, Pipe and Pipeline Stds—ASME. Available online: https://www.asme.org/codes-standards/find-codes-standards/stp-pt-003-hydrogen-standardization-interim-report-for-tanks-piping-and-pipelines (accessed on 9 May 2023).
- 158. CHMC 1-2014; Test Methods for Evaluating Material Compatibility in Compressed Hydrogen Applications-Metals. CSA Group: Toronto, ON, Canada, 2014.
- 159. Kaushal, G.; Bala, N.; Kaur, N.; Singh, H.; Prakash, S. Comparative high-temperature corrosion behavior of Ni-20Cr coatings on T22 boiler steel produced by HVOF, D-Gun, and cold spraying. *Metall. Mater. Trans. A* **2014**, *45*, 395–410. [CrossRef]
- 160. Singh, G.; Bala, N.; Chawla, V. Oxidation behaviour of HVOF sprayed NiCrAlY and NiCrAlY-20SiC coatings on T-91 boiler tube steel. *Prot. Met. Phys. Chem. Surf.* **2020**, *56*, 134–150. [CrossRef]
- 161. Eklund, J.; Phother, J.; Sadeghi, E.; Joshi, S.; Liske, J. High-temperature corrosion of HVAF-sprayed Ni-based coatings for boiler applications. *Oxid. Met.* **2019**, *91*, 729–747. [CrossRef]
- 162. Wetegrove, M.; Duarte, M.J.; Taube, K.; Rohloff, M.; Gopalan, H.; Scheu, C.; Dehm, G.; Kruth, A. Preventing Hydrogen Embrittlement: The Role of Barrier Coatings for the Hydrogen Economy. *Hydrogen* **2023**, *4*, 307–322. [CrossRef]
- 163. Nemanič, V. Hydrogen permeation barriers: Basic requirements, materials selection, deposition methods, and quality evaluation. *Nucl. Mater. Energy* **2019**, *19*, 451–457. [CrossRef]
- 164. Levchuk, D.; Koch, F.; Maier, H.; Bolt, H. Deuterium permeation through Eurofer and α-alumina coated Eurofer. *J. Nucl. Mater.* **2004**, *328*, 103–106. [CrossRef]
- 165. Serra, E.; Bini, A.C.; Cosoli, G.; Pilloni, L. Hydrogen Permeation Measurements on Alumina. *J. Am. Ceram. Soc.* **2005**, *88*, 15–18. [CrossRef]
- 166. Stöver, D.; Buchkremer, H.P.; Hecker, R. Hydrogen and deuterium permeation through metallic and surface-oxidized chromium. *Surf. Coat. Technol.* **1986**, *28*, 281–290. [CrossRef]
- 167. Levchuk, D.; Levchuk, S.; Maier, H.; Bolt, H.; Suzuki, A. Erbium oxide as a new promising tritium permeation barrier. *J. Nucl. Mater.* **2007**, 367–370, 1033–1037. [CrossRef]
- 168. Checchetto, R.; Gratton, L.M.; Miotello, A.; Tosello, C. Deuterium permeation through SiO2 thin film deposited on stainless steel substrate. *J. Non-Cryst. Solids* **1997**, 216, 65–70. [CrossRef]
- 169. Levchuk, D.; Bolt, H.; Döbeli, M.; Eggenberger, S.; Widrig, B.; Ramm, J. Al–Cr–O thin films as an efficient hydrogen barrier. *Surf. Coat. Technol.* **2008**, 202, 5043–5047. [CrossRef]
- 170. RLee, W.; Frank, R.C.; Swets, D.E. Diffusion of hydrogen and deuterium in fused quartz. J. Chem. Phys. 1962, 36, 1062–1071.
- 171. Tamura, M.; Noma, M.; Yamashita, M. Characteristic change of hydrogen permeation in stainless steel plate by BN coating. *Surf. Coat. Technol.* **2014**, *260*, 148–154. [CrossRef]
- 172. Tamura, M. Hydrogen permeation characteristics of TiN-Coated stainless steels. J. Mater. Sci. Eng. 2015, 5, 197–201.

173. Forcey, K.S.; Perujo, A.; Reiter, F.; Lolli-Ceroni, P.L. The formation of tritium permeation barriers by CVD. *J. Nucl. Mater.* **1993**, 200, 417–420. [CrossRef]

- 174. Wang, P.; Liu, J.; Wang, Y.; Shi, B. Investigation of SiC films deposited onto stainless steel and their retarding effects on tritium permeation. *Surf. Coat. Technol.* **2000**, *128–129*, 99–104. [CrossRef]
- 175. Checchetto, R.; Bonelli, M.; Gratton, L.; Miotello, A.; Sabbioni, A.; Guzman, L.; Horino, Y.; Benamati, G. Analysis of the hydrogen permeation properties of TiN-TiC bilayers deposited on martensitic stainless steel. *Surf. Coat. Technol.* 1996, 83, 40–44. [CrossRef]
- 176. Archakov, Y.I.; Grebeshkova, I.D. Ability of clad steels to resist hydrogen attack. Chem. Pet. Eng. 1966, 2, 388–395. [CrossRef]
- 177. Nugent, M.; Silfies, T.; Kowalski, P.; Sutton, N. Recent Applications of Evaluations of Equipment in HTHA Service. In *NACE COR-ROSION*; NACE, OnePetro: Richardson, TX, USA, 2018; p. NACE-2018. Available online: https://onepetro.org/NACECORR/proceedings-abstract/CORR18/All-CORR18/125786 (accessed on 21 February 2024).
- 178. Saini, N.; Pandey, C.; Mahapatra, M.M. Effect of diffusible hydrogen content on embrittlement of P92 steel. *Int. J. Hydrogen Energy* **2017**, 42, 17328–17338. [CrossRef]
- 179. American Welding Society; Committee on Filler Metal. Standard Methods for the Determination of Diffusible Hydrogen Content of Martinsitic, Bainitic, and Ferritic Steel Weld Metal Produced by Arc Welding. The Society. 1986. Available online: <a href="https://pubs.aws.org/Download\_PDFS/A4.3-93\_R2006PV.pdf">https://pubs.aws.org/Download\_PDFS/A4.3-93\_R2006PV.pdf</a> (accessed on 7 January 2024).
- 180. Fangnon, E.; Malitckii, E.; Latypova, R.; Vilaça, P. Prediction of hydrogen concentration responsible for hydrogen-induced mechanical failure in martensitic high-strength steels. *Int. J. Hydrogen Energy* **2023**, *48*, 5718–5730. [CrossRef]
- 181. Malitckii, E.; Fangnon, E.; Vilaça, P. Study of correlation between the steels susceptibility to hydrogen embrittlement and hydrogen thermal desorption spectroscopy using artificial neural network. *Neural Comput. Appl.* **2020**, *32*, 14995–15006. [CrossRef]
- 182. Zhang, G.; Wang, X.; Xiong, Y.; Shi, Y.; Song, J.; Luo, D. Mechanism for adsorption, dissociation and diffusion of hydrogen in hydrogen permeation barrier of α-Al2O3: A density functional theory study. *Int. J. Hydrogen Energy* **2013**, *38*, 1157–1165. [CrossRef]
- 183. Zhang, G.; Dou, S.; Lu, Y.; Shi, Y.; Lai, X.; Wang, X. Mechanisms for adsorption, dissociation and diffusion of hydrogen in hydrogen permeation barrier of α-Al2O3: The role of crystal orientation. *Int. J. Hydrogen Energy* **2014**, 39, 610–619. [CrossRef]
- 184. Depover, T.; Escobar, D.P.; Wallaert, E.; Zermout, Z.; Verbeken, K. Effect of hydrogen charging on the mechanical properties of advanced high strength steels. *Int. J. Hydrogen Energy* **2014**, *39*, 4647–4656. [CrossRef]
- 185. Danford, M.D. Hydrogen Trapping and the Interaction of Hydrogen with Metals. 1 July 1987. Available online: https://ntrs.nasa.gov/citations/19870016030 (accessed on 8 January 2024).
- 186. Mertens, G.; Duprez, L.; Cooman, B.C.D.; Verhaege, M. Hydrogen Absorption and Desorption in Steel by Electrolytic Charging. *Adv. Mater. Res.* **2007**, *15–17*, 816–821. [CrossRef]
- 187. Vernerey, F.J.; McVeigh, C.; Liu, W.K.; Moran, B.; Tewari, D.; Parks, D.M.; Olson, G.B. The 3-D computational modeling of shear-dominated ductile failure in steel. *JOM* **2006**, *58*, 45–51. [CrossRef]
- 188. Needleman, A. Computational Modeling of Material Failure. Appl. Mech. Rev. 1994, 47, S34–S42. [CrossRef]
- 189. Dujc, J.; Brank, B.; Ibrahimbegovic, A. Multi-scale computational model for failure analysis of metal frames that includes softening and local buckling. *Comput. Methods Appl. Mech. Eng.* **2010**, *199*, 1371–1385. [CrossRef]
- 190. Barrera, O.; Bombac, D.; Chen, Y.; Daff, T.D.; Galindo-Nava, E.; Gong, P.; Haley, D.; Horton, R.; Katzarov, I.; Kermode, J.R.; et al. Understanding and mitigating hydrogen embrittlement of steels: A review of experimental, modelling and design progress from atomistic to continuum. *J. Mater. Sci.* **2018**, *53*, 6251–6290. [CrossRef]
- 191. Cheng, G.; Chen, K.; Zhang, Y.; Venkatesh, T.; Wang, X.; Li, Z.; Yang, J. Probing the effects of hydrogen on the materials used for large-scale transport of hydrogen through multi-scale simulations. *Renew. Sustain. Energy Rev.* **2023**, *182*, 113353. [CrossRef]
- 192. Roadmap on Multiscale Materials Modeling—IOPscience. Available online: https://iopscience.iop.org/article/10.1088/1361-651 X/ab7150/meta (accessed on 8 January 2024).
- 193. Al-Jabr, K.A.; Multiscale Modeling of Hydrogen Embrittlement for Multiphase Material. May 2014. Available online: http://hdl.handle.net/10754/316598 (accessed on 8 January 2024).
- 194. Morrissey, L. A Multiscale Analysis on the Effect of Atomistic Processes on Mechanical Properties. Ph.D. Thesis, Memorial University of Newfoundland, St. John's, NL, Canada, 2020. Available online: https://research.library.mun.ca/15073/ (accessed on 8 January 2024).
- 195. Chavoshi, S.Z.; Hill, L.T.; Bagnoli, K.E.; Holloman, R.L.; Nikbin, K.M. A combined fugacity and multi-axial ductility damage approach in predicting high temperature hydrogen attack in a reactor inlet nozzle. *Eng. Fail. Anal.* 2020, 117, 104948. [CrossRef]
- 196. Wang, Y.; Li, J. Phase field modeling of defects and deformation. Acta Mater. 2010, 58, 1212–1235. [CrossRef]
- 197. Martínez-Pañeda, E.; Golahmar, A.; Niordson, C.F. A phase field formulation for hydrogen assisted cracking. *Comput. Methods Appl. Mech. Eng.* **2018**, 342, 742–761. [CrossRef]
- 198. Wu, J.-Y.; Nguyen, V.P.; Nguyen, C.T.; Sutula, D.; Sinaie, S.; Bordas, S.P.A. Chapter One—Phase-field modeling of fracture. *Adv. Appl. Mech.* **2020**, *53*, 1–183. [CrossRef]
- 199. Moelans, N.; Blanpain, B.; Wollants, P. An introduction to phase-field modeling of microstructure evolution. *Calphad* **2008**, 32, 268–294. [CrossRef]
- 200. Wang, M.; Akiyama, E.; Tsuzaki, K. Effect of hydrogen and stress concentration on the notch tensile strength of AISI 4135 steel. *Mater. Sci. Eng. A* **2005**, *398*, 37–46. [CrossRef]

201. Olden, V.; Thaulow, C.; Johnsen, R.; Østby, E.; Berstad, T. Influence of hydrogen from cathodic protection on the fracture susceptibility of 25%Cr duplex stainless steel—Constant load SENT testing and FE-modelling using hydrogen influenced cohesive zone elements. *Eng. Fract. Mech.* 2009, 76, 827–844. [CrossRef]

- 202. Thomas, R.L.S.; Scully, J.R.; Gangloff, R.P. Internal hydrogen embrittlement of ultrahigh-strength AERMET 100 steel. *Metall. Mater. Trans. A* **2003**, *34*, 327–344. [CrossRef]
- 203. Alvaro, A.; Jensen, I.T.; Kheradmand, N.; Løvvik, O.M.; Olden, V. Hydrogen embrittlement in nickel, visited by first principles modeling, cohesive zone simulation and nanomechanical testing. *Int. J. Hydrogen Energy* **2015**, *40*, 16892–16900. [CrossRef]
- 204. Valverde-González, A.; Martínez-Pañeda, E.; Quintanas-Corominas, A.; Reinoso, J.; Paggi, M. Computational modelling of hydrogen assisted fracture in polycrystalline materials. *Int. J. Hydrogen Energy* 2022, 47, 32235–32251. [CrossRef]
- 205. Harris, Z.D.; Lawrence, S.K.; Medlin, D.L.; Guetard, G.; Burns, J.T.; Somerday, B.P. Elucidating the contribution of mobile hydrogen-deformation interactions to hydrogen-induced intergranular cracking in polycrystalline nickel. *Acta Mater.* **2018**, *158*, 180–192. [CrossRef]
- 206. Cui, C.; Bortot, P.; Ortolani, M.; Martínez-Pañeda, E. Computational predictions of hydrogen-assisted fatigue crack growth. *Int. J. Hydrogen Energy* **2024**, *72*, 315–325. [CrossRef]
- 207. Kumar, G.R.; Muralidharan, A.; Rajyalakshmi, G.; Swaroop, S. Atom probe tomography analysis of hydrogen distribution in laser peened Ti6Al4V alloy to control hydrogen embrittlement. *Int. J. Adv. Manuf. Technol.* **2021**, *114*, 1395–1408. [CrossRef]
- 208. Wen, C.; Zhang, Y.; Wang, C.; Xue, D.; Bai, Y.; Antonov, S.; Dai, L.; Lookman, T.; Su, Y. Machine learning assisted design of high entropy alloys with desired property. *Acta Mater.* **2019**, *170*, 109–117. [CrossRef]
- 209. Feng, S.; Zhou, H.; Dong, H. Using deep neural network with small dataset to predict material defects. *Mater. Des.* **2019**, *162*, 300–310. [CrossRef]
- 210. Xiong, J.; Shi, S.-Q.; Zhang, T.-Y. A machine-learning approach to predicting and understanding the properties of amorphous metallic alloys. *Mater. Des.* **2020**, *187*, 108378. [CrossRef]
- 211. Ahmed, N.; Aldaw, M.; Ahmed, R.; Teodoriu, C. Modeling of necking area reduction of carbon steel in hydrogen environment using machine learning approach. *Eng. Fail. Anal.* **2024**, *156*, 107864. [CrossRef]
- 212. Campari, A.; Darabi, M.A.; Alvaro, A.; Ustolin, F.; Paltrinieri, N.; A Machine Learning Approach to Predict. the Materials' Susceptibility to Hydrogen Embrittlement. 2023. Available online: https://ntnuopen.ntnu.no/ntnu-xmlui/bitstream/handle/11 250/3105129/033.pdf?sequence=1 (accessed on 13 April 2024).
- 213. Subedi, A.; Campari, A.; Alvaro, A.; Thapa, B.S.; Paltrinieri, N. Evaluation of the Factors Determining Hydrogen Embrittlement in Pipeline Steels: An Artificial Intelligence Approach. 2023. Available online: https://rpsonline.com.sg/proceedings/esrel2023/pdf/P510.pdf (accessed on 13 April 2024).
- 214. Kim, S.-G.; Shin, S.-H.; Hwang, B. Machine learning approach for prediction of hydrogen environment embrittlement in austenitic steels. *J. Mater. Res. Technol.* **2022**, *19*, 2794–2798. [CrossRef]
- 215. Xu, K. Hydrogen embrittlement of carbon steels and their welds. In *Gaseous Hydrogen Embrittlement of Materials in Energy Technologies*; Elsevier: Amsterdam, The Netherlands, 2012; pp. 526–561. Available online: https://www.sciencedirect.com/science/article/pii/B9781845696771500144 (accessed on 14 August 2024).
- 216. Subedi, A.; Campari, A.; Thapa, B.S.; Paltrinieri, N. Safety Evaluation of Hydrogen Pipeline Transport: An Approach Based on Machine Learning. *Chem. Eng. Trans.* **2023**, *105*, 121–126.

**Disclaimer/Publisher's Note:** The statements, opinions and data contained in all publications are solely those of the individual author(s) and contributor(s) and not of MDPI and/or the editor(s). MDPI and/or the editor(s) disclaim responsibility for any injury to people or property resulting from any ideas, methods, instructions or products referred to in the content.